



Western Michigan University
ScholarWorks at WMU

Dissertations

Graduate College

12-2008

Switch On and Switch Off Nanosensors for the Detection of Nerve Gas Agents

Shankar Varaganti
Western Michigan University

Follow this and additional works at: <https://scholarworks.wmich.edu/dissertations>

 Part of the Chemistry Commons

Recommended Citation

Varaganti, Shankar, "Switch On and Switch Off Nanosensors for the Detection of Nerve Gas Agents" (2008). *Dissertations*. 819.

<https://scholarworks.wmich.edu/dissertations/819>

This Dissertation-Open Access is brought to you for free and open access by the Graduate College at ScholarWorks at WMU. It has been accepted for inclusion in Dissertations by an authorized administrator of ScholarWorks at WMU. For more information, please contact wmu-scholarworks@wmich.edu.



SWITCH ON AND SWITCH OFF NANOSENSORS FOR THE DETECTION OF
NERVE GAS AGENTS

by

Shankar Varaganti

A Dissertation
Submitted to the
Faculty of The Graduate College
in partial fulfillment of the
requirements for the
Degree of Doctor of Philosophy
Department of Chemistry
Dr. Ekkehard Sinn, Advisor

Western Michigan University
Kalamazoo, Michigan
December 2008

UMI Number: 3340205

INFORMATION TO USERS

The quality of this reproduction is dependent upon the quality of the copy submitted. Broken or indistinct print, colored or poor quality illustrations and photographs, print bleed-through, substandard margins, and improper alignment can adversely affect reproduction.

In the unlikely event that the author did not send a complete manuscript and there are missing pages, these will be noted. Also, if unauthorized copyright material had to be removed, a note will indicate the deletion.

UMI[®]

UMI Microform 3340205

Copyright 2009 by ProQuest LLC.

All rights reserved. This microform edition is protected against unauthorized copying under Title 17, United States Code.

ProQuest LLC
789 E. Eisenhower Parkway
PO Box 1346
Ann Arbor, MI 48106-1346

Copyright by
Shankar Varaganti
2008

ACKNOWLEDGMENTS

I express my gratitude to everyone who has helped me in finishing this project. I want to start by first thanking my advisor Dr. Subra Muralidharan. The support he gave me was immense, from organizing my work to implementing new thoughts in my research.

I acknowledge my committee members Dr. Ekkehard Sinn, Dr. John Miller, Dr. Yirong Mo, and Dr. Muralidhar Ghantasala, for their thoughtful insights in making my thesis near perfect.

I would like to thank Dr. John Miller for his guidance during my crunch situation. It was because of his unflinching support, faith and pivotal role that made me complete my doctoral studies at Western Michigan University.

I also am greatly indebted to Dr. Ekkehard Sinn for all his guidance and thoughtfulness during my troubled times.

I express my thanks to Dr. Subodh Dutta. It was he who taught me the nuances of synthetic techniques, which constituted a major part of my project. I also render my thanks to Dr. Raymond Sung for his cooperation in learning to work with the NMR and IR instruments.

I am grateful to the chemistry department at Western Michigan University for giving me an opportunity to do my Ph.D.

Acknowledgments—Continued

I also want to thank the office co-coordinators Pam and Annie for their help in all the paper work and documentation.

I must also thank Beth Sodt and Chun Wang (Wendy), my colleagues, for allowing me to share some of the synthetic procedures involving Quantum Dots and Stilbene analogs. I also express my thanks to Aruna who helped me with grasping chromatographic techniques, and also my other friends who were there with me in my good and bad years.

I thank my dad Mr. Lakshmaiah, mom Mrs. Balamani and my wife Jyothi for all their best wishes, support and faith they reposed in me.

Finally, I greatly acknowledge the funding from Department of Energy, Office of Basic Energy Sciences.

Shankar Varaganti

TABLE OF CONTENTS

ACKNOWLEDGMENTS	ii
LIST OF TABLES	xi
LIST OF FIGURES.....	xii
LIST OF SCHEMES.....	xix
LIST OF ABBREVIATIONS	xx
CHAPTER	
I. INTRODUCTION.....	1
1.1 Chemical Warfare Agents (CWA)	1
1.2 History and Classification of Nerve Agents	4
1.2.1 Tabun	5
1.2.2 Sarin	6
1.2.3 Soman	6
1.2.4 VX.....	7
1.3 Mechanism of Action of Nerve Agents on Human Beings	8
1.4 Treatment for Nerve Agent Exposure	10
1.5 Detection Techniques of Nerve Agents.....	11
1.6 Central Hypothesis	18
1.7 Objectives of the Present Study.....	19
1.8 Association Constant Calculation Methods.....	21
1.8.1 Stern-Volmer Equation	21

Table of Contents—Continued

CHAPTER		
	1.8.2 Benesi-Hildebrand Equation.....	22
	1.9 Instrumentation.....	23
II. BUILDING BLOCKS OF NANOSENSORS		25
	2.1 Introduction to Silica Nanoparticles.....	25
	2.2 Synthesis of Silica Nanoparticles	26
	2.3 Synthesis of Silica Nanoparticles by Stober Method	27
	2.4 Silanization of Silica Nanoparticles	28
	2.5 Results and Discussion.....	30
	2.6 Introduction to Quantum Dots.....	31
	2.7 Synthesis of ZnS: Mn/ZnS Quantum Dots.....	34
	2.8 UV-Vis Spectra of ZnS:Mn/ZnS (1/16 th) QDs.....	35
	2.9 Introduction to Stilbene Compound	37
	2.10 Synthesis of Stilbene Monomer.....	38
III. SYNTHESIS AND SPECTRAL STUDIES OF 4,4'-BIPYRIDINE TRYPTOPHAN RUTHENIUM COMPLEX		45
	3.1 Introduction	45
	3.2 Synthetic Methods.....	47
	3.2.1 Synthesis of 2,2'-Bipyridine-4,4'-Dicarboxylic Acid	47
	3.2.2 Preparation of cis-(bpy) ₂ RuCl ₂ .2H ₂ O.....	50
	3.2.3 Preparation of 4,4'-Bipyridine Tryptophan Ligand.....	51

Table of Contents—Continued

CHAPTER		
	3.2.4 Preparation of Ru(bpy) ₂ (4,4'-Bpy Tryptophan) Complex....	57
	3.2.5 Emission of 4,4'-Bpy Tryptophan [12.5x10 ⁻⁶ M] Vs Variable DCP [50 μM to 2.5 mM] (at Exci 280 nm).....	61
	3.2.6 Emission of 4,4'-Bpy Tryptophan [12.5x10 ⁻⁶ M] Vs Variable HCl (at Exci 280 nm).....	62
	3.2.7 Emission of 4,4'-Bpy Tryptophan [20x10 ⁻⁶ M] Vs Variable DMMP (at Exci 280 nm).....	63
	3.2.8 Emission of Ru(bpy) ₂ (4,4'-Bpy Tryptophan) [7.5X10 ⁻⁶ M] Vs Variable DCP [.87 μM to 7.83 μM] (at Exci 290 nm).....	64
	3.2.9 Emission of Ru(bpy) ₂ (4,4'-Bpy Tryptophan) [10X10 ⁻⁶ M] Vs Variable HCl [60 μM to 510 μM] (at Exci 290 nm).....	65
	3.3.0 Emission of Ru(bpy) ₂ (4,4'-Bpy Tryptophan) [5X10 ⁻⁶ M] Vs Variable DMMP.....	66
	3.3.1 Preparation of Zinc (4,4'-Bpy Tryp) ₂ Complex.....	67
	3.3.2 Emission of 10μM Zn(4,4'-Bpy Tryp) ₂ Complex Vs Various DCP Concentrations	69
	3.3.3 Emission of 10μM Zn(4,4'-Bpy Tryp) ₂ Complex Vs Various HCl Concentrations	70
	3.3.4 Emission of 10μM Zn(4,4'-Bpy Tryp) ₂ Complex Vs Various DMMP Concentrations.....	71
	IV. SYNTHESIS AND SPECTRAL STUDIES OF 5,5'-BIPYRIDINE TRYPTOPHAN RUTHENIUM COMPLEX	73
	4.1 Synthetic Methods.....	73
	4.1.1 Synthesis of 5,5'-Bipyridine Tryptophan	73

Table of Contents—Continued

CHAPTER

4.1.2 Emission of 5,5'-Bpy Tryptophan [12.5×10^{-6} M] Vs Variable DCP [50 μ M to 5 mM] [(at Exci 290 nm) (sol. Acetonitrile).....	78
4.1.3 Emission of 5,5'-Bpy Tryptophan [15×10^{-6} M] Vs Variable HCl [0 μ M to 54 μ M] [(at Exci 290 nm) (sol. Acetonitrile)]	80
4.1.4 Emission of 5,5'-Bpy Tryptophan [7×10^{-6} M] Vs Variable DMMP [0 μ M to 345 μ M] [(at Exci 290 nm) (sol. Acetonitrile)]	80
4.1.5 Preparation of Ru(bpy) ₂ (5,5'-Bpy Tryptophan) Complex....	82
4.1.6 Emission of Ru(bpy) ₂ (5,5'-Bpy Tryptophan) Complex [5×10^{-6} M] Vs Variable DCP [50 μ M to 875 μ M] (at Exci 290 nm).....	85
4.1.7 Emission of Ru(bpy) ₂ (5,5'-Bpy Tryptophan) Complex [10×10^{-6} M] Vs Variable HCl [0 μ M to 450 μ M] (at Exci 290 nm).....	87
4.1.8 Emission of Ru(bpy) ₂ (5,5'-Bpy Tryptophan) Complex [7.5×10^{-6} M] Vs Variable DMMP [0 μ M to 450 μ M] (at Exci 290 nm).....	87
4.1.9 Preparation of Zinc (5,5'-Bpy Tryptophan) ₂ Complex.....	88
4.2.0 Emission of 11.75 μ M Zn(5,5'Bpy Tryp) ₂ Complex Vs DCP [0 μ M to 282.5 μ M] (at Exci 290 nm)	89
4.2.1 Emission of 11.75 μ M Zn(5,5'Bpy Tryp) ₂ Complex Vs Variable HCl [0 μ M to 508 μ M] (at Exci 290 nm).....	90
4.2.2 Emission of 11.75 μ M Zn(5,5'Bpy Tryp) ₂ Complex Vs Variable DMMP [0 μ M to 280 μ M] (at Exci 290 nm)	92

Table of Contents—Continued

CHAPTER

V. SYNTHESIS AND SPECTRAL STUDIES OF FULL SENSOR SYSTEM.....	94
5.1 Introduction	94
5.2 Spectral Properties of Stilbene Monomer.....	96
5.2.1 Emission of Stilbene Monomer with DCP(excitation 290 nm).....	96
5.2.2 Emission of Stilbene Monomer with HCl	96
5.2.3 Emission of Stilbene Monomer with DMMP.....	97
5.3 Synthesis and Spectral Studies of Silica Nanoparticles with Stilbene Monomer	98
5.3.1 Synthesis Silica NPs with Stilbene Monomer	98
5.3.2 IR Spectra of Silica NPs with Stilbene Monomer.....	99
5.3.3 Emission of Silica NPs with Stilbene Monomer	100
5.3.4 Emission of Silica NPs with Stilbene Monomer Vs Various DCP	100
5.3.5 Emission of Silica NPs with Stilbene Monomer Vs Various HCl.....	101
5.4 Synthesis of Silica NPs + Stilbene Monomer + 4,4'-Bpy Tryp Ruthenium Complex (Sensor I) and its Spectral Characterization.....	103
5.4.1 Synthetic Scheme of Sensor I	103
5.4.2 Emission of Silica NP + Stilbene Monomer (9.45 μ M) + Ru(bpy) ₂ (4,4'-Bpy Tryptophan) (4.7 μ M) (Sensor I) Vs Various DCP.....	104

Table of Contents—Continued

CHAPTER

5.4.3 Emission of Silica NP + Stilbene Monomer (9.45 μ M) + Ru(bpy) ₂ (4,4'-Bpy Tryptophan) (4.7 μ M) (Sensor I) Vs Various HCl	105
5.4.4 Emission of Silica NP + Stilbene Monomer (9.45 μ M) + Ru(bpy) ₂ (4,4'-Bpy Tryptophan) (4.7 μ M) (Sensor I) Vs Various DMMP	106
5.5 Synthesis of Silica NPs + Stilbene Monomer + 5,5'-Bpy Trypruthenium Complex (Sensor II) and its Spectral Characterization.....	107
5.5.1 Synthetic Procedure of Sensor II.....	108
5.5.2 Emission of Silica NP + Stilbene Monomer (9.45 μ M) + Ru(bpy) ₂ (5,5'-Bpy Tryptophan) (4.7 μ M) (Sensor II) Vs Various DCP	109
5.5.3 Emission of Silica NP + Stilbene Monomer (9.45 μ M) + Ru(bpy) ₂ (5,5'-Bpy Tryptophan)(4.7 μ M) (Sensor II) Vs Various HCL	110
5.5.4 Emission of Silica NP + Stilbene Monomer (9.45 μ M) + Ru(bpy) ₂ (5,5'-Bpy Tryptophan) (4.7 μ M) (Sensor II) Vs Various DMMP	111
5.6 Synthesis of Silica NPs + Stilbene Monomer + 4,4'-Bpy Tryp Zinc Complex (Sensor III) and its Spectral Characterization.....	112
5.6.1 Synthetic Scheme of Sensor III	112
5.6.2 Emission of Sensor III with DCP	113
5.7 Synthesis of Silica NPs + Stilbene Monomer + 5,5'-Bpy Tryp Zinc Complex (Sensor IV) and its Spectral Characterization.....	114
5.7.1 Synthetic Scheme of Sensor IV.....	114

Table of Contents—Continued

CHAPTER	
5.7.2 Emission of Sensor IV with DCP	115
5.8 Synthesis of ZnS: Mn/ZnS QDs + Stilbene Monomer + 4,4'- Bpy Tryp Ruthenium Complex (Sensor V) and its Spectral Characterization.....	116
5.8.1 Synthetic Scheme of Sensor V.....	116
5.8.2 Emission of Sensor V Vs DCP	116
5.8.3 Emission of Sensor V Vs HCl	118
5.8.4 Emission of Sensor V Vs DMMP	119
VI. CONCLUSION.....	121
6.1 Conclusion.....	121
6.1.1 Sensor I	123
6.1.2 Sensor II	123
6.1.3 Sensor III.....	123
6.1.4 Sensor IV.....	124
6.1.5 Sensor V.....	124
REFERENCES	125

LIST OF TABLES

1.1 Chemical Warfare Agents.....	2
1.2 Physical Properties and Toxicity of Nerve Agents.....	7
3.1 Optical Rotation of 4,4'-Bpy Tryptophan.....	56
3.2 Association Constants of 4,4'-Bpy Tryptophan and its Complexes.....	72
4.1 Association Constants of 5,5'-Bpy Tryptophan and its Complexes.....	93
5.1 Association Constants of Sensor Systems	120
6.1 Association Constants and Behavior of Sensors Developed	122

LIST OF FIGURES

1.1	Chemical Structures of G and V Agents.....	5
1.2	The Reactivity of Tabun with Acetylcholine Esterase Enzyme (Adapted from ref.9).....	6
1.3	Interaction of a Nerve Agent with AChE (Adapted from ref.7).....	9
1.4	Mechanism of Sarin Toxicity (Taken from ref.11).....	9
1.5	Mechanism of Action of Pralidoxime (2-PAM) on AChE (Adapted from ref.7).....	11
1.6	Colorimetric Detection of Acetylcholinesterase Inhibitors (Adapted from ref.21).....	12
1.7	Nerve Agent Detection by Using Organophosphorus Hydrolase Enzyme (Adapted from ref.19).....	13
1.8	Bending of Self Assembled Cu ²⁺ /L-Cysteine Bilayer Coated Microcantilever with DMMP (Taken from ref.23).....	13
1.9	Hydrogen-Bond Acidic Linear Polymers Used in SAW Sensors (Adapted from ref.13).....	14
1.10	General Scheme of PET Indicator Molecules for the Detection of Nerve Agents (Adapted from ref.3).....	15
1.11	Fluorescent Sensor for Nerve Agent by Swager (Adapted from ref. 27).....	16
1.12	Fluorescent (PET) Sensor for Nerve Gas by Julius Rebek (Taken from ref. 28).....	17
1.13	Fluorescent Sensor for Nerve Gas Sensing by Walt (Adapted from ref. 29).....	17
1.14	NMCR Assembly of Proposed Nanosensor to Detect Nerve Agents (Adapted from ref. 30).....	18
1.15	NMCR Sensor Designed in this Work.....	20

List of Figures—Continued

2.1	TEM Image of Silica Nanoparticles.....	28
2.2	TEM Image of Silinized Silica Nanoparticles	29
2.3	IR Spectra of Silica NPs and Silanized Silica NPs	30
2.4	Size Tunable Fluorescence Spectra of CdSe Qds (Taken from ref. 49)	32
2.5	Chemical Modification Methods of QDs (Taken from ref. 49).....	33
2.6	UV-Vis Spectrum of ZnS:Mn/ZnS (1/16 th) QDs in Acetonitrile.....	35
2.7	Excitation Spectrum of ZnS:Mn/ZnS (1/16 th) QDs in Acetonitrile.....	36
2.8	Emission Spectrum of ZnS:Mn/ZnS (1/16 th) QDs in Acetonitrile	36
2.9	Schematic Diagram of Stilbene Conversion	37
2.10	Synthetic Scheme for the Preparation of Stilbene Monomer (Adapted from ref. 68)	39
2.11	¹ H NMR Spectrum of Stilbene Intermediate	40
2.12	¹ H NMR Spectrum of Stilbene Monomer.....	41
2.13	LCMS ESI (–ve mode) of Stilbene	42
2.14	UV-Vis Spectrum of Stilbene Monomer	42
2.15	Excitation Spectrum of Stilbene Monomer.....	43
2.16	Emission Spectrum of Stilbene Monomer	43
3.1	¹ H NMR Spectrum of 4,4'-Dimethyl-2,2'-Bipyridine.....	48
3.2	¹³ C NMR Spectrum of 4,4'-Dimethyl-2,2'-Bipyridine.....	49
3.3	¹ H NMR Spectrum of 2,2'-Bipyridine-4,4'-Dicarboxylic Acid	50
3.4	¹ H NMR Spectrum of cis-(bpy) ₂ RuCl ₂ .2H ₂ O	51

List of Figures—Continued

3.5	^1H NMR spectrum of 4,4'-Bpy Tryptophan.....	52
3.6	^{13}C NMR spectrum of 4,4'-Bpy Tryptophan	53
3.7	^1H - ^1H COSY NMR Spectrum of 4,4'-Bpy Tryptophan.....	53
3.8	LC-MS ESI Negative Spectrum of 4,4'-Bpy Tryptophan.....	54
3.9	UV-Vis Spectrum of 12.5 μM 4,4'-Bpy Tryptophan.....	54
3.10	Excitation Spectrum of 4,4'-Bpy Tryptophan.....	55
3.11	Emission Spectrum of 4,4'-Bpy Tryptophan	55
3.12	^1H NMR Spectrum of $\text{Ru}(\text{bpy})_2(4,4'\text{-Bpy Tryptophan})$	58
3.13	LC-MS ESI Positive Spectrum of $\text{Ru}(\text{bpy})_2(4,4'\text{-Bpy Tryptophan})$	59
3.14	UV-Vis Spectrum of $\text{Ru}(\text{bpy})_2(4,4'\text{-Bpy Tryptophan})$	59
3.15	Emission Spectrum of $\text{Ru}(\text{bpy})_2(4,4'\text{-Bpy Tryptophan})$	60
3.16	Emission Spectrum of 4,4'-Bpy Tryptophan with Various DCP Concentrations.....	61
3.17	Association Constant of 4,4'-Bpy Tryptophan with DCP	61
3.18	Emission Spectrum of 4,4'-Bpy Tryptophan with Various HCl Concentrations	62
3.19	Emission Spectrum of 4,4'-Bpy Tryptophan with Various DMMP Concentrations	63
3.20	Emission Spectrum of $\text{Ru}(\text{bpy})_2(4,4'\text{-Bpy Tryptophan})$ with Various DCP Concentrations.....	64
3.21	Association Constant of $\text{Ru}(\text{bpy})_2(4,4'\text{-Bpy Tryptophan})$ with DCP.....	64
3.22	Emission Spectrum of $\text{Ru}(\text{bpy})_2(4,4'\text{-Bpy Tryptophan})$ with HCl	65
3.23	Association Constant of $\text{Ru}(\text{bpy})_2(4,4'\text{-Bpy Tryptophan})$ with HCl	66

List of Figures—Continued

3.24	Emission Spectrum of Ru(bpy) ₂ (4,4'-Bpy Tryptophan) with DMMP	66
3.25	Emission Spectrum of Zn(4,4'-Bpy Tryp) ₂ with DCP	69
3.26	Association Constant of Zn(4,4'-Bpy Tryp) ₂ with DCP	69
3.27	Emission Spectrum of 10μM Zn(4,4'-Bpy Tryp) ₂ Complex with HCl	70
3.28	Emission Spectrum of 10μM Zn(4,4'-Bpy Tryp) ₂ Complex with DMMP....	71
4.1	¹ H NMR of 5,5'-Bipyridine Tryptophan Ligand.....	74
4.2	¹³ C NMR of 5,5'-Bipyridine Tryptophan Ligand	75
4.3	¹ H- ¹ H COSY NMR of 5,5'-Bipyridine Tryptophan Ligand	75
4.4	¹ H- ¹³ C HETCOR NMR of 5,5'-Bipyridine Tryptophan Ligand.....	76
4.5	LC-MS ESI (-Ve) of 5,5'-Bipyridine Tryptophan Ligand	76
4.6	UV-Vis Spectrum of 5,5'-Bipyrdine Tryptophan Ligand	77
4.7	Excitation Spectrum of 5,5'-Bipyridine Tryptophan Ligand	77
4.8	Emission Spectrum of 5,5'-Bipyridine Tryptophan Ligand.....	78
4.9	Emission Spectrum of 5,5'-Bpy Tryptophan with DCP	78
4.10	Association Constant of 5,5'-Bpy Tryptophan with DCP	79
4.11	Emission Spectrum of 5,5'-Bpy Tryptophan with HCl	80
4.12	Emission Spectrum of 5,5'-Bpy Tryptophan with DMMP	80
4.13	Association Constant of 5,5'-Bpy Tryptophan with DCP	81
4.14	¹ H NMR of Ru(bpy) ₂ (5,5'-Bpy Tryptophan) Complex	83
4.15	LC-MS ESI (+Ve) mode of Ru(bpy) ₂ (5,5'-Bpy Tryptophan) Complex	84
4.16	UV-Vis Spectrum of Ru(bpy) ₂ (5,5'-Bpy Tryptophan) Complex.....	84

List of Figures—Continued

4.17	Emission Spectrum of Ru(bpy) ₂ (5,5'-Bpy Tryptophan) Complex	85
4.18	Emission Spectrum of Ru(bpy) ₂ (5,5'-Bpy Tryptophan) Complex with DCP	85
4.19	Association Constant of Ru(bpy) ₂ (5,5'-Bpy Tryptophan) Complex with DCP	86
4.20	Emission Spectrum of Ru(bpy) ₂ (5,5'-Bpy Tryptophan) Complex with HCl	87
4.21	Emission Spectrum of Ru(bpy) ₂ (5,5'-Bpy Tryptophan) Complex with DMMP	87
4.22	Emission Spectrum of Zn(5,5'Bpy Tryp) ₂ Complex with DCP	89
4.23	Association Constant of Zn(5,5'Bpy Tryp) ₂ Complex with DCP	89
4.24	Emission Spectrum of Zn(5,5'Bpy Tryp) ₂ Complex with HCl	90
4.25	Association Constant of Zn(5,5'Bpy Tryp) ₂ Complex with HCl	91
4.26	Emission Spectrum of Zn(5,5'Bpy Tryp) ₂ Complex with DMMP	92
4.27	Association Constant of Zn(5,5'Bpy Tryp) ₂ Complex with DMMP	92
5.1	Emission Spectrum of Stilbene Monomer with DCP	96
5.2	Emission Spectrum of Stilbene Monomer with HCl	96
5.3	Association Constant of Stilbene Monomer with HCl	97
5.4	Emission Spectrum of Stilbene Monomer with DMMP	97
5.5	IR Spectra of Silica NPs with Stilbene Monomer	99
5.6	Emission Spectrum of Silica NPs with Stilbene Monomer	100
5.7	Emission Spectrum of Silica NPs with Stilbene Monomer with Various DCP	100

List of Figures—Continued

5.8	Association Constant of Silica NPs with Stilbene Monomer with Various DCP	101
5.9	Emission Spectrum of Silica NPs with Stilbene Monomer Vs Various HCl	101
5.10	Association Constant of Silica NPs with Stilbene Monomer Vs Various HCl	102
5.11	Emission Spectrum of Sensor I with Various DCP Concentrations	104
5.12	Association Constant of Sensor I with DCP	104
5.13	Emission Spectrum of Sensor I with HCl	105
5.14	Association Constant of Sensor I with HCl	105
5.15	Emission Spectrum of Sensor I with DMMP	106
5.16	Emission Spectrum of Sensor II with DCP	109
5.17	Association Constant of Sensor II with DCP	109
5.18	Emission Spectrum of Sensor II with HCl	110
5.19	Association Constant of Sensor II with HCl	110
5.20	Emission Spectrum of Sensor II with DMMP	111
5.21	Emission Spectrum of Sensor III with DCP	113
5.22	Association Constant of Sensor III with DCP	113
5.23	Emission Spectrum of Sensor IV with DCP	115
5.24	Emission Spectrum of Sensor V with DCP	116
5.25	Association Constant of Sensor V with DCP	117
5.26	Emission Spectrum of Sensor V with HCl	118
5.27	Association Constant of Sensor V with HCl	118

List of Figures—Continued

5.28 Emission Spectrum of Sensor V with DMMP	119
5.29 Association Constant of Sensor V with DMMP	119

LIST OF SCHEMES

3.1 Synthetic Scheme of Preparation of 2,2'-Bipyridine-4,4'-Dicarboxylic Acid.....	47
3.2 Synthetic Scheme of Preparation of cis-(bpy) ₂ RuCl ₂ .2H ₂ O	50
3.3 Synthetic Scheme of Preparation of 4,4'-Bpy Tryptophan	51
3.4 Synthetic Scheme of Preparation of Ru(bpy) ₂ (4,4'-Bpy Tryptophan) Complex.....	57
3.5 Synthetic Scheme of Preparation of 4,4'-Bipyridine Tryptophan Zinc Complex.....	68
4.1 Synthetic Scheme of Preparation of 5,5'-Bpy Tryptophan	73
4.2 Synthetic Scheme of Preparation of Ru(bpy) ₂ (5,5'-Bpy Tryptophan) Complex.....	82
4.3 Synthetic Scheme of Preparation of 5,5'-Bipyridine Tryptophan Zinc Complex.....	88
5.1 Synthesis of Silica NPs with Stilbene Monomer	99
5.2 Synthesis of Sensor I.....	103
5.3 Synthesis of Sensor II.....	108
5.4 Synthesis of Sensor III	112
5.5 Synthesis of Sensor IV	114

LIST OF ABBREVIATIONS

- CWA (Chemical Warfare Agents)
- NA (Nerve Agents)
- DFP (Diethyl Fluoro Phosphate)
- DCP (Diethyl Chloro Phosphate)
- DMMP (Dimethyl Methyl Phosphonate)
- AChE (Acetylcholine Esterase)
- ACh (Acetylcholine)
- 3-PAMC1 (Pralidoxime Chloride)
- OPH (Organophosphorus Hydrolase)
- SAW (Surface Acoustic Wave)
- PET (Photo-induced Electron Transfer)
- FLA (Fluoresceinamine)
- NMCR (Nanoparticle, Monomer, Complex and Receptor)
- FRET (Fluorescence Resonance Energy Transfer)
- TEM (Transmission Electron Microscope)
- NMR (Nuclear Magnetic Resonance)
- LC-MS (Liquid Chromatography Mass Spectrometry)
- NPs (Nanoparticles)
- TEOS (Tetraethyl Ortho Silicate)
- APTS (3-Aminopropyltriethoxysilane)

List of Abbreviations—Continued

QDs (Quantum Dots)

TNT (Trinitro toluene)

SDS (Sodium Dodecyl Sulfate)

OPV (Oligophenylene Vinylene)

LED (Light Emitting Diode)

MLCT (Metal to Ligand Charge Transfer)

CHAPTER I

INTRODUCTION

1.1 Chemical Warfare Agents (CWA)

The use of poisonous gases as weapons started centuries ago. In 431 BC, sulfur was burned on the walls of the cities of Plataea and Belium in the Athenian and Spartan Wars. British used picric acid and sulfur in the Crimean War (1854-1856) and the Boer War (1880-1881).¹ In 1915, German troops used around 6000 cylinders of chlorine gas on French troops causing 5-10000 casualties.² Italians used mustard gas against Ethiopia in 1935.¹ Japan used chemicals on China in 1937.¹ Chemicals were used in both World Wars and in Cold War.³ The Iraqi government carried out poison attacks on civilians in both Iraq and Iran in 1986 and on the Kurdish population in northern Iraq in 1988.¹ These are only a few incidents which were reported; there are many other incidents which caused casualties and deaths that went unrecorded in the chronicles of time. All these incidents have been proved to be a hindrance for world peace and have become an important international concern.

According to the Organization for the Prohibition of Chemical Weapons and the Chemical Weapons Convention, substances are considered chemical weapons if they, through a “chemical effect on living processes, may cause death, temporary loss of performance, or permanent injury to people or animals”.⁴ CWA’s were used in both

World Wars and in Cold War. Chemical Warfare Agents (CWA) are classified into several groups based on their mode of action; nerve agents, asphyxian/blood agents, vesicant agents, choking/pulmonary agents, lachrymatory agents, blistering agents, vomit agents, tear gases and cytotoxic proteins.^{3,4} Chemical Warfare Agents are usually in gaseous form, but they also exist in liquid and solid forms. A CWA is very easy to use even though it is highly toxic and lethal even at low levels. A typical CWA will not lose its activity for a long time even on reaction with heat, air and water in the atmosphere.

Table 1.1 Chemical Warfare Agents¹

Name	Code	Chemical name	Site of action
Nerve agents			
a) Tabun	GA	Ethyl-N-	AChE
b) Sarin	GB	dimethylphosphoroamidocyanidate	AChE
c) Soman	GD	Isopropylmethylphosphonofluoridate	AChE
d) VX	VX	Pinacolyl methylphosphonofluoridate O-Ethyl S-[2-(diisopropylamino)ethyl] methylphosphonothlate	AChE
Vesicants			
a) Sulfur mustard	HD	2,2'-Dichlorodiethyl sulfide	Eyes, Skin and lung
b) Nitrogen mustard	HN1	2,2'-Dichloro-N-methyldiethylamine	
c) Lewisite I	L1	Dichloro(2-chlorovinyl)arsine	eyes and lung

Table 1.1—Continued

Pulmonary agents			
a) Phosgene	CG		Lung
b) Chlorine	CL		Lung
Cyanides			
a) HCN	AC	Hydrogen cyanide	Cytochrome oxidase
b) CK	CK	Cyanogen chloride	Cytochrome oxidase

Table 1.1 shows the different types of chemical warfare agents and their site of action.

Organophosphorus compounds (nerve gases) and their structural simulants were developed as the most dangerous CWA during and after World War II.⁵ The ease of synthesis helps terrorists to use nerve gases widely as weapons. The Japanese extremist group, Aum Shinrikyo, used sarin gas in Matsumoto in June 1994, killing seven people and more than three hundred casualties. In 1995 five two-man teams of the same group used nerve gas by puncturing a dozen liquid sarin filled plastic bags with an umbrella, causing twelve deaths and thousands of injuries.⁶ The use of chemical weapons against civilians by terrorist groups is a real threat and there is a urgent need for detectors and sensors that are able to warn about CWA danger.

1.2 History and Classification of Nerve Agents

The organophosphorus cholinesterase inhibitors commonly known as nerve agents (NA), and these compounds are structurally related to highly toxic phosphoric acid esters.⁶ Organophosphorus compounds are closely related to insecticides and pesticides. The first organophosphate compounds were synthesized in 1854.⁷ The first nerve agent was developed in 1936 by German scientist Dr. Gerhard Schroeder. He made this compound for a chemical company as a pesticide,⁷ and later discovered that this compound had extremely bad effects on nervous systems and could be poisonous.

Nerve gas agents can be classified according to the following criteria:

- 1) Boiling point: volatile and non volatile.
- 2) Country of origin: Agents originally developed in Germany were designated as “G series” agents, these include GA (Tabun), GB (Sarin), GD (Soman) and GF (Cyclo sarin).⁷
- 3) Toxicity: “V series” agents, V stand for venomous and include VE, VG, VM and VX. V agents are up to 10 times more poisonous than G agents.

Figure 1.1 shows the chemical structure of G, V agents and the nerve gas simulants DFP (Diethyl Fluoro Phosphate), DCP (Diethyl Chloro Phosphate) and DMMP (Dimethyl methyl phosphonate). Nerve gas agents are very toxic, So nerve gas agent simulants which are in similar chemical structures are used in this research.

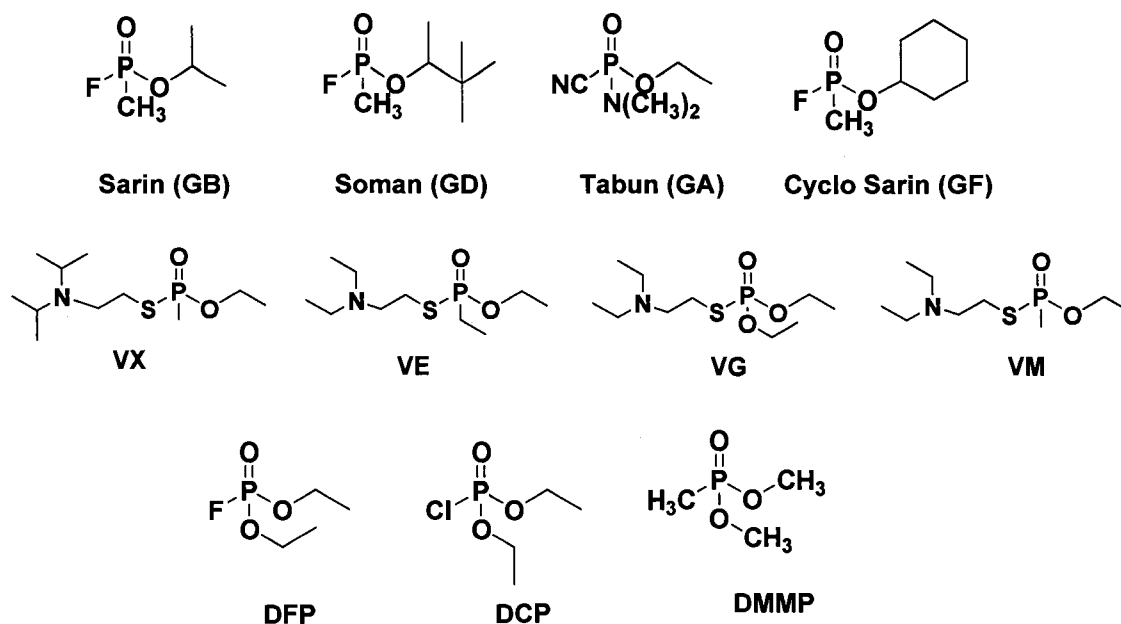


Figure 1.1 Chemical Structures of G and V Agents

1.2.1 Tabun

Tabun (Ethyl N,N-dimethylphosphoramidocyanidate), the first known nerve agent, also called GA, was discovered accidentally by German scientist Dr. Gerhard Schroeder in 1937. It is a clear, colorless liquid with a faint fruity odor. Tabun is one of the most highly toxic nerve agents with a LD₅₀ of 14-21mg/kg body weight (dermal) and 0.014mg/kg (intravenous).⁸ A small drop of Tabun can cause pinpoint pupils, dim vision, and headache. Tabun has a high persistency. Heavily splashed liquid tabun can persist one to two days depending on climate conditions. Tabun has a 5.6 times higher vapor density than air. The higher vapor density allows the agent to flow into low elevations such as trenches, bunkers and into buildings potentially causing more damage. Figure 1.2 shows the nerve agent tabun reactivity with Acetylcholine esterase (AChE) enzyme. Serine hydroxyl group of enzyme reacts with tabun and forms phosphodiester bond.



Figure 1.2 The Reactivity of Tabun with Acetylcholine Esterase Enzyme (Adapted from ref.9)

1.2.2 Sarin

Sarin [2-(fluoro-methylphosphoryl)oxypropane] is also known as GB. Sarin is colorless, odorless liquid at room temperature. Sarin is very difficult to produce. Sarin can cause sudden death upon inhalation or through skin contact. Sarin is the most volatile compound with very little persistence and evaporates as fast as water or kerosene. Sarin has 2.9 times higher vapor density than air and tends to flow downwards.

1.2.3 Soman

Soman [3-(fluoro-methyl-phosphoryl)oxy-2,2-dimethyl-butane] also known as GD, was discovered in 1944. Soman is a volatile, corrosive and colorless liquid with a faint odor when it is pure. Soman has a persistency between Sarin and Tabun; It can persist one or two days depending on climate conditions. Soman has higher toxicity to the brain compared to other nerve agents.

1.2.4 VX

VX [S-2(diisopropylamino) O-ethylmethylphosphonothioate] is the most toxic nerve agent ever made and was discovered by Ranjit Ghosh and J.F.Newman in 1951. VX is a thick, clear to straw colored liquid and gives off a colorless vapor. VX is highly persistent in the environment and may last several weeks. VX has high vapor density and its density is nine times higher than air.

Table 1.2 Physical Properties and Toxicity of Nerve Agents⁷

	Vapor pressure mm Hg at 20°C	Volatility Mg/m ³ at 25°C	Odor	Solubility	LD ₅₀ gm/person	LC ₅₀ MgXmin/m ³
Tabun(GA)	.037	576-610	Fruity	9.8g/100g at 25°C	1	100-400
Sarin(GB)	2.1	16400-22000	Odorless	Miscible	1.7	50-100
Soman(GD)	0.40	3060-3900	Fruity	2.1g/100g at 20°C	0.35	25-70
Cyclosarin(GF)	0.07	59 ppm	Odorless	3.7g/100g at 25°C	unknown	unknown
VX	0.0007	3-30	Odorless	Miscible at <9.4°C slight at 25°C	0.01	5-50

Table 1.2 shows the physical properties and toxicity of nerve gas agents.

1.3 Mechanism of Action of Nerve Agents on Human Beings

Acetylcholine (ACh) is a central neurotransmitter and hydrolysis of ACh is the vital mode of regulation of the neural response system.¹⁰ The enzyme AChE hydrolyzes approximately 10,000 ACh molecules per second into inactive products like acetic acid and choline,⁶ and also maintains the concentration of neurotransmitter ACh within the synaptic cleft of the nervous system. Organophosphate nerve agents inhibit the activity of AChE. The phosphorus atom of the nerve agent covalently binds to the serine hydroxyl group in the catalytic site (esteratic site) of acetylcholine esterase and forms a phosphate ester bond. This bonding blocks the enzyme from interaction with its normal substrate ACh and causes accumulation of ACh rather than the normal breakdown. If nerve agents are not removed from AChE (by treating with Oxime) within a short time after exposure, AChE will undergo an aging process where AChE becomes resistant to hydrolysis and is considered as irreversibly bound to the nerve agents. The inhibition of AChE by nerve gases leads to the headache, nausea, vomiting, diarrhea, bradycardia, respiratory failure and sometimes paralysis and death depending on the dose. The interaction and mechanism of the nerve agent with the enzyme can be seen below in Figures 1.3 and 1.4.

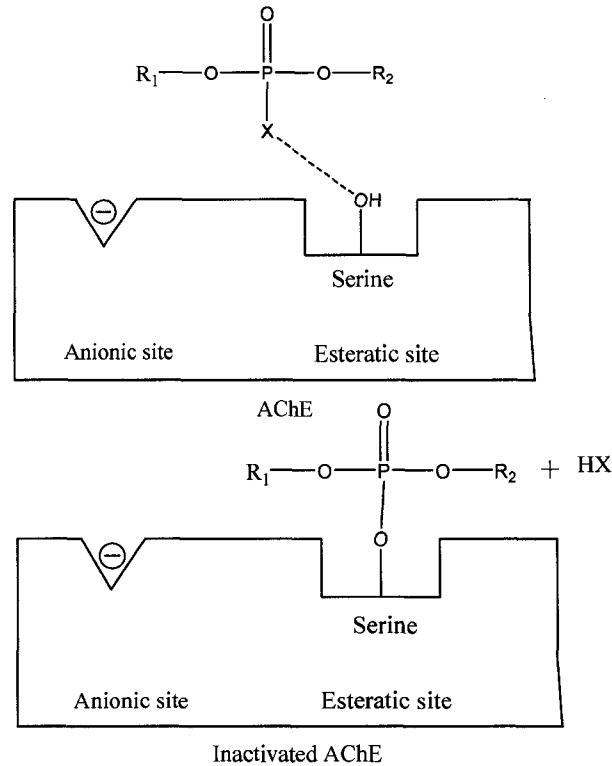


Figure 1.3 Interaction of a Nerve Agent with AChE (Adapted from ref.7)

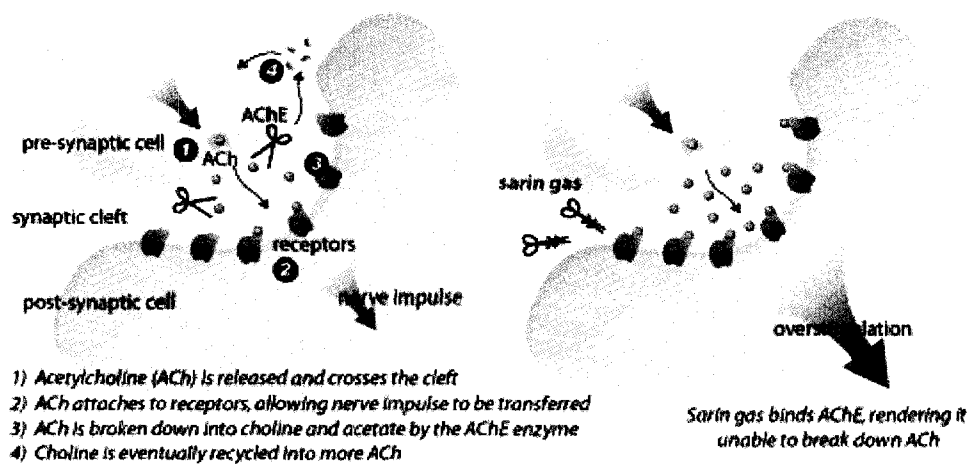


Figure 1.4 Mechanism of Sarin Toxicity (Taken from ref.11)

1.4. Treatment for Nerve Agent Exposure

Nerve agent poisoning occurs due to the inhibition of Acetylcholine esterase enzyme. Nerve agent treatment basically involves reactivation of the enzyme. When a person is exposed to a nerve agent, the primary step is to take off the clothes and accessories of victim and wash with plenty of water, diluted (0.5%) bleach, and with soap and water depending on the exposure.

Four drugs: atropine, pralidoxime chloride (3-PAMC1), diazepam, and tropicamide have been used as antidotes for the nerve agent poisoning.¹² Treatment of nerve agents relies on two approaches. First, competitive antagonist, like atropine, will bind at the acetylcholine receptors there by blocking any binding by nerve agent, so that the acetylcholine present within the synapse cannot work. Second, an oxime (pralidoxime chloride) detaches the nerve agent from cholinesterase, thus reactivating the enzyme (as shown in Figure 1.5). Diazepam is used to treat seizures associated with nerve agent exposure, and tropicamide is used to reverse meiosis and relieve ocular pain caused by nerve agent toxicity.

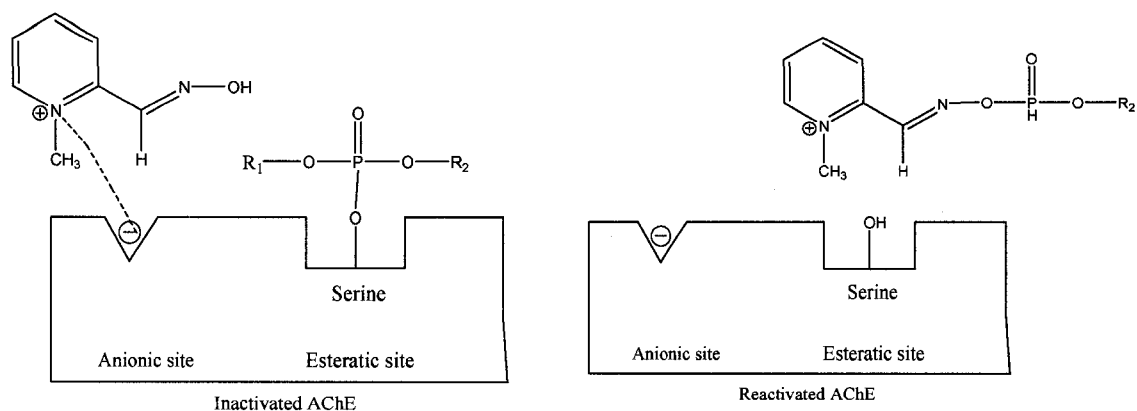


Figure 1.5 Mechanism of Action of Pralidoxime (2-PAM) on AChE (Adapted from ref.7)

1.5 Detection Techniques of Nerve Agents

The development towards the detection of nerve agents is very important because of their high toxicity and use as chemical weapons for terrorists or war actions. A lot of research is being devoted towards the development of new and improved methods for the detection of highly toxic nerve agents. There are several types of detection methods for nerve agents based on different techniques, including surface acoustic wave detectors,¹³⁻¹⁵ enzymatic assays,¹⁶⁻¹⁹ mass spectrometry, interferometry²⁰ and colorimetric detectors.^{21, 22}

Colorimetric detection methods were used to detect organophosphorus ester pesticides or nerve agent compounds in water. In this technique cholinesterase (horse serum cholinesterase or eel cholinesterase) impregnated paper was used as a source of detection with the help of a chromogenic substrate (2,6-dichloroindo phenyl acetate). If

organophosphorus compounds are present in the water they will inhibit acetylcholine esterase and won't show any color changes with the substrate.²¹ If organophosphorus compounds are absent in the water, the enzyme is active and will react with the substrate giving a blue color as shown in Figure 1.6.

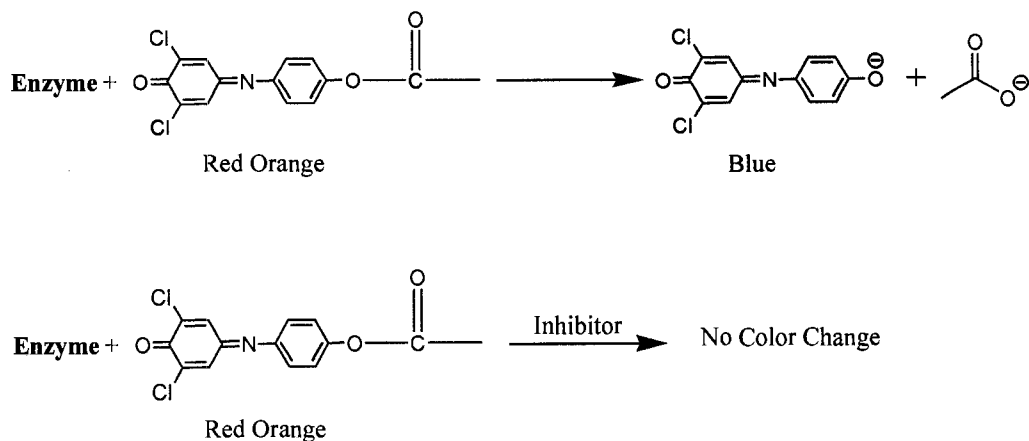


Figure 1.6 Colorimetric Detection of Acetylcholinesterase Inhibitors (Adapted from ref.21)

Enzymatic assays are also used for the detection of nerve agents; In this technique organophosphorus hydrolase (OPH) is used as an enzyme because of its unique ability to hydrolyze organophosphorus compounds and nerve agents. OPH selectively catalyzes a hydrolytic reaction at the P-O, P-S, P-F or P-CN bonds in neurotoxins. These hydrolyzed products are detected with various devices such as pH meter,¹⁶ emission,¹⁷ gas chromatography and flame-photometric detectors.¹⁹ Enzymatic assays are very sensitive because contaminations in the sample will destroy the enzymatic activity and slow response time. The hydrolysis of organophosphorus pesticides with OPH is shown in Figure 1.7.

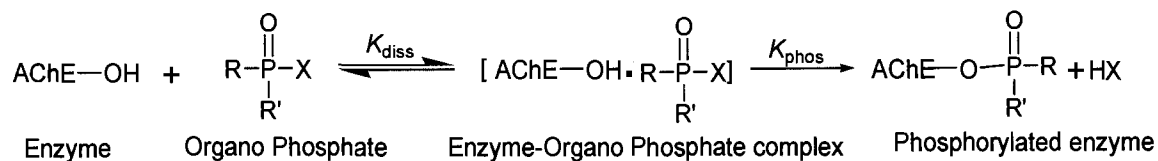


Figure 1.7 Nerve Agent Detection by Using Organophosphorus Hydrolase Enzyme (Adapted from ref.19)

Hai-Feng Ji et al used a microcantilever technique to detect nerve agents. In this technique they used a self-assembled bilayer of Cu^{2+} /L-Cysteine on a gold surface as a microcantilever. This Cu^{2+} /L-Cysteine bilayer recognizes the phosphoryl group due to the formation of strong $\text{P}=\text{O}-\text{Cu}^{2+}$ bonds. Nerve agents are absorbed onto the gold surface and cause bending of the microcantilever. Figure 1.8. shows the bending of self assembled Cu^{2+} /L-Cysteine bilayer coated microcantilever with DMMP.

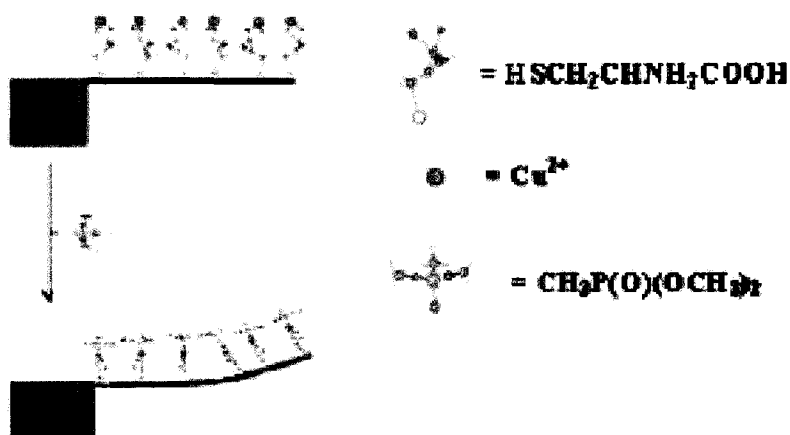


Figure 1.8 Bending of Self Assembled Cu^{2+} /L-Cysteine Bilayer Coated Microcantilever with DMMP (Taken from ref.23)

Surface acoustic wave (SAW) detectors are also used in the detection of nerve agents. Hydrogen bond acidic hyperbranched polymers (Fig 1.9) interact with hydrogen bond basic nerve agents to produce a response. SAW detection involves the change in frequency of the sensor after exposure to a nerve agent as a function of both modulus and mass. Polymers coated on SAW sensors interact with nerve agents and cause a change in mass that results in a change in the frequency of the sensor.¹³

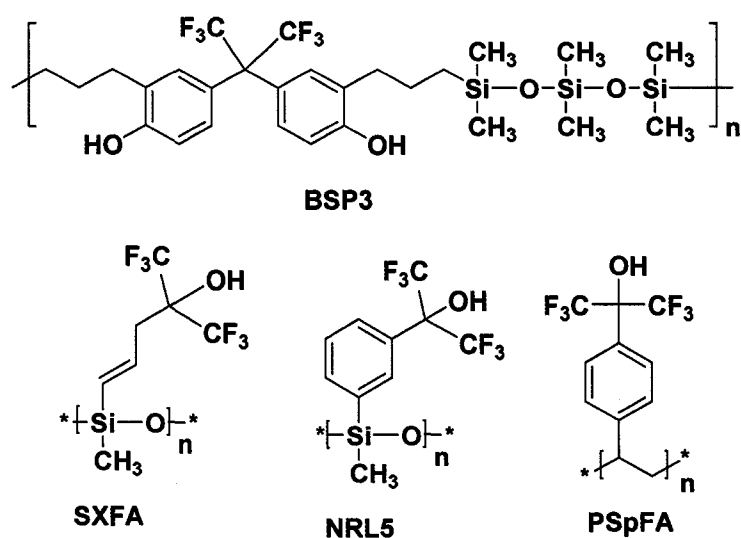


Figure 1.9 Hydrogen-Bond Acidic Linear Polymers Used in SAW Sensors (Adapted from ref.13)

All the above detection methods have limitations such as weak response, limited selectivity, false positives, low sensitivity, cost, and real-time recognition. Optical or chemosensors are simple and inexpensive and overcome all the above mentioned limitations, sometimes detection can even be performed with the naked eye. Fluorescent sensors are designed to undergo change in the absorptive or emissive behavior in

presence of target analytes. There are many different analytical techniques developed based on changes in the fluorescence properties of a molecule in different environments; These fluorescence changes include quenching, Forster resonance energy transfer, photo-induced electron transfer (PET) (Figure 1.10) and surface modified fluorescence.

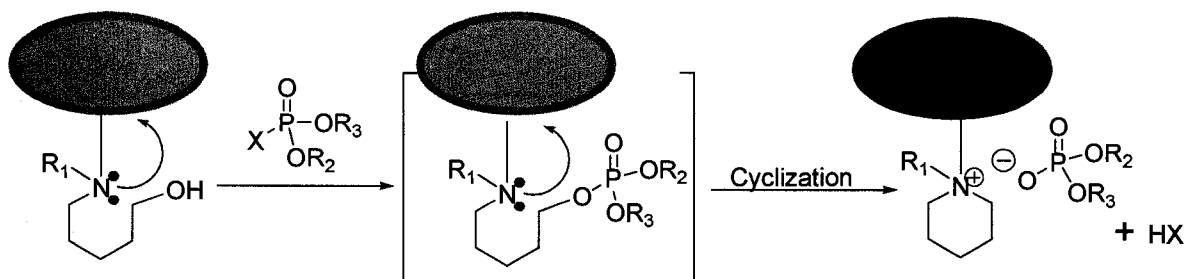


Figure 1.10 General Scheme of PET Indicator Molecules for the Detection of Nerve Agents (Adapted from ref.3)

Recently the use of fluorescence sensors towards the detection of nerve agents gained attention because of their ease of operation and high response rate. Detection of nerve agents by using chromo-fluorogenic sensors first described by Schonemann in 1944, was based on the oxidation of amines in the presence of organophosphorus compounds. The mechanism of action is based in the formation of a peracid from the organophosphorus compound which is then involved in the oxidation of an amine to give a color change. In 1957, Bernard Gehauf *et al* proved that the mixture of indole and sodium perborate(1:2) in water-acetone(1:1v/v) will change pale yellow to green in the presence of nerve agent due to the oxidation of indole to indoxyl.

Swager *et al* have developed a fluorescent based sensor for the detection of nerve agents.²⁷ Nerve agents react with hydroxyl group of AChE enzyme and form the

(pyrene) was attached to the amine with a spacer (methylene) and then exposed to nerve agents. Reaction with the nerve agents causes quenching of the fluorophore near the amine via PET resulting in increase in the emission.²⁸

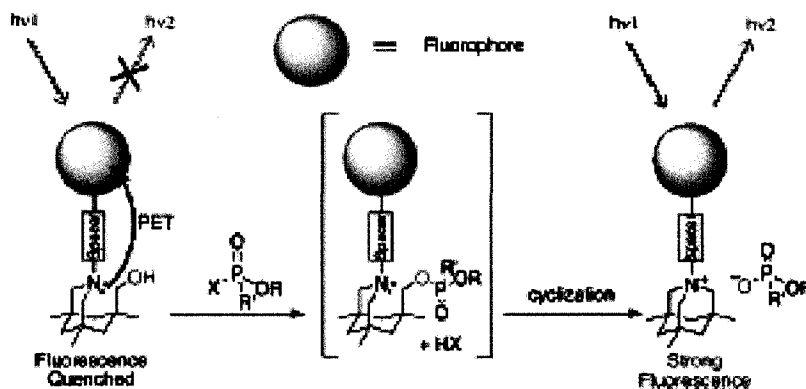


Figure 1.12 Fluorescent (PET) Sensor for Nerve Gas by Julius Rebek (Taken from ref. 28)

Walt *et al.* developed a fluorescent sensor based on microbeads. They coated microbeads with fluoresceinamine (FLA) dye and poly (2-vinylpyridine) and then reacted the beads with the nerve agent stimulant, DCP. FLA's amine group quantum yield increases upon reaction with the phosphoryl group of nerve agents (Figure 1.13).

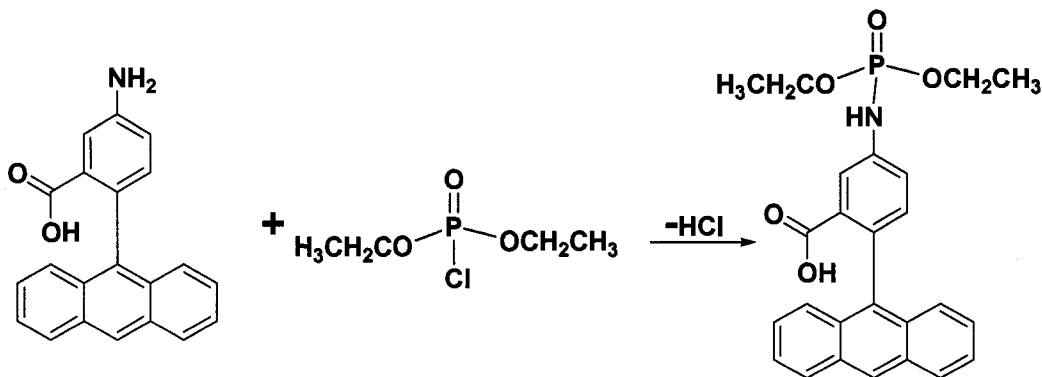


Figure 1.13 Fluorescent Sensor for Nerve Gas Sensing by Walt (Adapted from ref. 29)

1.6 Central Hypothesis

The central hypothesis of this research is to develop nanosensors to detect the nerve agents based on a bottom-up approach. The bottom up approach will provide systematic layer by layer assembly of molecular moieties (Figure 1.14) (nanoparticle, monomer, complex and receptor) which show high selectivity and sensitivity towards nerve agent simulants. The advantage of this bottom-up approach is that the building blocks of nanosensors can be selected based upon differing target analytes such as nerve agents, explosives, biotoxins, viruses etc, resulting in highly ordered nanostructures.

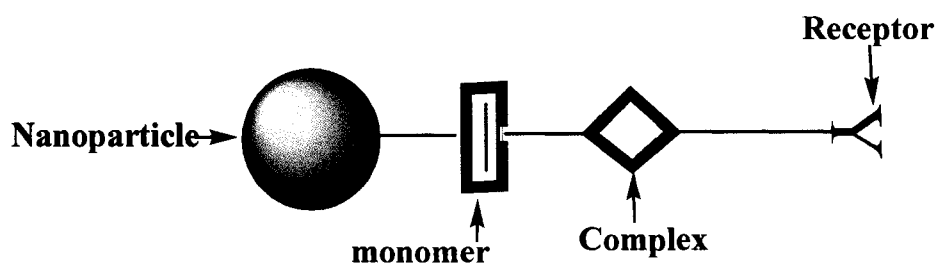


Figure 1.14 NMCR Assembly of Proposed Nanosensor to Detect Nerve Agents (Adapted from ref. 30)

In the NMCR (nanoparticle, monomer, complex and receptor) assembly a highly conjugated aromatic compound with a free nitrogen atom interacts with the phosphoryl group of a nerve agent thus acting as a receptor in the nanosensor. After the interaction, this receptor will form an adduct which shows an emission change and can be used as a fluorescence sensor. These receptor molecules are attached to metal complexes (nanomolecules) of ruthenium, europium or zinc complexes to show a visible change in the fluorescence. The main purpose of ruthenium complexes is for fluorescence resonance energy transfer (FRET). Here, the strength of the interaction of receptor

moieties with target molecules is increased considerably when the receptor is also attached to another moiety which does not have significant interaction. These nanomolecules are attached to conjugated aromatic compounds such as stilbene analogs (monomer) to increase the signal intensity. The monomers are then attached to either silica nanoparticles or quantum dots (nanoparticles) to produce a highly ordered nanosensor assembly. The nanoparticles give uniform assembly and more surface area for reaction with nerve agents. Hence, the sensor based on NMCR concept provides high selectivity and sensitivity towards nerve agents.

1.7 Objectives of the Present Study

Figure 1.15 gives the complete information of the nanosensors synthesized and characterized using NMR, LCMS, and elemental analysis. 4, 4'-Bipyridine tryptophan and 5, 5'-Bipyridine tryptophan ligands were synthesized, characterized and used as receptors in the NMCR sensors. Ruthenium, zinc and europium metal complexes of these ligands were synthesized, characterized and used as Complexes. Silica nanoparticles and ZnS:Mn/ZnS quantum dots are used as nanoparticles. Highly conjugated aromatic stilbene type compounds are used as monomers. Nerve agents are very toxic, so we used nerve agent analogs such as DCP and DMMP to detect nerve agents.

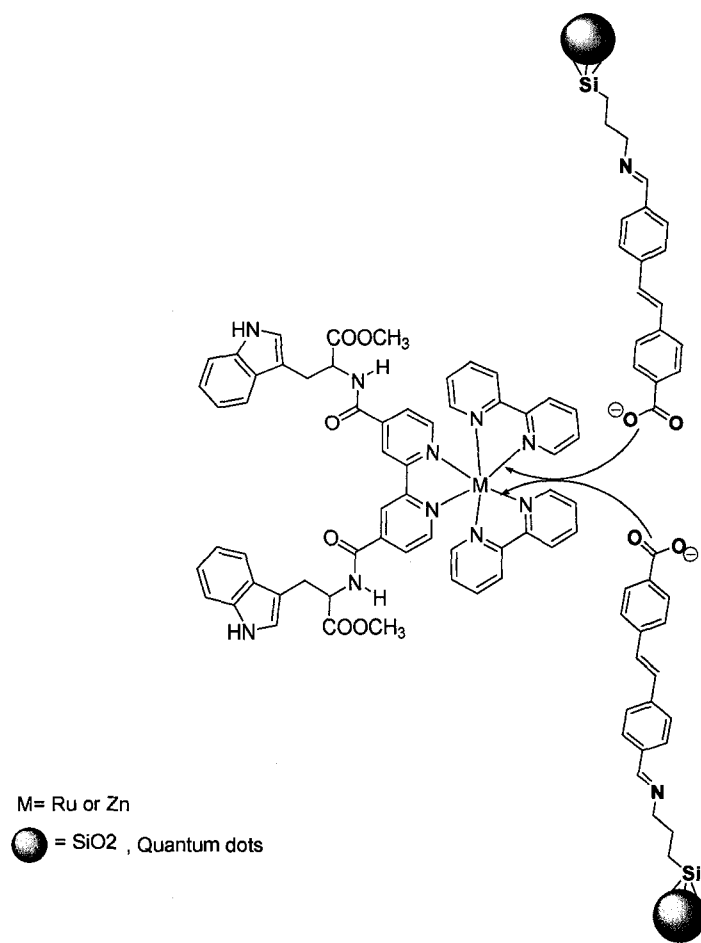


Figure 1.15 NMCR Sensor Designed in this Work

1.8 Association Constant Calculation Methods

The interaction of compounds (nanosensors) with the target analytes (DCP, DMMP, or HCl) was quantitated by using association constant. Association constant describes the bonding affinity between two molecules at equilibrium. There are several approaches for calculating the association constant, like C/I method, Stern-Volmer method and Benesi-Hildebrand method.

1.8.1 Stern-Volmer Equation³¹

Stern-Volmer equation is better used in the photophysical intermolecular deactivation processes such as fluorescence quenching process. There are two types of quenching phenomena, dynamic and static.

a) Dynamic Quenching

$$I_0/I = 1 + K_D [Q]$$

I_0 = Fluorescence intensity of the receptor in the absence of the target analyte

I = Fluorescence Intensity of the receptor in the presence of the target analyte

K_D = Quenching Constant

Q = Quencher concentration

b) Static Quenching

$$I_0/I = 1 + K_{SV} [Q]$$

I_0 = Fluorescence intensity of the receptor in the absence of the target analyte

I = Fluorescence Intensity of the receptor in the presence of the target analyte

K_{SV} = Association Constant [product of the true quenching constant K_q and the excited state life time (τ^0)]

Q = Quencher concentration

Both dynamic and static quenching processes give a linear Stern-Volmer plots, if there is any deviation from the plot and if it is not linear, a modified Stern-Volmer equation is used.

c) Modified Stern-Volmer Method

Modified Stern-Volmer equation is used to determine both K_D and K_{SV} .

$$[I_0/I-1] / [T] = (K_D + K_{SV}) + K_D K_{SV} [T]$$

K_D = Dynamic association constant

K_{SV} = Static association constant

1.8.2 Benesi-Hildebrand Equation³²

A Benesi-Hildebrand equation is used to calculate the donor-acceptor interactions in fluorescence and absorbance studies.

$$(I_0 / I - I_0) = (a / b - a) (1 / K_B [\text{substrate}] + 1)$$

I_0 and I are fluorescence intensity of the sensor molecule in the absence and presence of the incoming target molecule respectively. K_B is the binding constant while a

and b are constants. $(I_0 / I - I_0)$ was plotted as a function of incoming target molecule and the binding constant was calculated from the ratio between the y-intercept and the slope.

I used Benesi-Hildebrand equation to calculate association constants of synthesized compounds and sensor with DCP, HCl and DMMP.

1.9 Instrumentation

All synthesized compounds were characterized by ^1H NMR, ^{13}C NMR, FT-IR, LC/MS, UV-Vis, emission, and fluorescence spectroscopy. Silica Nanoparticles were characterized by transmission electron microscopy (TEM). Absorbance, emission and fluorescence data of all compounds were taken in acetonitrile, unless mentioned. Most of the compounds are excited at 290 nm to get the emission spectra.

All compounds were characterized by using below mentioned instruments.

1. Emission and Excitation: Fluorescence data collected in this thesis is performed on Edinburgh fluorescence spectrophotometer.
2. Nuclear Magnetic Resonance (NMR): NMR studies are performed by using JEOL eclipse (400 MHz) instrument.
3. Liquid chromatography-Mass spectrometry (LC-MS): LC-MS studies were performed on Shimadzu 2010EV Mass Spectrometer by using both, Atmospheric Pressure Chemical Ionization (APCI) and Electro Spray Ionization (ESI)

techniques with UV detector. FAB mass results were performed at Michigan State University.

4. UV-Vis spectra: UV-Vis absorption spectra were performed either on Perkin Elmer UV/Vis Lambda20 Spectrophotometer or on Shimadzu UV-2101 PC UV-Vis scanning spectrophotometer.
5. FT-IR spectra: FT-IR spectra were taken on Broker Equinox 55 FT-IR spectrometer.
6. TEM: Silica nanoparticles were characterized by JEOL JEM-1230 transmission electron microscope.

CHAPTER II

BUILDING BLOCKS OF NANOSENSORS

2.1 Introduction to Silica Nanoparticles

Nanoparticles are very useful in the electronics, optics, engineering, chemical, biotechnology and biomedical industries. The study of nanostructured organic-inorganic hybrid materials with variable properties and well defined multidimensional architectures has become very active area of research. One of the most important aspects in the nanotechnology field is the preparation and development of nanomaterials, such as nanoparticles (NPs).³³⁻³⁴ Nanoparticles can be made with different materials and with different sizes as small as 1 nm. The size of the nanoparticles is very important in making sensors or any nanotechnology applications because the quality of these applications is highly dependent on the size and size distribution of nanoparticles. For instance, the size of the silica nanoparticles depends on five factors:³⁵

- a) Concentration of TEOS(Tetra Ethyl Ortho Silicate): The size of silica nanoparticles increases with increasing TEOS concentration.
- b) Concentrations of ammonia and volume of water: Ammonium hydroxide acts as a catalyst; Increasing the ammonia concentration increases the rate of hydrolysis and condensation of TEOS resulting in bigger particles. Increasing water volume gives smaller sized silica nanoparticles.³⁶

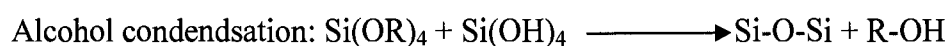
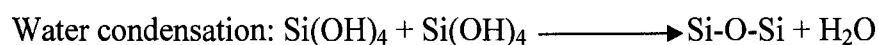
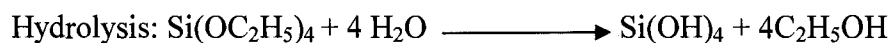
- c) Size of the alcohol: Alcohol plays a vital role in controlling the size and monodispersity of nanoparticles. Both the size and concentration of alcohol is very important. Particle size increases with increasing chain length of alcohol or increasing concentration of alcohol.
- d) Reaction temperature: Increasing temperature results in smaller nanoparticles³⁷

Monodispersed, monolayer forming nanoparticles are very important in building of portable nanosensors. Monodispersed silica nanoparticles occupy a very important position in the nanotechnology field because of its broad range of applications and ease of synthesis.³⁸ Silica nanoparticles have several advantages because of its large hydrodynamic radius, large surface area, photochemical inertness and transparency to light. Silica nanoparticles can also be derivatized with different functional groups such as amino, carboxylic and cyano groups.³⁹

2.2 Synthesis of Silica Nanoparticles

Spherical silica nanoparticles are generally made by one of two chemical approaches: reverse micro emulsion or sol-gel synthesis. In the reverse micro emulsion technique monodisperse spherical colloids are created by the controlled aqueous environment within surfactant confined micelles in a nonpolar solvent.⁴⁰ In the late 1960s, Stober and coworkers developed a mild synthetic protocol for growing monodispersed spherical silica nanoparticles based on the sol-gel chemistry of silicon alkoxides. Stober's method involves the hydrolysis and condensation of tetraethoxysilicate

in an ethanol solution in the presence of water. Ammonia serves as a catalyst to create monodisperse, spherical, electrostatically stabilized particles.⁴¹ In Stober method, hydrolysis and condensation of silicon alkoxides takes place and produce silica nanoparticles.



2.3 Synthesis of Silica Nanoparticles by Stober Method

100 mL of ethanol was taken into a 250 mL clean round bottom flask and 4.5mL of TEOS, 4.5mL of Ammonia (25 wt %) and 3mL of deionized water were introduced and stirred at 40° C for 3hrs. Addition of another 2.5mL TEOS was introduced into the system and stirred again for 3 more hours. The system was diluted with 1.5L of deionized water. At the end of the reaction, a turbid solution of silica nanoparticles was observed. Ethanol, water and excess ammonia were removed by rotary evaporation. Silica nanoparticles were characterized using Transmission Electron Microscopy (TEM) (Figure 2.1) and Infrared (IR) spectroscopy.

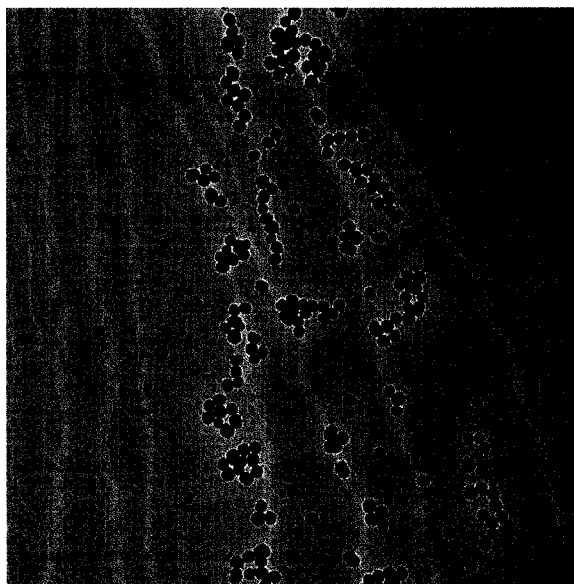


Figure 2.1 TEM Image of Silica Nanoparticles

2.4 Silanization of Silica Nanoparticles

Silanization of silica nanoparticles were done by using 3-aminopropyltriethoxysilane (APTS). Silanization of Si-NP can be done via two methods namely, a one pot method and a two pot method.⁴² In the one pot method, APTS is added after the addition of TEOS and the reaction is continued for 10 hours. In this method formation of silica nanoparticles and silanization takes place at same time. Obtained silanized silica nanoparticles were washed several times with hot ethanol to get rid of any unbound APTS and then collected by centrifugation. In the two pot method, first silica nanoparticles were synthesized by the Stober's method and dried. To these synthesized nanoparticles, APTS was added and the reaction was stirred for ten hours to obtain maximum surface coverage. I used the two pot method to silanize silica nanoparticles.

300 mg of silica nanoparticles were dispersed in 25 mL of absolute ethanol then 1 mL of APTS was added and stirred at room temperature overnight. The silica nanoparticles were then centrifuged and washed with hot ethanol to remove excess APTS and ammonia. Silanized silica nanoparticles were characterized by using TEM and IR spectroscopy.

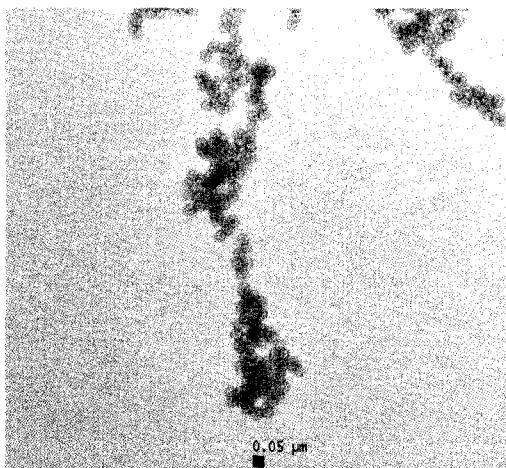


Figure 2.2 TEM Image of Silinized Silica Nanoparticles

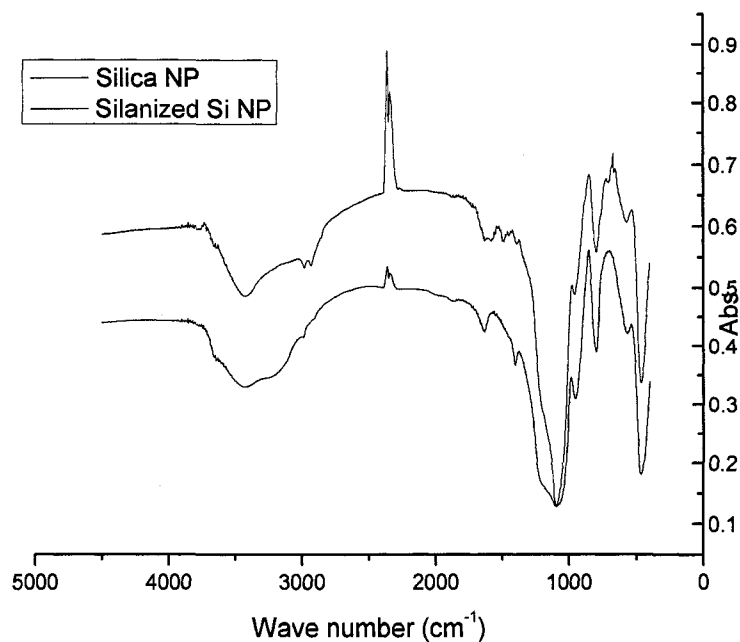


Figure 2.3 IR Spectra of Silica NPs and Silanized Silica NPs

2.5 Results and Discussion

TEM image (Figure 2.1) shows that the size of the silica nanoparticles were 45 to 50 nm and monodispersed. IR spectroscopy (Figure 2.3) shows the silanization of silica nanoparticles. The peak (two spikes) around 3000 cm^{-1} shows the presence of a primary amine in silanized silica NPs. Ethanol was used in the silanization of the nanoparticles, because ethanol forms H-bonds with Si-O^- and this solvent surface interaction creates a strong solvent layer around the nanoparticles, preventing the non specific adsorption on nanoparticles. Polar solvents such as ethanol and THF accelerate hydrolysis when compared to nonpolar solvents such as hexane and toluene. APTS hydrolyzes and polymerizes very fast in water but in ethanol, APTS polymerization is very slow.⁴³

2.6 Introduction to Quantum Dots

Quantum dots (QDs) are colloidal nanocrystalline semiconductor particles which have all three dimensions confined to the 1-10 nm length scale.⁴⁴ QDs are also called zero dimensional materials or semiconductor nanoparticles. QDs are made from group II-IV, III-V, or IV-VI materials.⁴⁵ QDs behave differently from bulk solids due to the quantum confinement effects which are caused by very small (1-10nm) sizes. Semiconductors have two energy levels, a fully occupied valance band and an unoccupied conduction band. Electronic excitation occurs when an electron moves from valance band to conduction band. Because of this movement, a hole (an empty level) is created in the valance band. The electron and hole are bound to each other by coulombic attraction, and the new particle is called as an exciton.⁴⁶ QDs are smaller in size when compare to the size of the exciton diameter and considered a good example of the particle in a box. The energies of the particle in the box depend on the size of the box. Therefore QDs are characterized by a band-gap energy between the valance and conduction bands which depends on the size of the quantum dot.⁴⁷ The band-gap of quantum dots increases as their size decreases and produces shorter emission wavelengths (Figure 2.4). The emission and the absorption of QDs depends on the energy and density of the electron states and can be altered by tuning QD particle sizes.

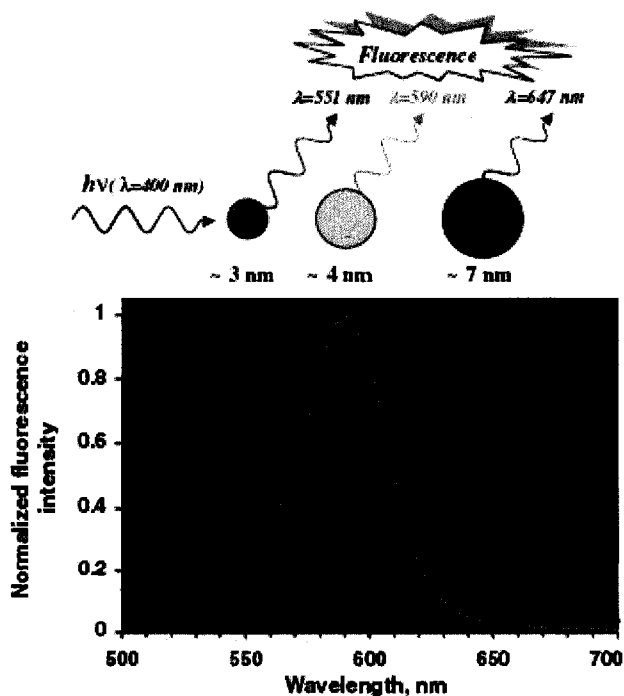


Figure 2.4 Size Tunable Fluorescence Spectra of CdSe Qds (Taken from ref. 49)

QDs are considered better than conventional organic fluorophores because of higher fluorescence quantum yields, narrow spectral line widths and better photoluminescence stability.⁴⁸ QDs are 100 times more stable and brighter than organic fluorophores against photobleaching. QDs can be excited over a wider range of wavelengths. The luminescence lifetime and two-photon absorption cross-section of QDs are greater than organic fluorophores.⁴⁹

QDs have so many advantages but are limited by their solubility in aqueous solutions. Modification of QDs makes them more water soluble. Surface modifications can be done several ways (Figure 2.5), however most of the time, surface modifications are done by amphiphilic molecules containing a thiol group strongly coordinated to the

QD surface and a polar group (-OH, -NH₂, and -COOH). Modifications can also give high quantum efficiencies and prevent QDs from aggregation.⁵⁰

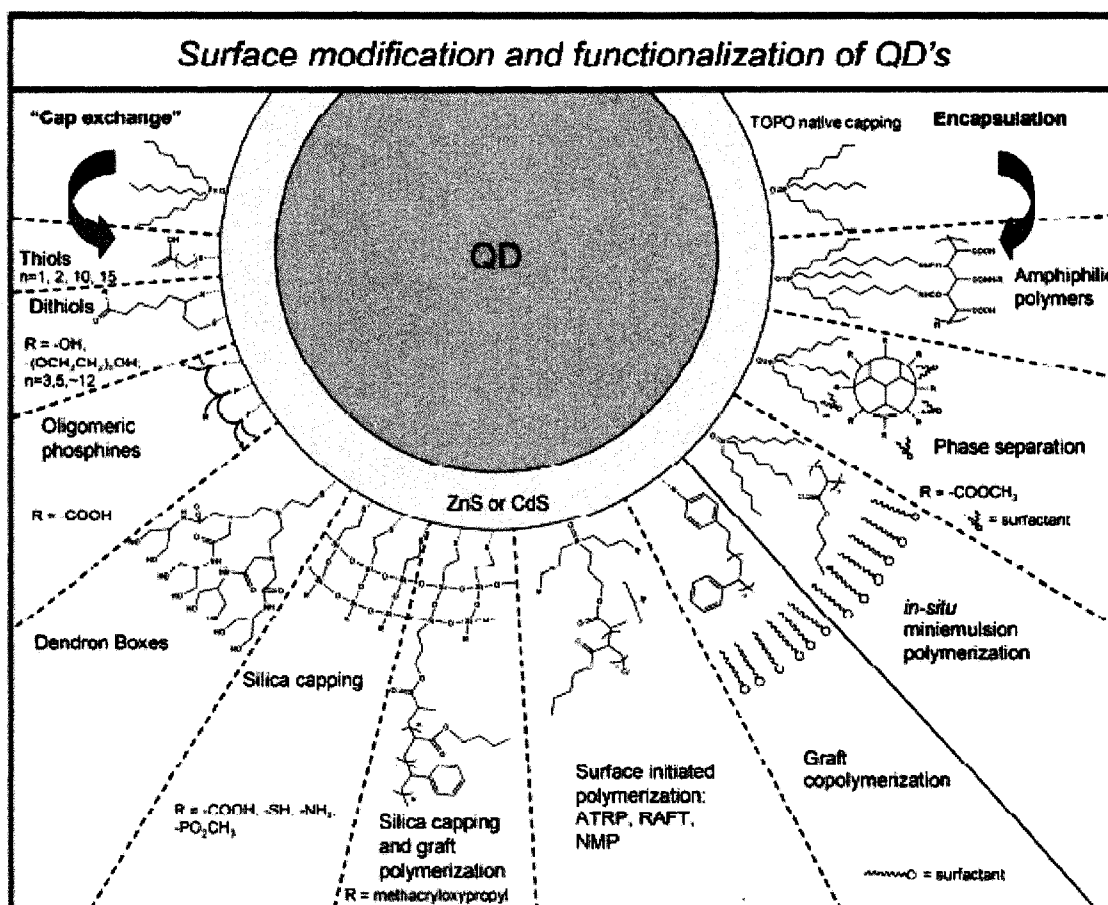


Figure 2.5 Chemical Modification Methods of QDs (Taken from ref. 49)

The emissive behavior of QDs strongly depends on surface structure. Interaction between an analyte and the surface of QDs change their physical properties. Thus QDs are very useful in sensing technologies. QDs can be used to detect small molecules, inorganic anions,⁵¹ and explosives such as trinitro toluene (TNT).⁵² They can also be used in fluorescence based immunoassays,⁵³ bioimaging applications,⁵⁴

monitoring DNA hybridization,⁵⁵ glucose sensing,⁵⁶ and checking protein-ligand complementarities.⁵⁷

2.7 Synthesis of ZnS: Mn/ZnS Quantum Dots

QDs are used as sensors in so many fields because of their narrow spectral line widths, high emission quantum yields and size-tunable emission profiles. We used QDs with a zinc sulfide core surrounded by a layer of manganese doped zinc sulfide as our sensor. These QDs were synthesized by literature procedures⁵⁸ and optimized by my colleague, Elizabeth Sadt. I used the same procedure for the synthesis of my QDs.

Preparation of Zn(DS)₂ 11.22g of Sodium dodecyl sulfate (SDS) was added to 400mL of ethanol. This mixture was heated to about 70 °C (or until steaming a little bit, there will still be a bit of SDS that is not dissolved). 5.28g of zinc acetate was added separately to a 70mL:10mL methanol/water mixture and stirred on a hot plate. When the zinc acetate dissolved, the mixture was added to the SDS mixture (volume of the two mixed species should give around 300mL of total solution). The solution was refluxed until only around 100 mL was left in the beaker. Once removed from heat, the beaker was placed in an ice bath until crystals are completely formed. Crystals were filtered off and washed with ethanol. The solids were dried overnight in a vacuum dessicator over anhydrous CaCl₂. This Zn(DS)₂ salt was used in the preparation of QDs.

Synthesis of ZnS: Mn/ZnS (1/16th) QDs. 0.015g of MnSO₄ were dissolved into 1000mL of milli-Q water and used as the doping solution. 0.039g of Na₂S were added into 100mL of milli-Q water and stirred for 15 minutes. Then, 0.5mL of doping solution was added to the above solution followed by the addition of 0.2975g of Zn(DS)₂. This solution was then stirred for 30 more minutes. After 30 minutes, the QD solution was cooled to -20 °C for 24 hours.

2.8 UV-Vis Spectra of ZnS:Mn/ZnS (1/16th) QDs

The above synthesized QDs were characterized by UV-Vis, Excitation and Emission Spectroscopy.

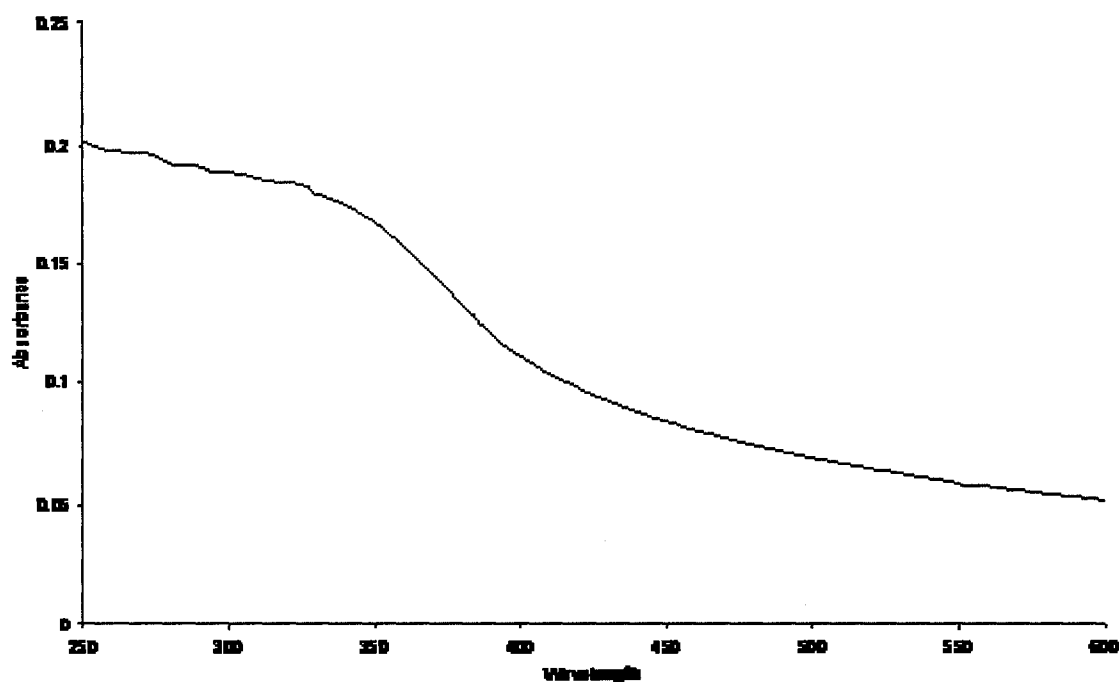


Figure 2.6 UV-Vis Spectrum of ZnS:Mn/ZnS (1/16th) QDs in Acetonitrile

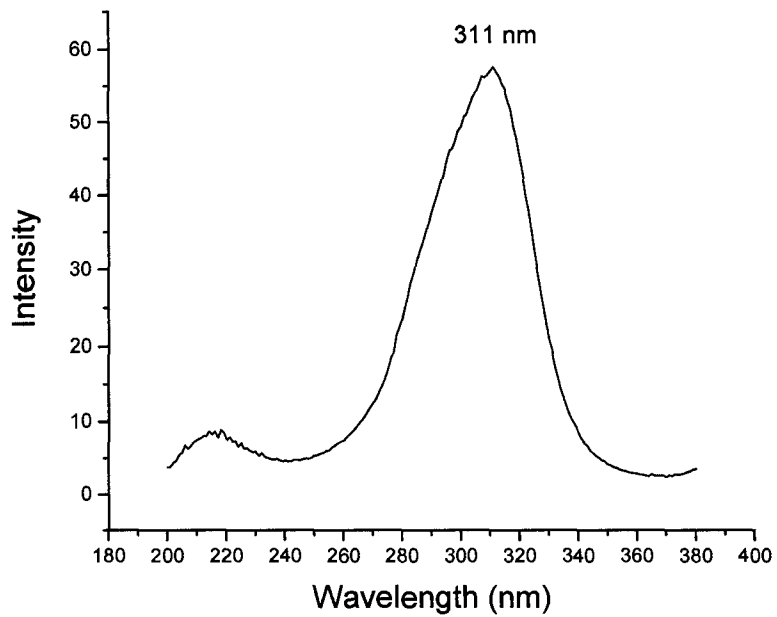


Figure 2.7 Excitation Spectrum of ZnS:Mn/ZnS (1/16th) QDs in Acetonitrile

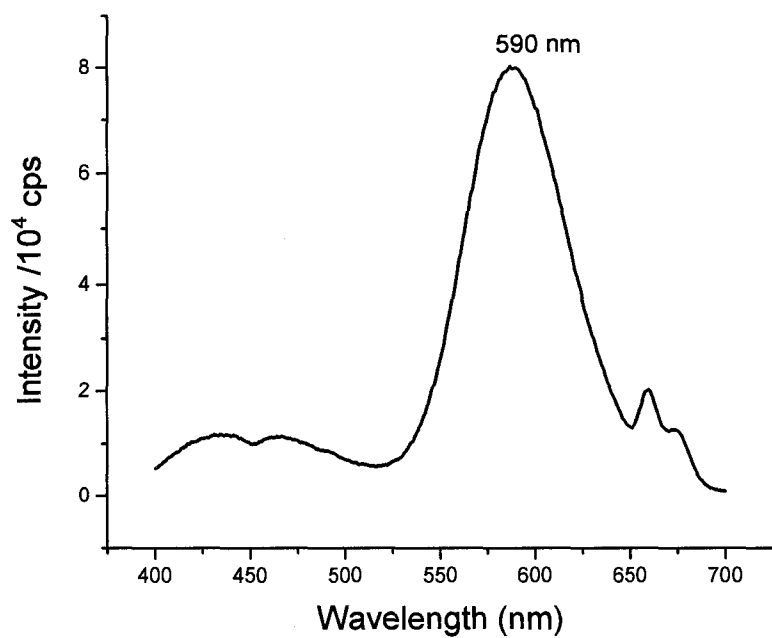


Figure 2.8 Emission Spectrum of ZnS:Mn/ZnS (1/16th) QDs in Acetonitrile

QDs were excited at 310 nm to get an emission spectra, this emission is very sharp and symmetric at 590 nm (Figure 2.8), which is due to the orange luminescence originating from Mn^{+2} .

2.9 Introduction to Stilbene Compound

The word “stilbene” was derived from the Greek word stilbos, which means shining. There are several types of stilbene compounds available with different sizes and different functional groups. Stilbene is a diphenylethene compound (Figure 2.9) where the double bond is substituted with phenyl group on both carbons. Stilbene type compounds are used in chemical sensors and are becoming a very active area of research because these highly conjugated systems have high fluorescence yields and high electroluminescence efficiency.⁵⁹

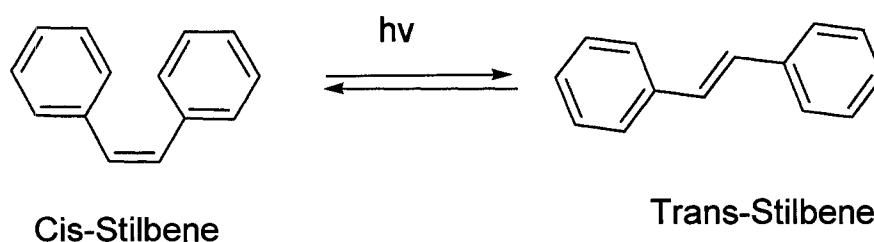


Figure 2.9 Schematic Diagram of Stilbene Conversion

Stilbene type compounds are also called Π -conjugated oligomers or oligophenylene vinylene (OPV) compounds. In OPVs, photoinduced electron transfer

happens between an electroactive donor and an acceptor.⁶⁰ OPVs have excellent charge transport properties, high stability, high luminescence efficiency and long lifetimes.^{61,62}

OPVs can convert nonspecific interactions into observable responses. Because of the above reasons OPVs are used in many fields, such as light emitting diodes (LEDs),^{59,63} field-effect transistors,⁶⁴ photovoltaic diodes,⁶⁵ and in chemical sensors.⁶⁶ Stilbene analog compounds were used in NMCR sensor assembly to amplify the signal intensity.

2.10 Synthesis of Stilbene Monomer

Synthesis of stilbene type compounds were prepared and optimized by my colleague Chun Wang (Wendy). I used her procedure to synthesis stilbene compounds. On stilbene I have attached aldehyde group on one end and acid group at the other end (Figure 2.10). Aldehyde group helps in attaching to the amino group of silica nanoparticle, and the acid group is helpful in binding to the ruthenium complex. There are several types of reactions available for the formation of double bond, of which Wittig reaction is most commonly used. In Wittig reaction formation of double bond takes place by the reaction of aldehyde or ketone with the ylide generated from a phosphonium salt.⁶⁷

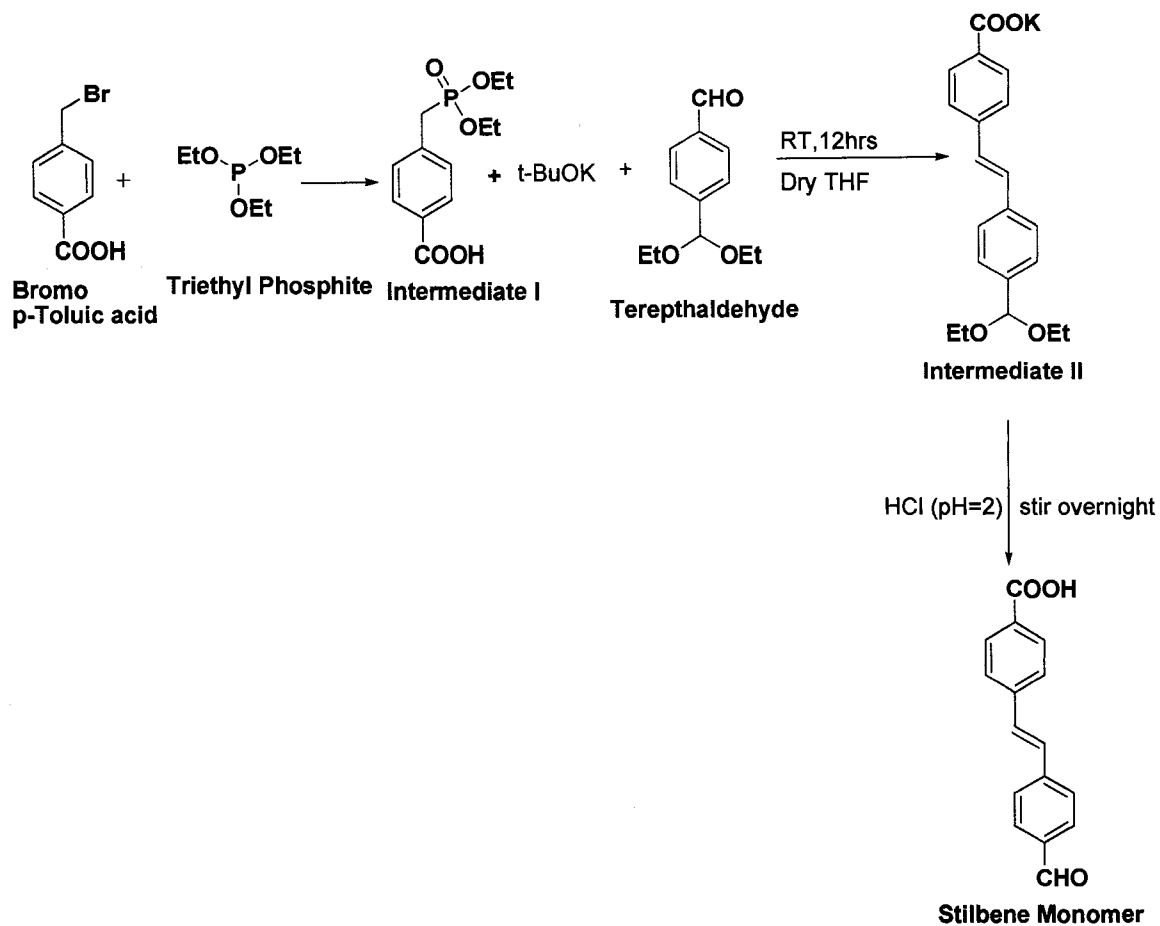


Figure 2.10 Synthetic Scheme for the Preparation of Stilbene Monomer (Adapted from ref. 68)

1g α -Bromo-p-toluic acid was dissolved in 35mL of anhydrous toluene, to this 0.92mL of triethylphosphite was added and refluxed over night. After coming down to room temperature, the crystals (intermediate I) were filtered off and washed with toluene and ether to remove impurities. Intermediate I was characterized by using NMR (Figure 2.11).

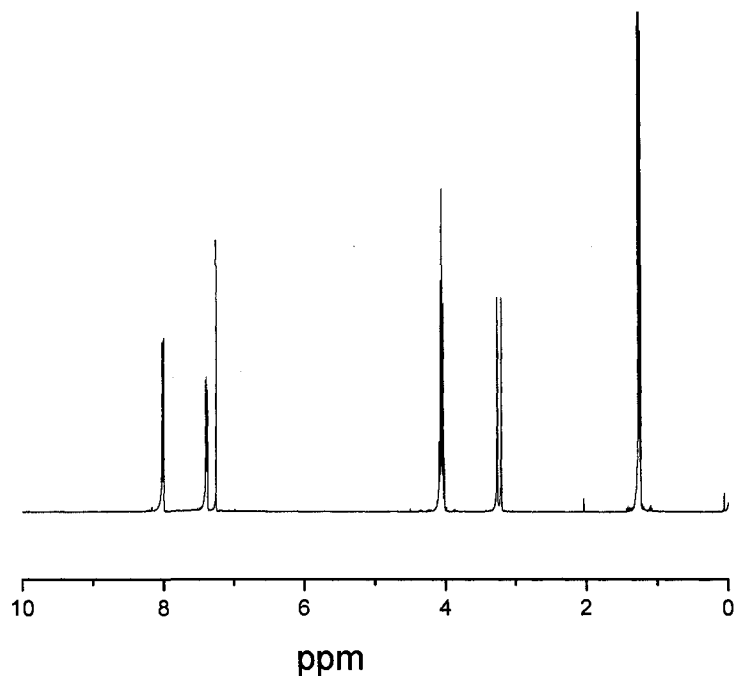


Figure 2.11 ¹H NMR Spectrum of Stilbene Intermediate

¹H NMR (400 MHz, CDCl₃): δ 1.25 (6H, t, $J = 6.9\text{Hz}$), 3.24 (2H, d, $J = 22.3\text{Hz}$), 4.07 (4H, m), 7.38 (2H, dd, $J = 8.3, 2.5\text{Hz}$), 8.01 (2H, d, $J = 7.6$).

100mg of stilbene intermediate I, was dissolved in distilled THF with vigorous stirring, to this 98 mg of potassium tert.butoxide was added and stirred for 15mins, then added 73 μL of terephthaldehyde and stirred over night at room temperature to obtain intermediate II.

Intermediate II is subjected to acidification with 6N HCl until the pH of the solution is reached to two. After the reaction mixture was stirred for two hours, the solvent was removed by rotary evaporation. A yellow color solid was obtained which was

washed with water, ethanol and ether to remove impurities. This compound was characterized by NMR (Figure 2.12), LCMS (Figure 2.13), UV-Vis (Figure 2.14), Excitation (Figure 2.15) and Emission spectroscopy (Figure 2.16).

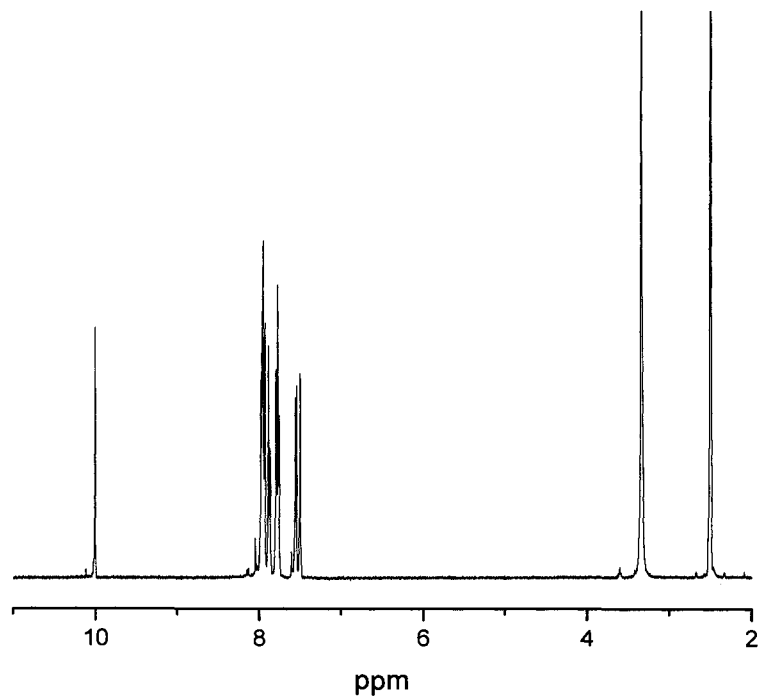


Figure 2.12 ¹H NMR Spectrum of Stilbene Monomer

¹H NMR (400 MHz, DMSO-d₆): δ 7.55 (1H, d, $J = 5.8$ Hz), 7.77 (3H, m), 7.87 (1H, d, $J = 8.0$ Hz), 7.92-7.97 (5H, m), 10.00 (1H, s).

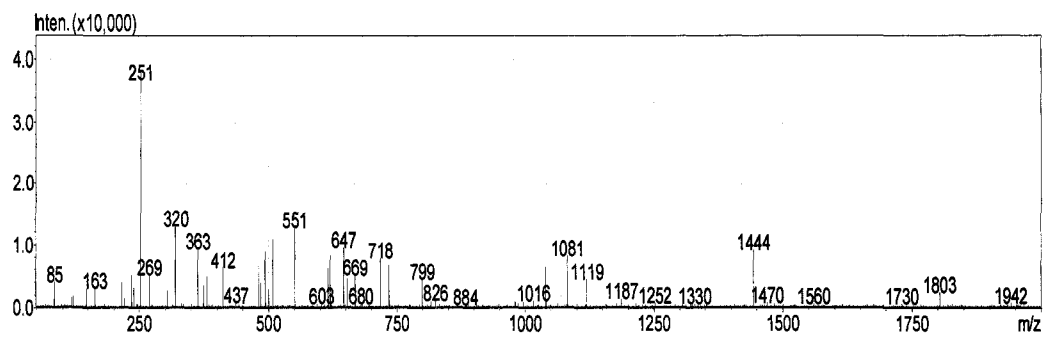


Figure 2.13 LCMS ESI (-ve mode) of Stilbene

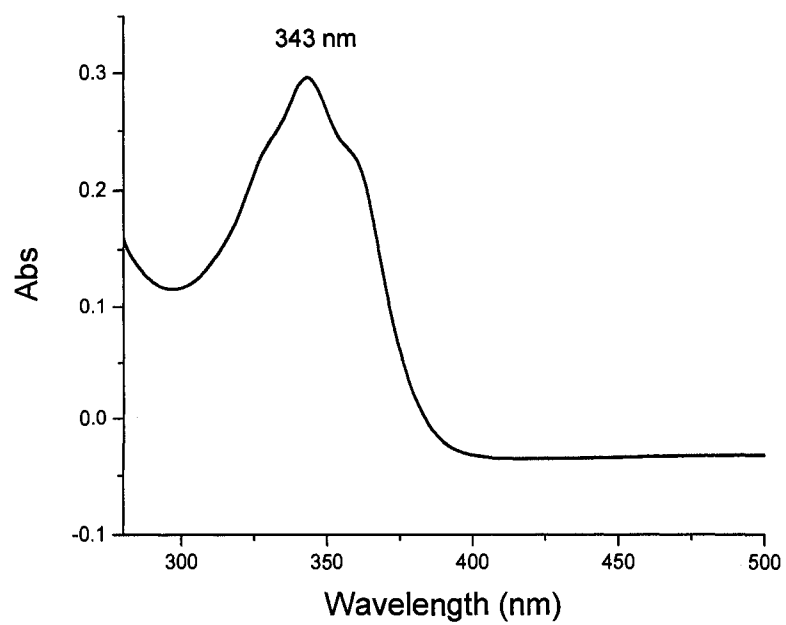


Figure 2.14 UV-Vis Spectrum of Stilbene Monomer

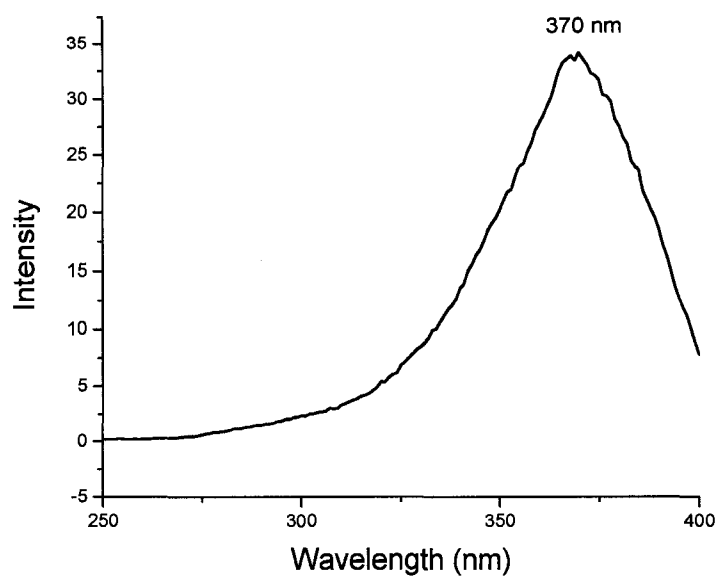


Figure 2.15 Excitation Spectrum of Stilbene Monomer

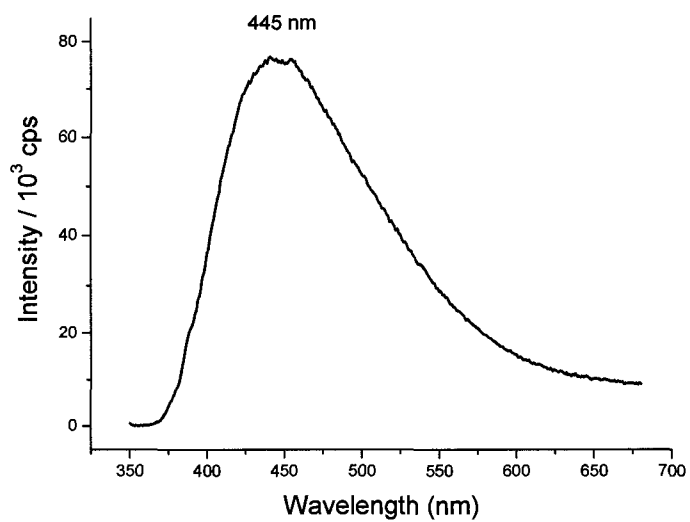


Figure 2.16 Emission Spectrum of Stilbene Monomer

All spectral studies were done in acetonitrile solution. Stilbene compound is not soluble in acetonitrile, so first stilbene compound was dissolved in very small amount

of DMSO and this solution was then added to acetonitrile solution. Stilbene has absorption maxima at 343 nm (Figure 2.14) and emission at 445 nm (Figure 2.16). Stilbene emission comes from π - π^* interaction.

CHAPTER III

SYNTHESIS AND SPECTRAL STUDIES OF 4,4'-BIPYRIDINE TRYPTOPHAN RUTHENIUM COMPLEX

3.1 Introduction

Sensor is a device which measures a physical quantity or chemical phenomenon and converts this into a signal which can be read by different types of instruments based on the type of signal. Receptors are the focal part of the sensor, which reacts with target analytes and exhibit a signal based on the type of reaction, and the type of leaving group. This results due to the interaction between a receptor and target moiety. There are a number of receptors based on the type of target. Receptors have active functional groups which react with the target analyte. In optical sensors the association of a receptor molecule with target analyte causes change in the optical properties of the receptor and shows a difference in the signal. There are different types of signals such as, fluorescence enhancement, fluorescence quenching and sometimes change in the peak position called as bathochromic shift (towards longer wavelength) or hypsochromic shift (towards shorter wavelength). Nerve gas agents are organophosphate compounds which contain negatively charged phosphate group; therefore, in sensors for nerve gas, receptors must have electron rich groups such as nitrogen or oxygen. Tryptophan is an amino acid which contains indole functional group. The nitrogen group of the indole functional group is electron rich and we think this can be used as a receptor for the nerve gas agent. Tryptophan also has an amine group, so we can attach this amine group to a highly conjugated bipyridine compound. Bipyridine compounds are considered as popular

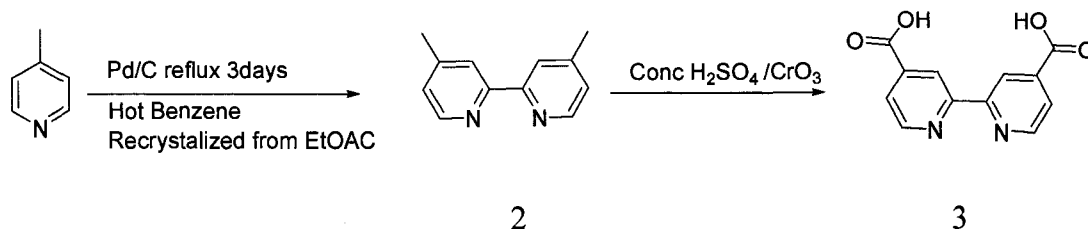
ligands in coordination chemistry and can be used as a chelating ligand which forms complexes with most transition metals.

2,2'-Bipyridine tryptophan ligand was synthesized and characterized by using NMR, LCMS, absorbance and fluorescence spectroscopy. The interaction of nerve gas analogs DCP, DMMP and DCP hydrolyzed product HCl with 2,2'-Bipyridine tryptophan ligand was quantitatively analyzed by using association constants.

Ruthenium bipyridyl complexes can be used as chemosensors because of its large extinction coefficients, longer lifetimes, and visible emission wavelengths. Optical properties of Ru metal can be tuned by its ligand behavior. Emission in ruthenium complexes is caused by the metal to ligand charge transfer (MLCT). In this chapter, the synthesis of Ru(bpy)₂(4,4'-Bpy Tryptophan) complex and Zinc (4,4'-Bpy tryp)₂ complex is discussed. The characterization of these complexes have been done using NMR, LCMS, absorbance and fluorescence spectroscopy. The interaction of nerve agent analogs with these complexes by using association constants have been analyzed.

3.2 Synthetic Methods

3.2.1 Synthesis of 2,2'-Bipyridine-4,4'-Dicarboxylic Acid



Scheme 3.1 Synthetic Scheme of Preparation of 2,2'-Bipyridine-4,4'-Dicarboxylic Acid

Freshly distilled 350 mL 4-picoline and 14g of palladium (10% on charcoal) were taken in a round bottom flask and refluxed for 3 days. To this solution 125mL of hot benzene was added and refluxing was continued for 30 mins. The mixture was filtered when hot to remove the catalyst. The filtrate was concentrated to 150 mL using rotary evaporator, almost colorless crystals of 4,4'-Dimethyl-2,2'-Bipyridine (2) was precipitated, and were recrystallized from ethyl acetate. The formation of the product was confirmed by ¹H NMR (Figure 3.1) and C¹³ NMR (Figure 3.2) and compared with the literature data.⁶⁹

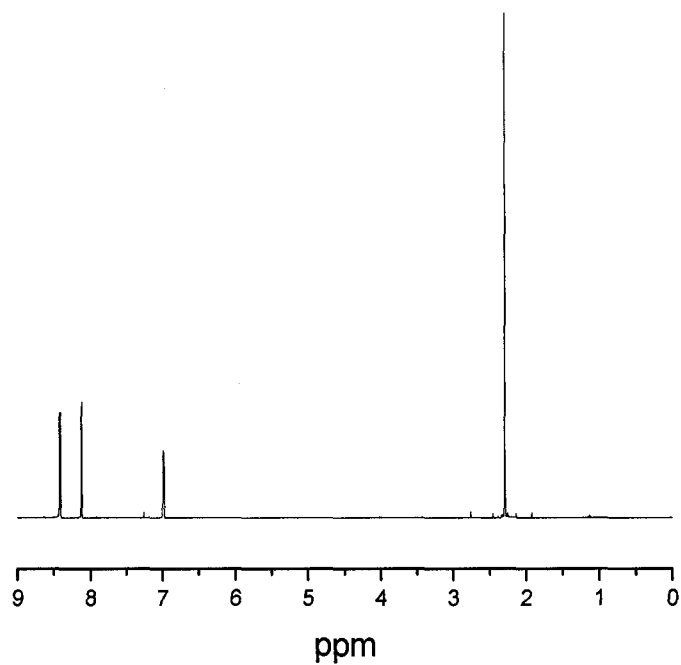


Figure 3.1 ^1H NMR Spectrum of 4,4'-Dimethyl-2,2'-Bipyridine

^1H NMR (400 MHz, CDCl_3): 2.29 (6H, s), 6.99 (2H, d, $J = 5.1\text{Hz}$), 8.11 (2H, s), 8.41 (2H, d, $J = 5.1\text{Hz}$)

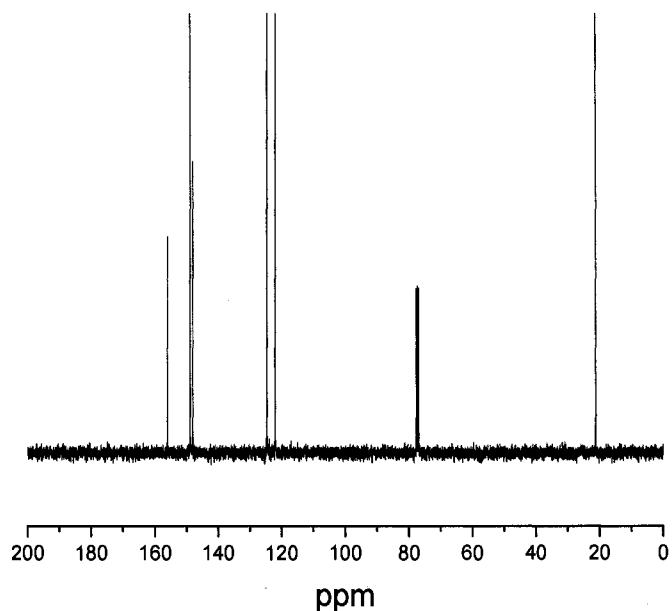


Figure 3.2 ^{13}C NMR Spectrum of 4,4'-Dimethyl-2,2'-Bipyridine

Compound 2(2g, 10.86 mmol) was dissolved in 25mL of Conc. H_2SO_4 and cooled to 0°C . CrO_3 (6.5g, 65.13 mmol) was added in small portions over a period of 45 mins. This mixture was heated to 75°C for 4h, stirred at room temperature for 10h and poured into ice/water mixture. The green precipitate was separated by centrifugation and washed several times with water. This green powder was then dissolved in water and added KOH until the solution was basic, the insoluble powder was filtered and washed with water. The aqueous solution was acidified with HCl to precipitate the compound 2,2'-Bipyridine-4,4'-dicarboxylic acid (3). This compound is washed with water, methanol and diethyl ether and dried. The formation of product was confirmed by ^1H NMR (Figure 3.3) and ^{13}C NMR and compared with the literature data.⁷⁰

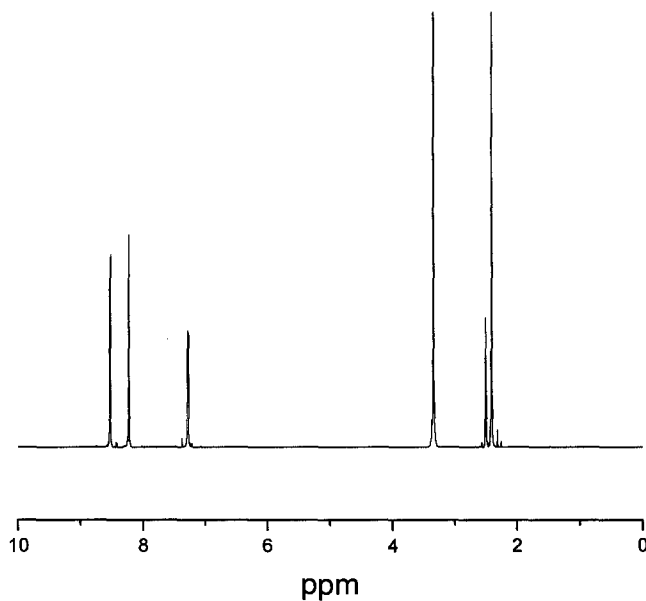
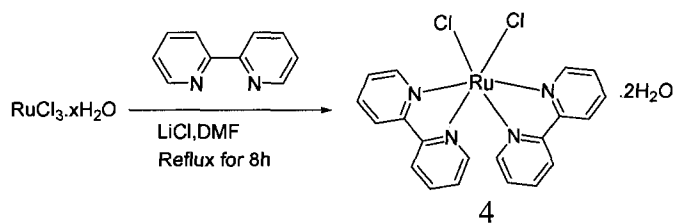


Figure 3.3 ^1H NMR Spectrum of 2,2'-Bipyridine-4,4'-Dicarboxylic Acid

3.2.2 Preparation of $\text{cis}-(\text{bpy})_2\text{RuCl}_2 \cdot 2\text{H}_2\text{O}$



Scheme 3.2 Synthetic Scheme of Preparation of $\text{cis}-(\text{bpy})_2\text{RuCl}_2 \cdot 2\text{H}_2\text{O}$

3.9g of $\text{RuCl}_3 \cdot 3\text{H}_2\text{O}$ (14.9 mmol), 4.68g of Bipyridine (30 mmol), and 4.2g of LiCl (1 mmol) were heated at reflux temperature for 8h in DMF. After the reaction mixture was cooled to room temperature, 125mL of reagent grade acetone was added and the resultant solution was cooled to 0°C overnight and crystals of $\text{cis}-(\text{bpy})_2\text{RuCl}_2 \cdot 2\text{H}_2\text{O}$

(4) were filtered off and washed with water and diethyl ether.⁷¹ The formation of product was confirmed by ¹H NMR (Figure 3.4) and compared with the literature data.

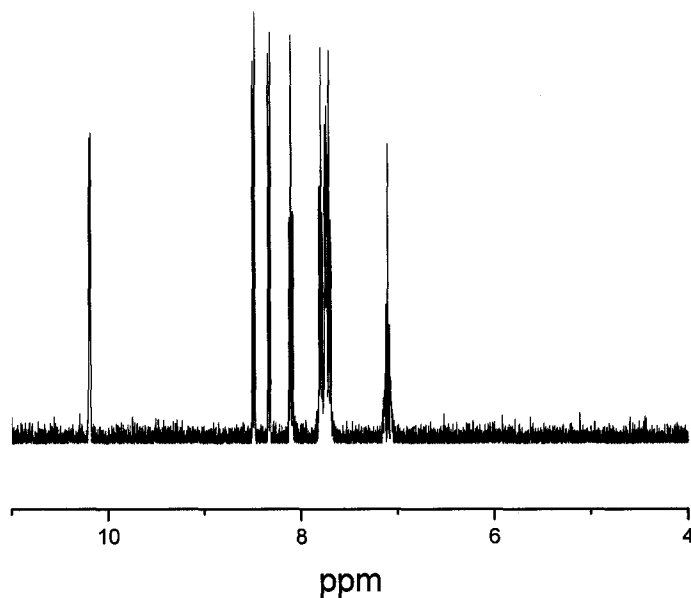
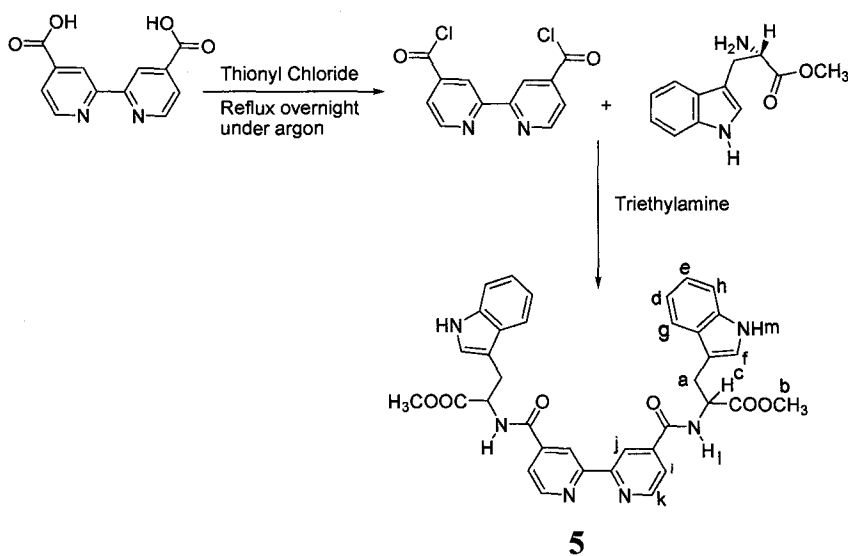


Figure 3.4 ¹H NMR Spectrum of cis-(bpy)₂RuCl₂.2H₂O

3.2.3 Preparation of 4,4'-Bipyridine Tryptophan Ligand



Scheme 3.3 Synthetic Scheme of Preparation of 4,4'-Bpy Tryptophan

300 mg of 4, 4'-Binicotinicacid and 15mL of thionyl chloride was taken in a three necked round bottom flask and refluxed overnight under Argon. After completely drying 30mL of benzene, 600mg of L-tryptophan methyl ester hydrochloride and 0.8 mL of triethylamine were added and refluxed overnight. To this solution 30mL of 0.1M sodium bicarbonate was added and extracted with chloroform. The obtained precipitate was filtered off and recrystallized with acetone which gave the pure compound (5). The formation of product was confirmed by ^1H NMR (Figure 3.5), ^{13}C NMR (Figure 3.6), COSY NMR (Figure 3.7), LC-MS (Figure 3.8), UV-Vis (Figure 3.9), Excitation (Figure 3.10) and Emission (Figure 3.11).

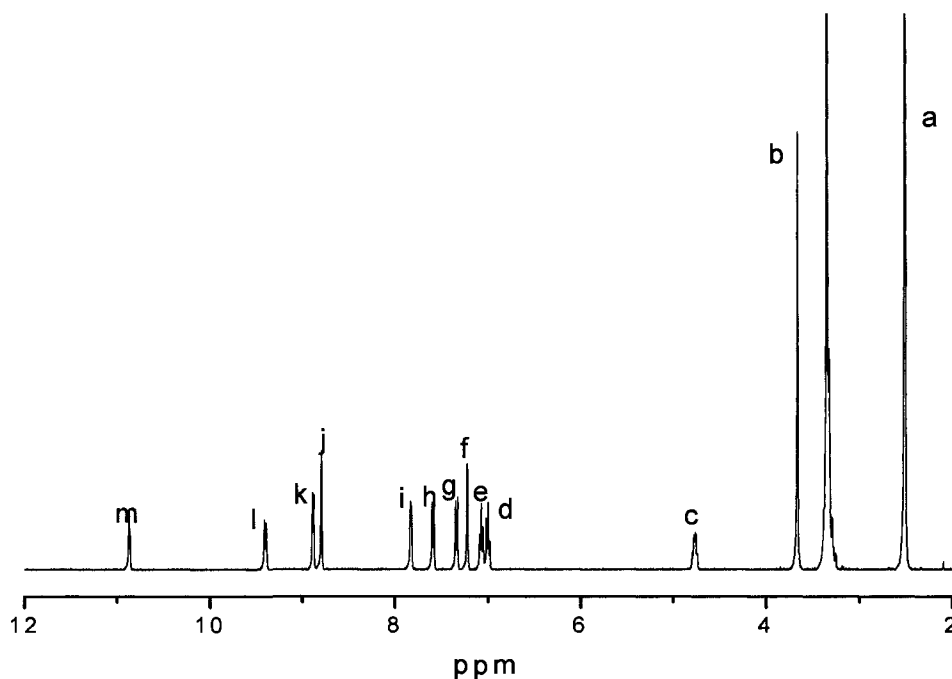


Figure 3.5 ^1H NMR spectrum of 4,4'-Bpy Tryptophan

^1H NMR (400 MHz, DMSO-d_6): 3.30-3.36 (4H, m), 3.66 (6H, s), 4.75 (2H, m), 6.99 (2H, t, $J = 7.7\text{Hz}$), 7.06 (2H, t, $J = 6.9\text{Hz}$), 7.21 (2H, d, $J = 2.2\text{Hz}$), 7.33 (2H, d, $J = 8.0\text{Hz}$),

7.58 (2H, d, $J = 8.0\text{Hz}$), 7.82 (2H, dd, $J = 4.8, 1.5\text{Hz}$), 8.79 (2H, s), 8.87 (2H, d, $J = 5.1\text{Hz}$), 9.39 (2H, d, $J = 7.7\text{Hz}$), 10.86 (2H, s).

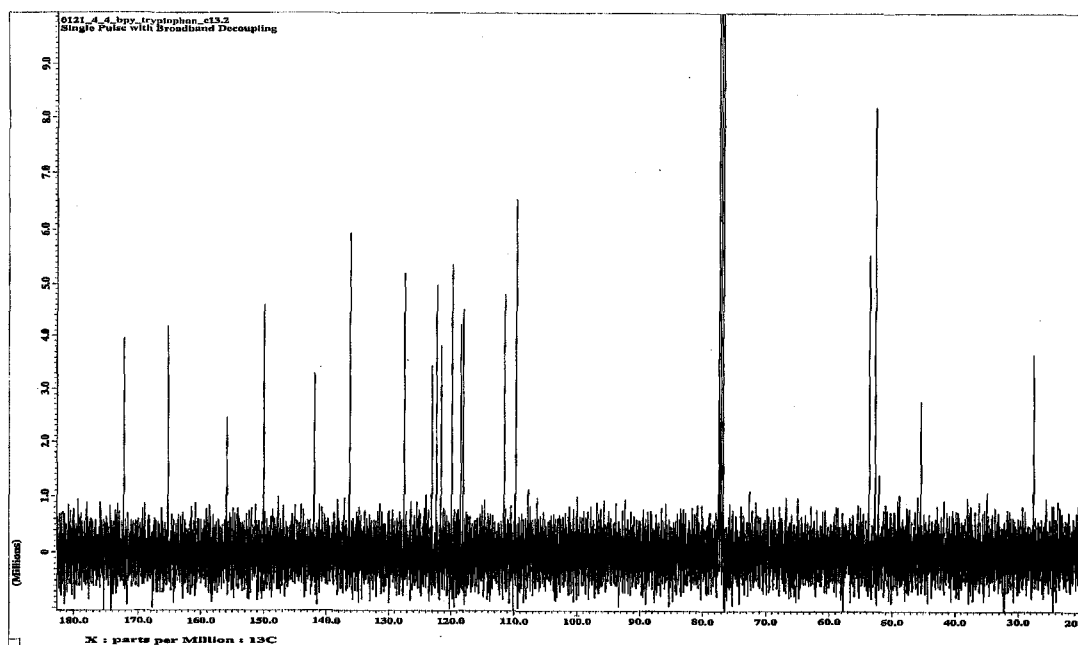


Figure 3.6 ^{13}C NMR spectrum of 4,4'-Bpy Tryptophan

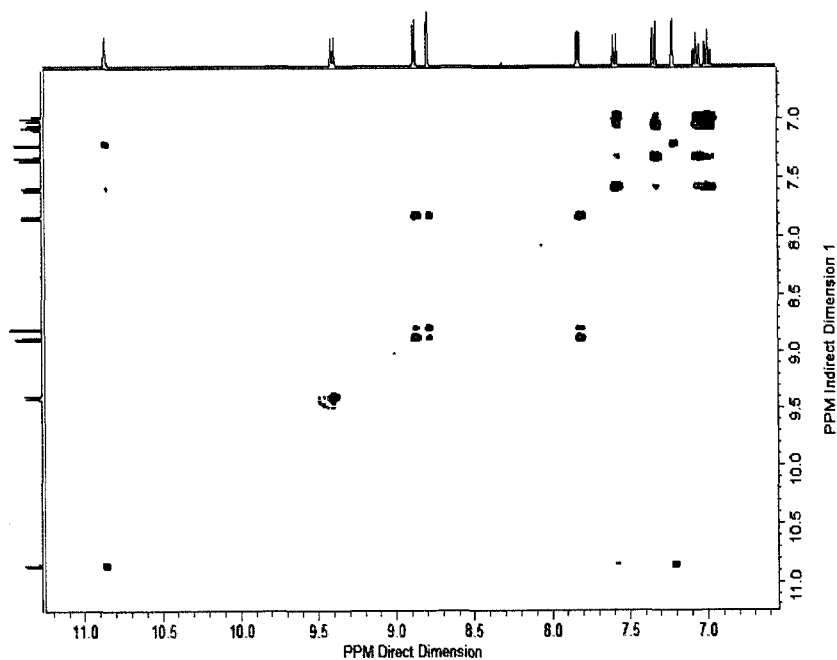


Figure 3.7 ^1H - ^1H COSY NMR Spectrum of 4,4'-Bpy Tryptophan

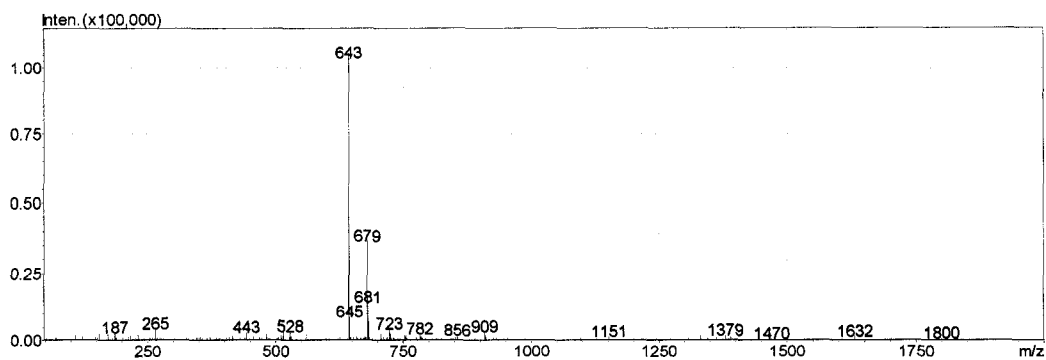


Figure 3.8 LC-MS ESI Negative Spectrum of 4,4'-Bpy Tryptophan

UV-Vis of 4,4'-BpyTryptophan

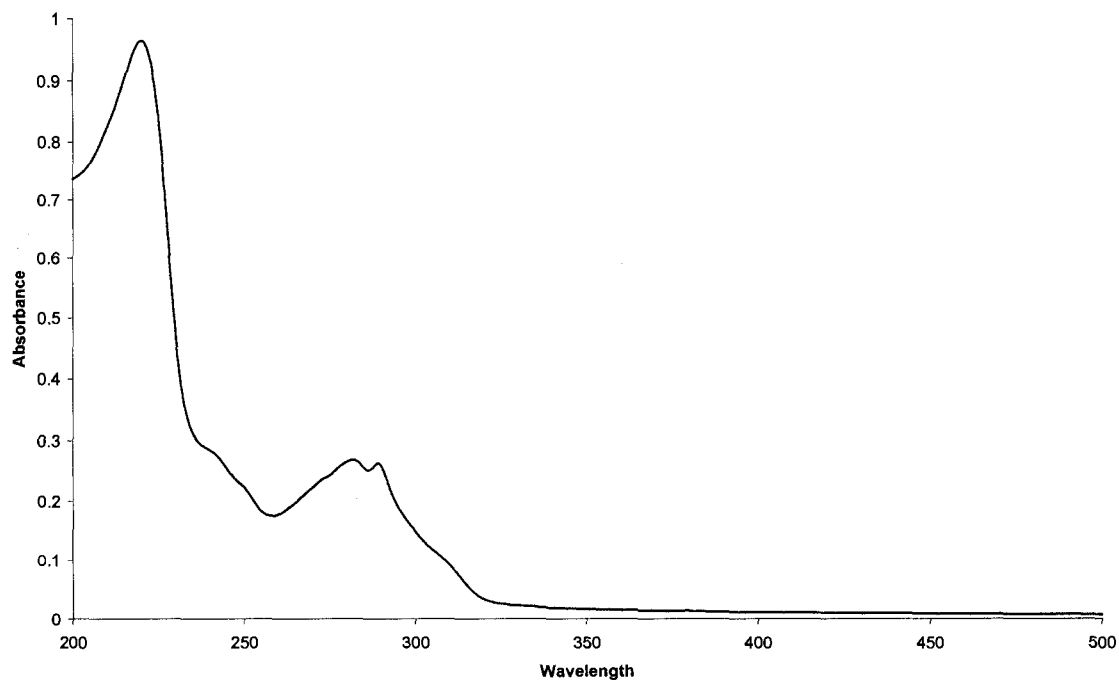


Figure 3.9 UV-Vis Spectrum of 12.5µM 4,4'-Bpy Tryptophan

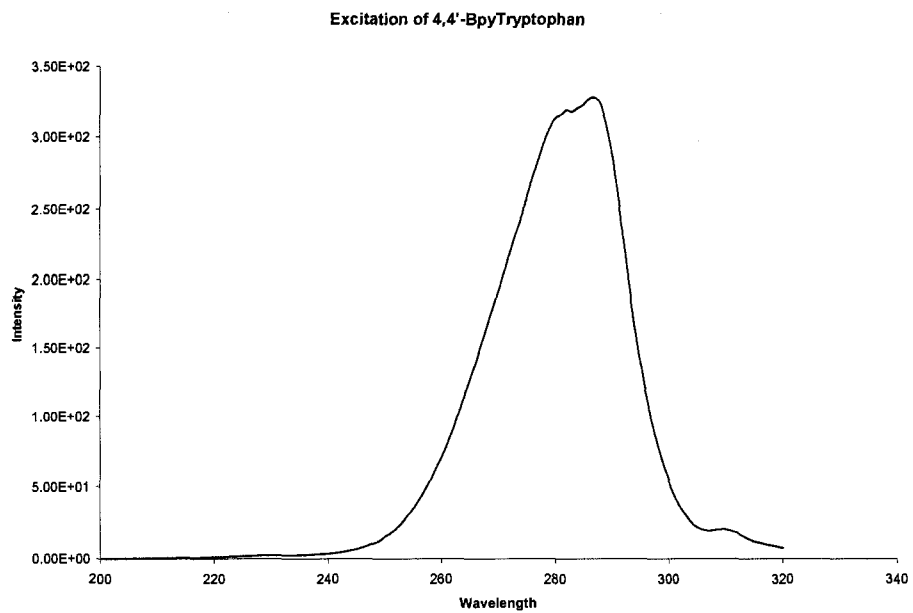


Figure 3.10 Excitation Spectrum of 4,4'-Bpy Tryptophan

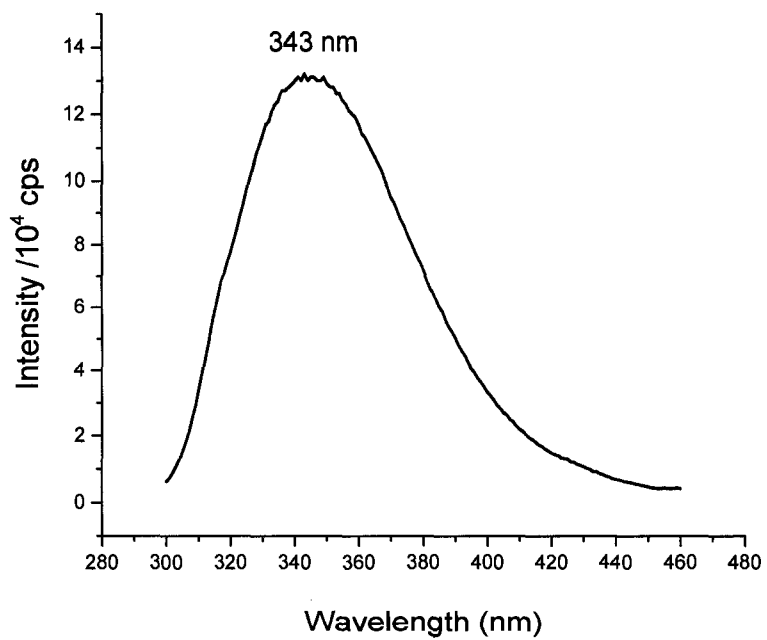


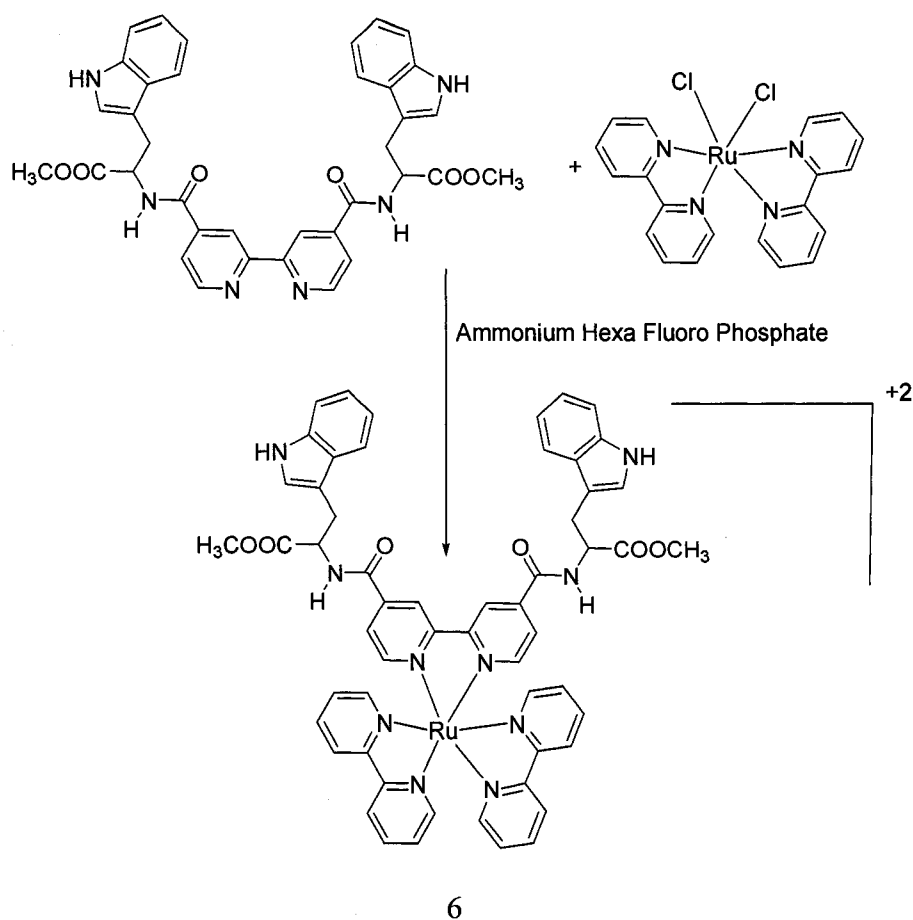
Figure 3.11 Emission Spectrum of 4,4'-Bpy Tryptophan

Tryptophan has maximum absorption at wavelength of 280 nm and its emission peak is solvatochromic, it ranges from 300 to 350 nm (change in color) depending on the polarity of the solvent.⁷² In our experiments, we used acetonitrile to check the emission and absorption. The synthesized 4,4'-Bpy Tryptophan compound has absorption maxima at 287 nm (Figure 3.9) and the emission maxima at 343 nm shows the tryptophan behavior. Tryptophan compounds are chiral compounds, table 3.1 shows the optical activity of 4,4'-Bipyridine tryptophan ligand.

Table 3.1 Optical Rotation of 4, 4'-Bpy Tryptophan

Concentration(C) (mol/L)	0.005	0.01	0.015
Optical Rotation(x) (degrees)	-0.137	-0.330	-0.483
Optical Activity(D) (degrees)	-27.4	-33.0	-32.2

3.2.4 Preparation of Ru(bpy)₂(4,4'-Bpy Tryptophan) Complex



Scheme 3.4 Synthetic Scheme of Preparation of Ru(bpy)₂(4,4'-Bpy Tryptophan) Complex

387mg of 4,4'-Bipyridine tryptophan ligand (5) and 243mg of cis-(bpy)₂ RuCl₂.2H₂O (4) were taken in a sealed tube and heated at 110° C overnight. After cooling to room temperature any unreacted compound was filtered off and to this solution 200mg of ammonium hexafluorophosphate was added. The precipitate obtained was filtered off and washed with cold water and cold ethanol to remove any impurities from the compound 4, 4'-Bpy Tryptophan ruthenium complex (6).

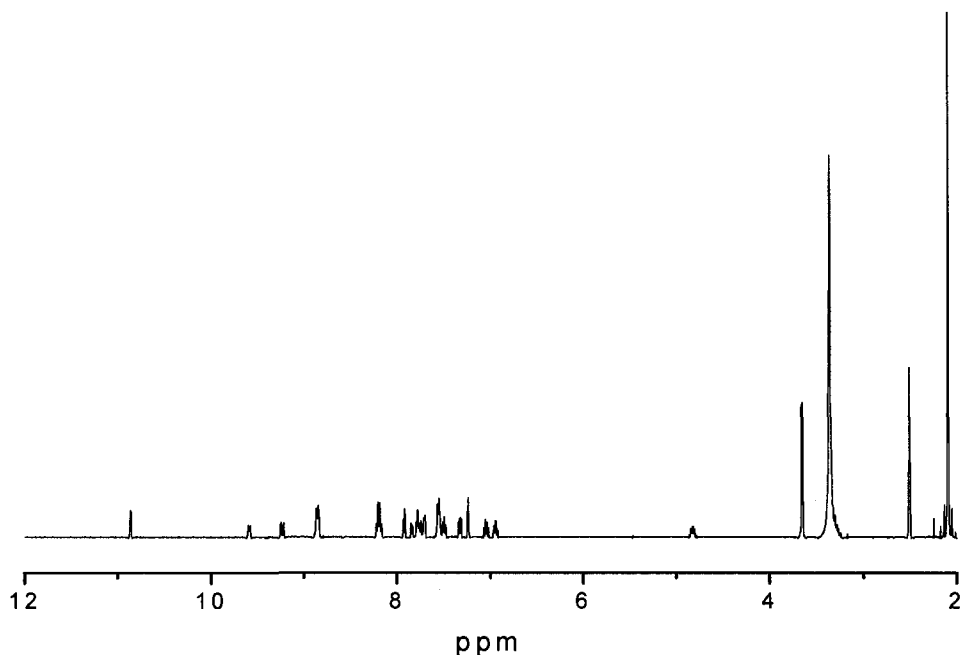


Figure 3.12 ^1H NMR Spectrum of $\text{Ru}(\text{bpy})_2(4,4'\text{-Bpy Tryptophan})$

^1H NMR (400 MHz, DMSO-d_6): 3.21-3.38 (2H, m, CHCH_2 -), 3.64 (6H, d, COOCH_3 , $J = 4.0\text{Hz}$), 4.81 (2H, m, NHCHCH_2), 6.93 (2H, t, Ar-H, $J = 8.0\text{Hz}$), 7.04 (2H, m, Ar-H), 7.20 (2H, s, Pyr-H), 7.31 (2H, dd, Ar-H, $J = 8.0, 3.3\text{Hz}$), 7.48 (2H, t, Bpy-H, $J = 6.5\text{Hz}$), 7.54 (4H, m, Ar-H, Bpy-H), 7.69-7.83 (6H, m, Bpy-H), 7.91 (2H, t, Bpy-H, $J = 5.5\text{Hz}$), 8.19 (4H, q, Bpy-H, $J = 8.0\text{Hz}$), 8.84 (4H, dd, Bpy-H, $J = 8.4, 3.6\text{Hz}$), 9.15 (2H, d, Bpy-H, $J = 13.9\text{Hz}$), 9.53 (2H, d, NH-CO , $J = 7.3\text{Hz}$), 10.85 (2H, s, Pyr-NH).

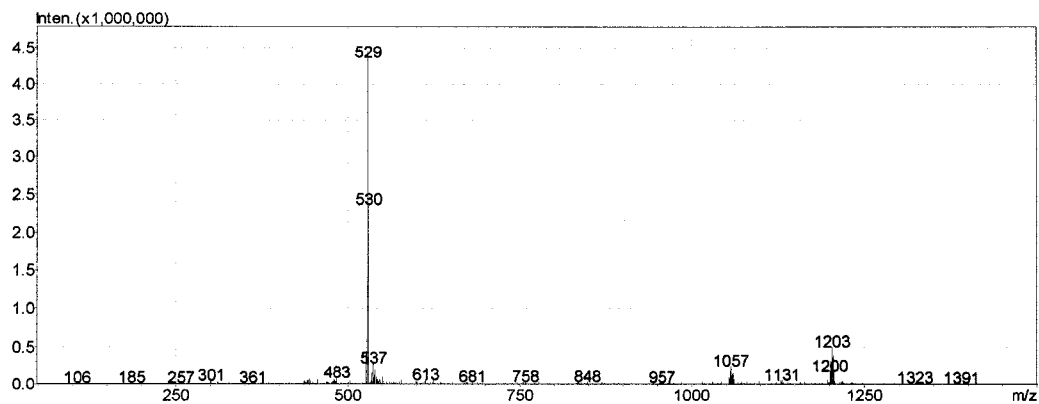


Figure 3.13 LC-MS ESI Positive Spectrum of Ru(bpy)₂(4,4'-Bpy Tryptophan)

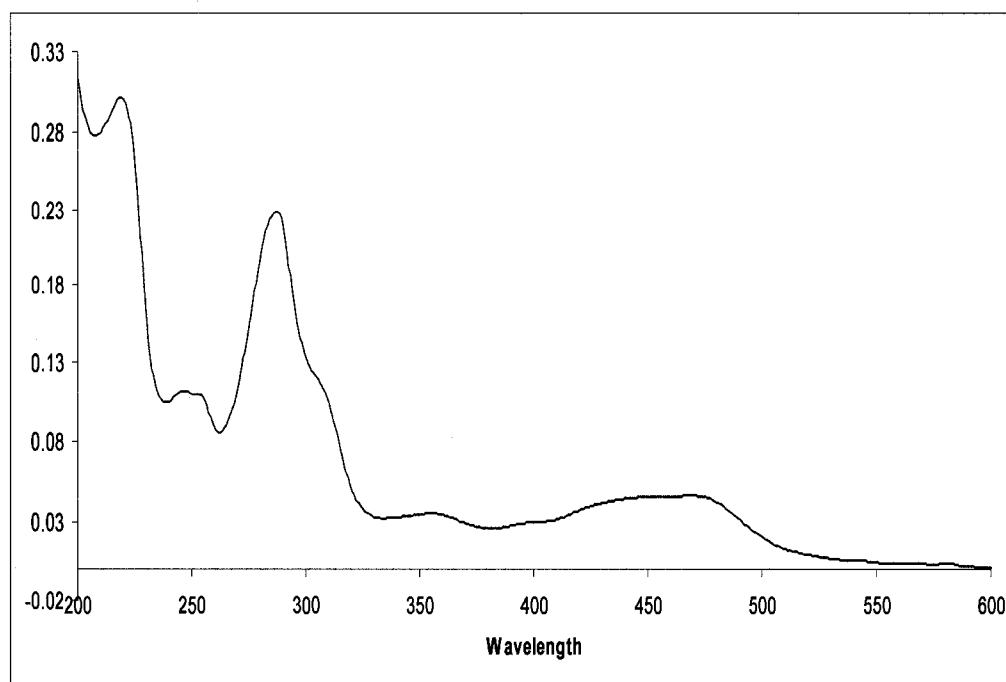


Figure 3.14 UV-Vis Spectrum of Ru(bpy)₂(4,4'-Bpy Tryptophan)

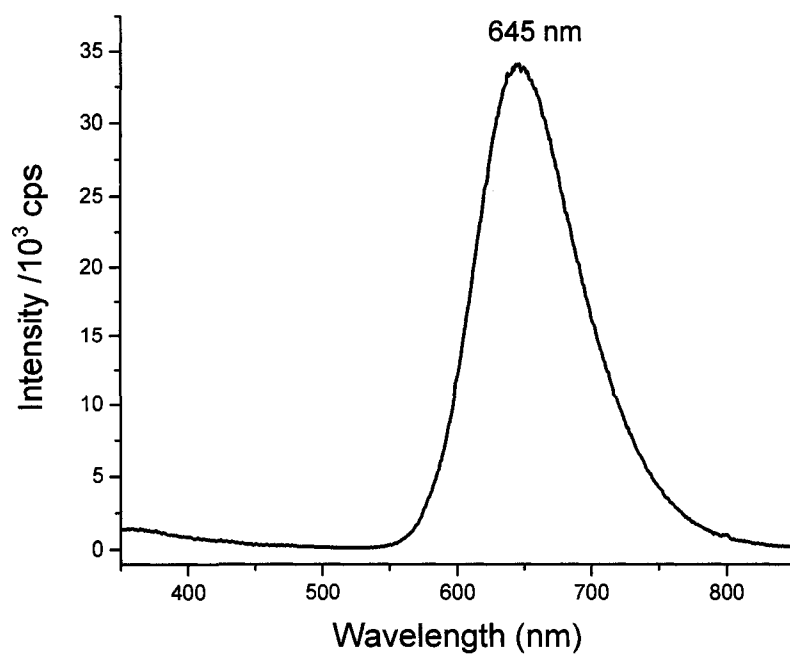


Figure 3.15 Emission Spectrum of Ru(bpy)₂(4,4'-Bpy Tryptophan)

Figure 3.13 shows the LCMS spectrum of the complex. Figures 3.14 and 3.15 show the absorption and emission spectra of Ru(bpy)₂(4,4'-Bpy Tryptophan) respectively. The absorption spectra shows two peaks, the peak at 290 nm shows tryptophan absorbance and the peak around 450 nm shows the ruthenium absorbance. The emission spectrum shows the maximum at 645 nm when excited at 290nm.

3.2.5 Emission of 4,4'-Bpy Tryptophan [12.5×10^{-6} M] Vs Variable DCP [50 μ M to 2.5 mM] (at Exci 280 nm)

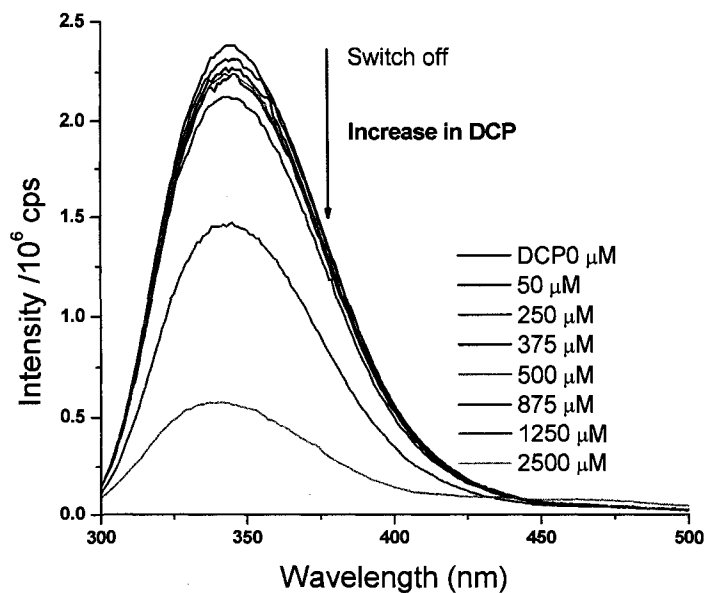


Figure 3.16 Emission Spectrum of 4,4'-Bpy Tryptophan with Various DCP Concentrations

Association Constant: ($146 \pm 60 \text{ M}^{-1}$)

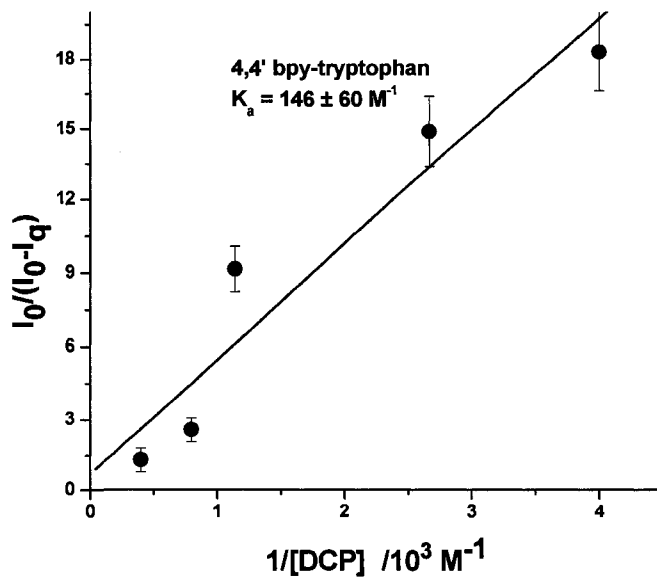


Figure 3.17 Association Constant of 4,4'-Bpy Tryptophan with DCP

Figure 3.16 shows the emission of 4,4'-Bpy Tryptophan ligand [12.5×10^{-6} M] with variable DCP [$50 \mu\text{M}$ to 2.5 mM] concentrations, excited at 280 nm . Initial emission was at 344 nm , when $50 \mu\text{M}$ DCP was added the emission quenched and continued with increased concentrations and hypsochromic shift was observed. The emission with 12.5 mM DCP was observed at 341 nm , and with 25 mM DCP the emission was observed at 340 nm . The above quenching was attributed to adduct formation between lone pair of nitrogen in tryptophan and DCP. The emission was quantified by calculating the association constant (Figure 3.17), which is a very small value ($146 \pm 60 \text{ M}^{-1}$), which may be due to tryptophan's low emission.

3.2.6 Emission of 4,4'-Bpy Tryptophan [12.5×10^{-6} M] Vs Variable HCl (at Exci 280 nm)

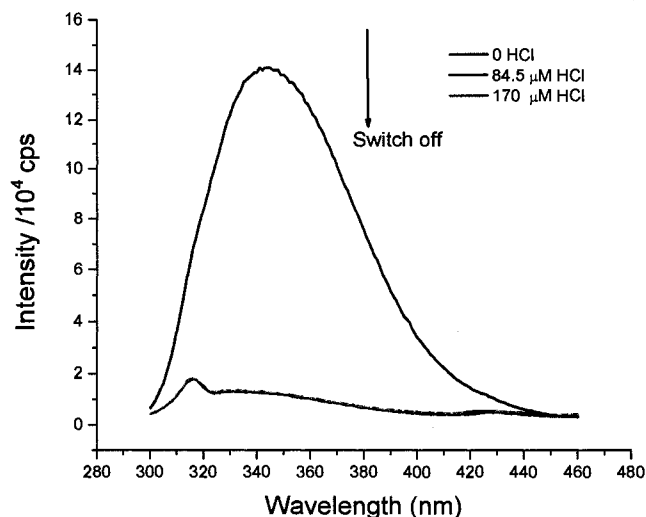


Figure 3.18 Emission Spectrum of 4,4'-Bpy Tryptophan with Various HCl Concentrations

Figure 3.18 shows the emission of $12.5 \mu\text{M}$ 4,4'-Bpy Tryptophan with variable HCl concentrations at excitation 280 nm . When $84.5 \mu\text{M}$ HCl was added the

emission quenched completely, on further addition the emission remained constant, which shows that the system reached saturated. The drastic change of emission may be due the decrease of pH after adding HCl. By lowering the pH HCl quenches fluorescence of the adducts. There is no association constant for this system, this is because of the fact that when very dilute acid is added, the emission quenches completely.

3.2.7 Emission of 4,4'-Bpy Tryptophan [20×10^{-6} M] Vs Variable DMMP (at Exci 280 nm)

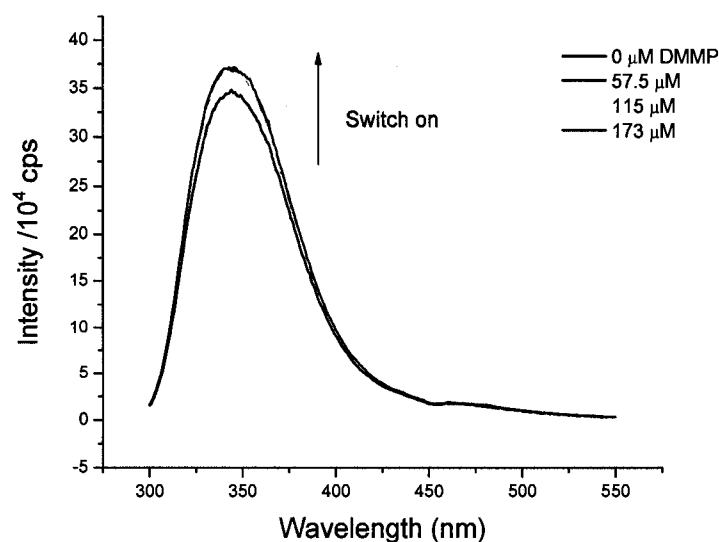


Figure 3.19 Emission Spectrum of 4,4'-Bpy Tryptophan with Various DMMP Concentrations

Figure 3.19 shows the emission of 4,4'-Bpy Tryptophan ligand with various DMMP concentrations. After adding the 57.5 μ M DMMP the emission increased and stays constant even on further addition of DMMP. When compared to the emission by DCP, the change in emission intensity with DMMP is very low, because DMMP is not expected to form a leaving group as easily as DCP and will not form adduct.

3.2.8 Emission of Ru(bpy)₂(4,4'-Bpy Tryptophan) [7.5X10⁻⁶ M] Vs Variable DCP [.87 μM to 7.83 μM] (at Exci 290 nm)

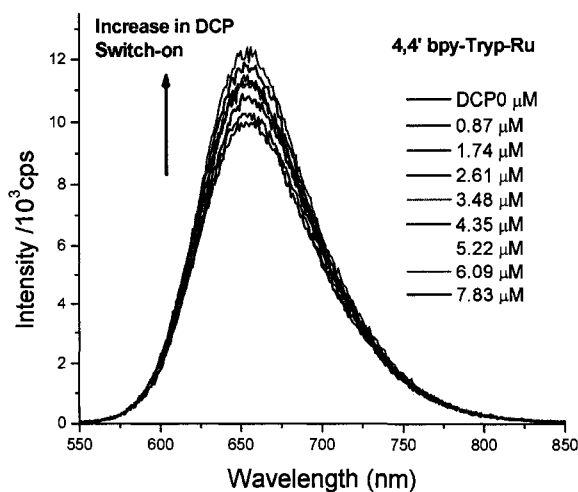


Figure 3.20 Emission Spectrum of Ru(bpy)₂(4,4'-Bpy Tryptophan) with Various DCP Concentrations

Association Constant : $K = (5.8 \pm 0.6) \times 10^4 \text{ M}^{-1}$

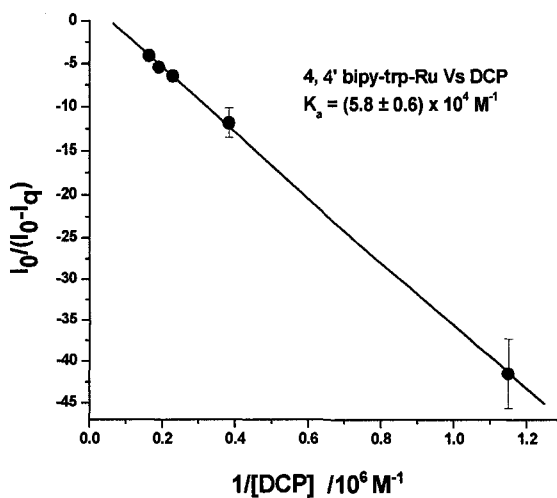


Figure 3.21 Association Constant of Ru(bpy)₂(4,4'-Bpy Tryptophan) with DCP

Figure 3.20 shows the emission of 7.5 μM Ru(bpy)₂(4,4'-Bpy Tryptophan) with various (.87 μM to 7.83 μM) DCP concentrations. By increasing concentration of DCP, emission of the complex increases. There are two emissions, one from tryptophan

and the other from ruthenium. There is metal to ligand charge transfer and the tryptophan emission is completely transferred and decreased when compared to the ruthenium emission. Calculated association constant (Figure 3.21) is due to the ruthenium emission and is very high when compared to the ligand association constant.

3.2.9 Emission of Ru(bpy)₂(4,4'-Bpy Tryptophan) [10X10⁻⁶ M] Vs Variable HCl [60 μM to 510 μM] (at Exci 290 nm)

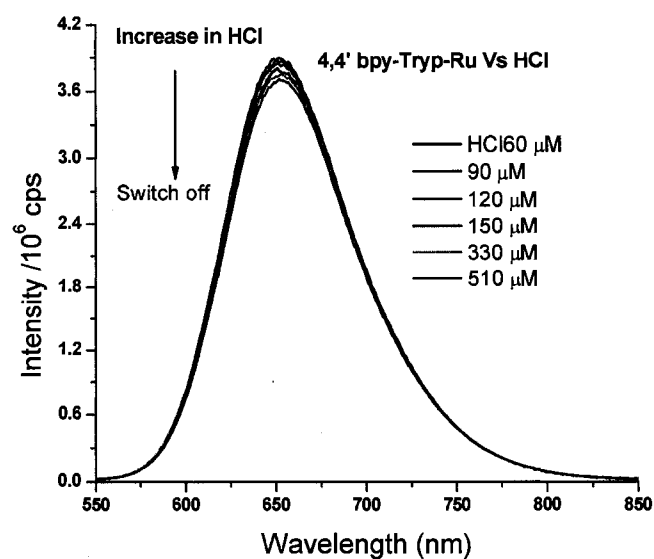


Figure 3.22 Emission Spectrum of Ru(bpy)₂(4,4'-Bpy Tryptophan) with HCl

Association Constant: $K = (1.0 \pm 0.4) \times 10^4 \text{ M}^{-1}$

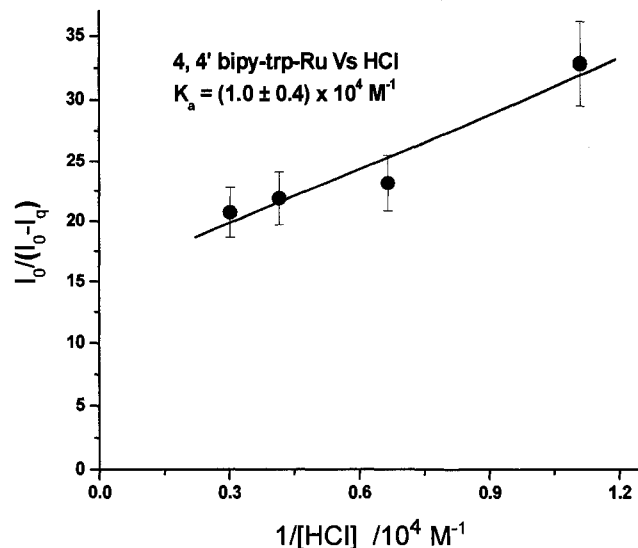


Figure 3.23 Association Constant of $\text{Ru}(\text{bpy})_2(4,4'\text{-Bpy Tryptophan})$ with HCl

Figure 3.22 shows the emission of $10 \mu\text{M}$ $\text{Ru}(\text{bpy})_2(4,4'\text{-Bpy Tryptophan})$ with various HCl ($60 \mu\text{M}$ to $510 \mu\text{M}$) concentrations. With increasing HCl concentration ruthenium shows decrease in emission and acts as a switch-off sensor. The calculated association constant is very high [$(1.0 \pm 0.4) \times 10^4 \text{ M}^{-1}$] (Figure 3.23).

3.3.0 Emission of $\text{Ru}(\text{bpy})_2(4,4'\text{-Bpy Tryptophan}) [5 \times 10^{-6} \text{ M}]$ Vs Variable DMMP

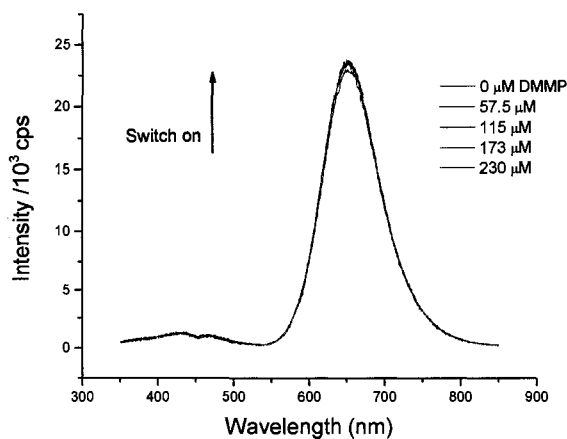
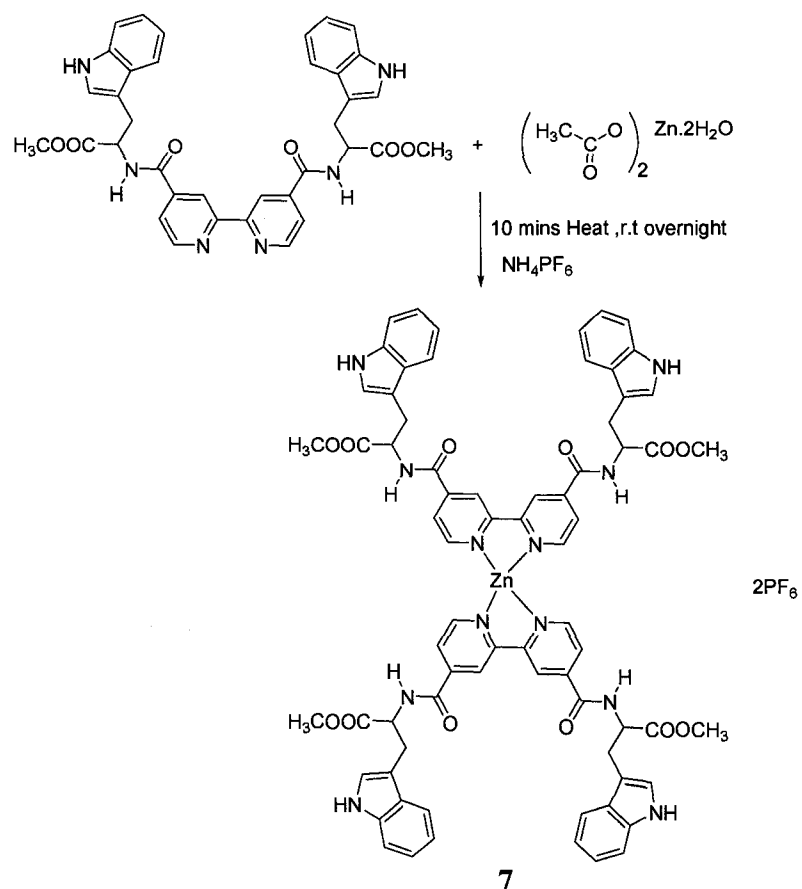


Figure 3.24 Emission Spectrum of $\text{Ru}(\text{bpy})_2(4,4'\text{-Bpy Tryptophan})$ with DMMP

Figure 3.24 shows emission of Ru(bpy)₂(4,4'-Bpy Tryptophan) complex with DMMP and there is a very small change in the emission intensity observed with increased DMMP concentration. As previously mentioned DMMP does not have any good leaving group and causes the low emission intensity change.

3.3.1 Preparation of Zinc (4,4'-Bpy tryp)₂ Complex

0.110 g (0.5 mmol) of zinc acetate dihydrate and 0.690 g (1mmol) of 4,4'-Bpy Tryptophan were dissolved in acetonitrile by warming for 10 mins, and then stirred over night at room temperature. To this 0.5 g of ammonium hexafluorophosphate was added to get the required complex. A light yellow color precipitate (7) was formed when ammonium hexafluorophosphate was added; this precipitate was filtered off and washed with cold ether to remove any impurities.



Scheme 3.5 Synthetic Scheme of Preparation of 4,4'-Bipyridine Tryptophan Zinc Complex

The above complex was characterized by using FAB mass spectroscopy and results shows the peak at 1352.40 as substantial evidence for the synthesized compound.

3.3.2 Emission of $10\mu\text{M Zn}(4,4'\text{-Bpy tryp})_2$ Complex Vs Various DCP Concentrations

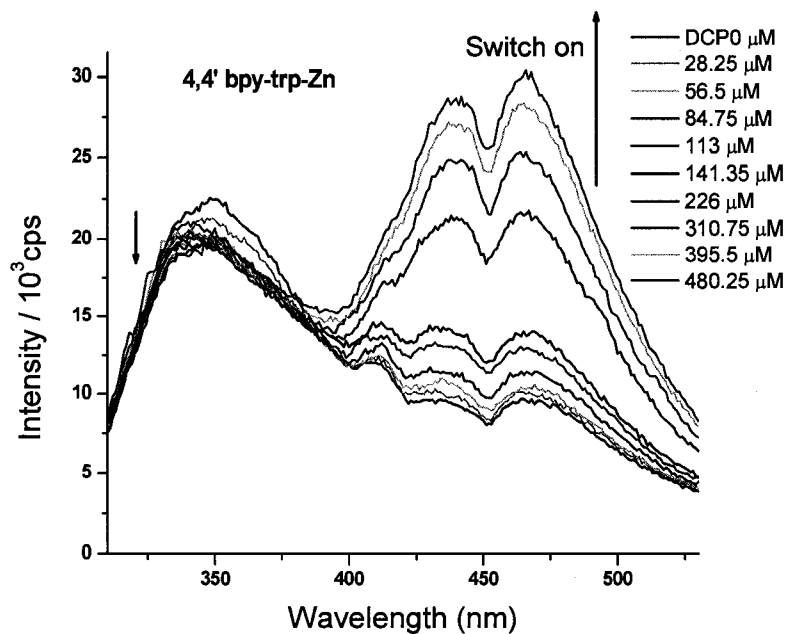


Figure 3.25 Emission Spectrum of $\text{Zn}(4,4'\text{-Bpy tryp})_2$ with DCP

Association Constant: $K = (5.4 \pm 0.6) \times 10^3 \text{ M}^{-1}$

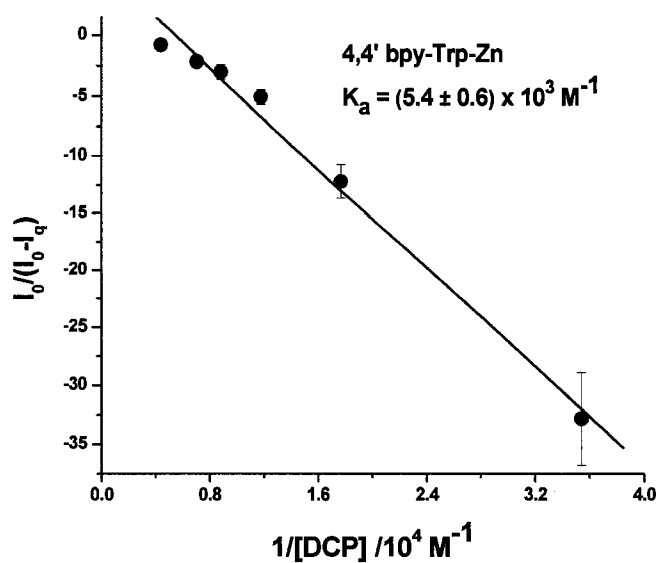


Figure 3.26 Association Constant of $\text{Zn}(4,4'\text{-Bpy tryp})_2$ with DCP

Figure 3.25 shows the emission of $10\mu\text{M Zn}(4,4'\text{-Bpy tryp})_2$ complex versus various DCP ($28.25\ \mu\text{M}$ to $480\ \mu\text{M}$) concentrations. The zinc complex has two emissions, the emission at $340\ \text{nm}$ shows tryptophan emission and the emissions at 440 and $460\ \text{nm}$ shows zinc emissions. Zinc has weak emission and there is no metal to ligand charge transfer, so the zinc complex shows two emissions. Increasing concentrations of DCP shows different behavior at both positions. Increasing DCP concentrations, decreases emission intensity in the tryptophan region and the emission is a hypsochromic shift. The zinc shows switch -on behavior with increasing DCP concentrations. When compared to ruthenium complex, the zinc complex has a weak association constant.

3.3.3 Emission of $10\mu\text{M Zn}(4,4'\text{-Bpy tryp})_2$ Complex Vs Various HCl Concentrations

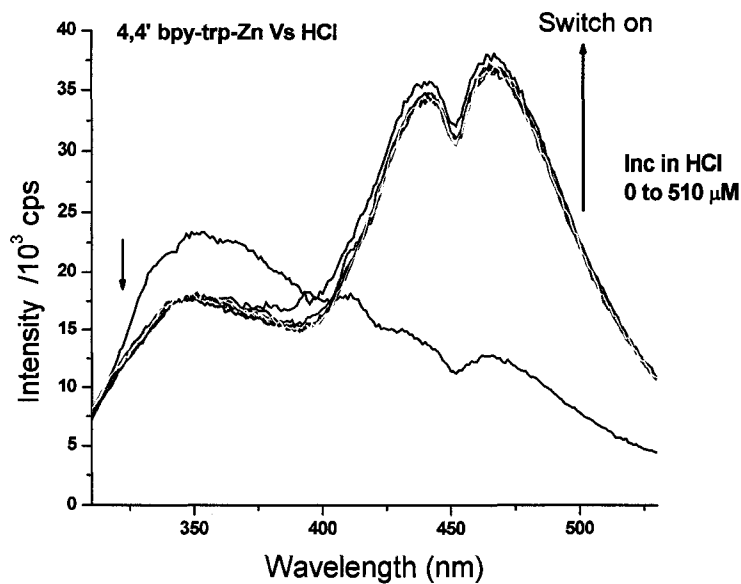


Figure 3.27 Emission Spectrum of $10\mu\text{M Zn}(4,4'\text{-Bpy tryp})_2$ Complex with HCl

3.3.4 Emission of $10\mu\text{M Zn}(4,4'\text{-Bpy tryp})_2$ Complex Vs Various DMMP Concentrations

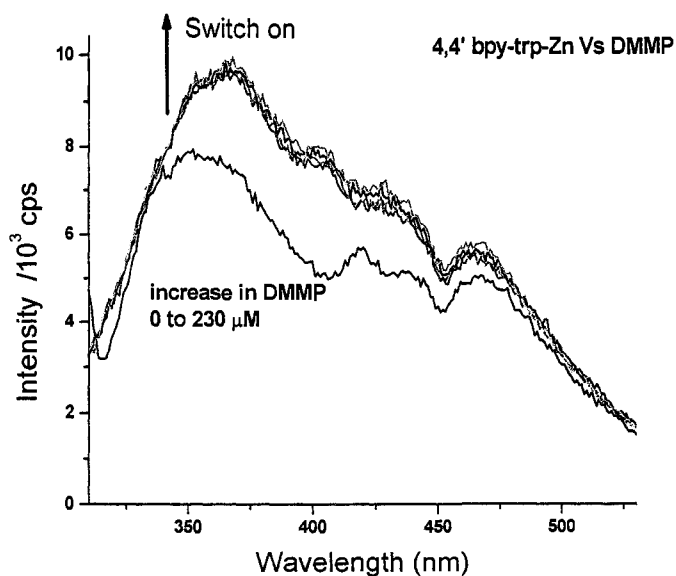


Figure 3.28 Emission Spectrum of $10\mu\text{M Zn}(4,4'\text{-Bpy tryp})_2$ Complex with DMMP

Figures 3.27 and 3.28 shows the emission of $\text{Zn}(4,4'\text{-Bpy tryp})_2$ complex with DCP and DMMP respectively. The HCl emission pattern is same as DCP (tryptophan shows switch off and zinc shows switch on) , but after adding very small amount of acid it changes completely and gets saturated. For DMMP $\text{Zn}(4,4'\text{-Bpy tryp})_2$ complex , switch on behavior is exhibited and it is very weak, it is also saturated after adding a very small concentration of DMMP.

Table 3.2 Association Constants of 4,4'-Bpy Tryptophan and its Complexes

	$K_{\text{DCP}} \text{ M}^{-1}$	$K_{\text{HCl}} \text{ M}^{-1}$	$K_{\text{DMMP}} \text{ M}^{-1}$
4,4'-Bipyridine tryptophan	146 ± 60		
Ru(bpy) ₂ (4,4'-Bpy Tryptophan)	$(5.8 \pm 0.6) \times 10^4$	$(1.0 \pm 0.4) \times 10^4$	No change
Zinc (4,4'-Bpy tryp) ₂	$(5.4 \pm 0.6) \times 10^3$		

Table 3.2 shows the association constants of 4,4'-Bipyridine tryptophan receptor and its ruthenium and zinc complexes with nerve gas analogs DCP, DMMP and hydrolyzed product HCl. 4,4' Ruthenium complex shows better sensitivity towards DCP when compared to the 4,4' zinc complex.

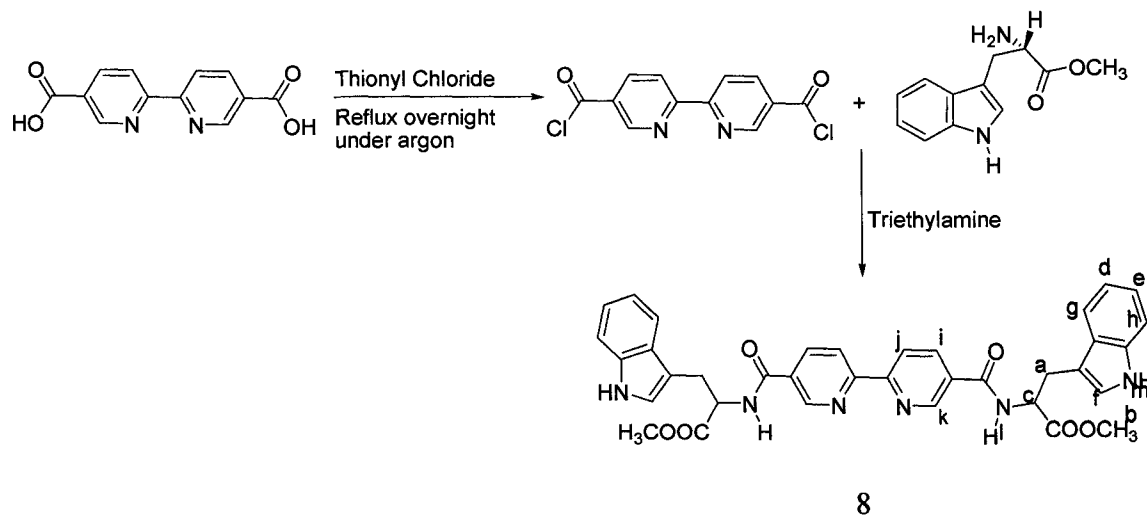
CHAPTER IV

SYNTHESIS AND SPECTRAL STUDIES OF 5,5'-BIPYRIDINE TRYPTOPHAN RUTHENIUM COMPLEX

4.1 Synthetic Methods

In chapter III, I discussed about 4,4'-Bpy Tryptophan ligand and its complexes with ruthenium and zinc metals. In this chapter I am going to discuss about 5,5'-Bpy Tryptophan ligand with ruthenium and zinc metals. Here, I am going to check whether changing the position of receptor at bipyridine position from 4,4' to 5,5' will have any effect on interaction of nerve agents.

4.1.1 Synthesis of 5,5'-Bipyridine Tryptophan



Scheme 4.1 Synthetic Scheme of Preparation of 5,5'-Bpy Tryptophan

300 mg of 2,2'-Bipyridine-5,5'-dicarboxylic acid and 15mL of thionyl chloride was taken in a three necked round bottom flask and refluxed overnight under Argon. On complete drying, 30mL of benzene, 600mg of L-tryptophan methyl ester

hydrochloride and 0.8 mL of triethylamine was added and refluxed overnight. To this 30mL of 0.1M sodium bicarbonate was added and extracted with chloroform. This solution was then rotary evaporated. The precipitate obtained was filtered off and recrystallized with acetone giving pure 5,5'-Bpy Tryptophan compound (8). Figure.4.1 shows the ^1H NMR, Figure 4.2.shows the ^{13}C NMR, Figure 4.3.shows the COSY NMR, Figure 4.4. shows the HETCOR NMR, Figure 4.5.shows the LCMS spectrum, Figure 4.6.shows the UV-Vis spectrum, Figure 4.7 shows excitation spectrum and Figure 4.8 shows the emission spectrum of 5,5'-Bipyridine tryptophan complex.

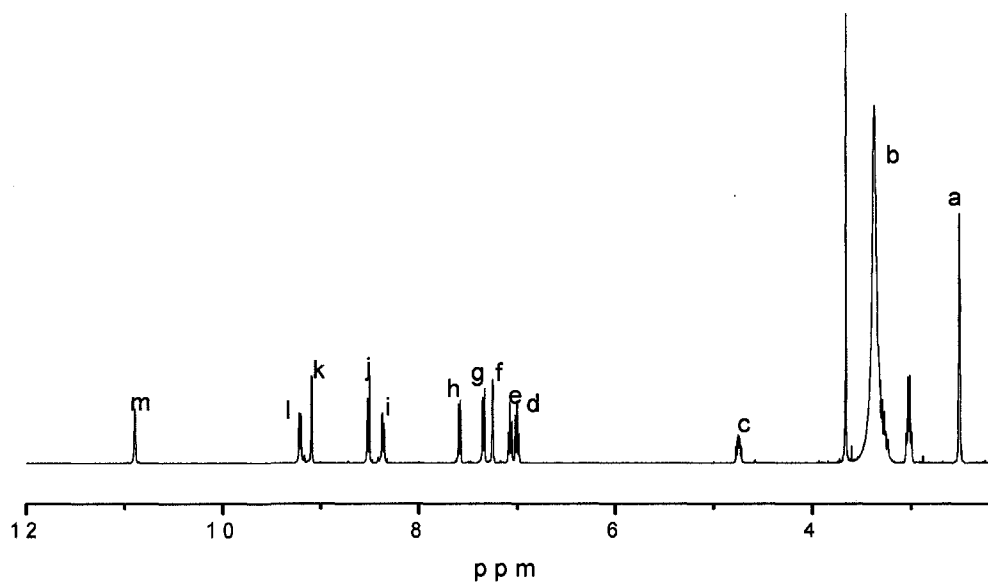


Figure 4.1 ^1H NMR of 5,5'-Bipyridine Tryptophan Ligand

^1H NMR (400 MHz, DMSO-d_6): 3.36-3.26 (2H, m), 3.66 (6H, s), 4.74 (2H, q, $J = 5.5\text{Hz}$), 7.00 (2H, t, $J = 7.7\text{Hz}$), 7.07 (2H, t, $J = 7.3\text{Hz}$), 7.24 (2H, s), 7.58 (2H, d, $J = 7.7\text{Hz}$), 8.36 (2H, dd, $J = 8.4, 2.2\text{Hz}$), 8.51 (2H, d, $J = 8.4\text{Hz}$), 9.09 (2H, s), 9.19 (2H, d, $J = 7.7\text{Hz}$), 10.88 (2H, s)

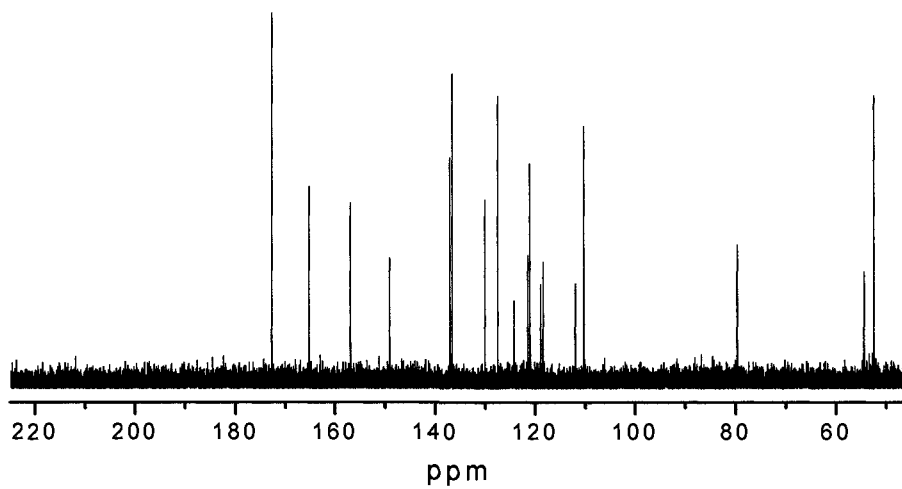


Figure 4.2 ^{13}C NMR of 5,5'-Bipyridine Tryptophan Ligand

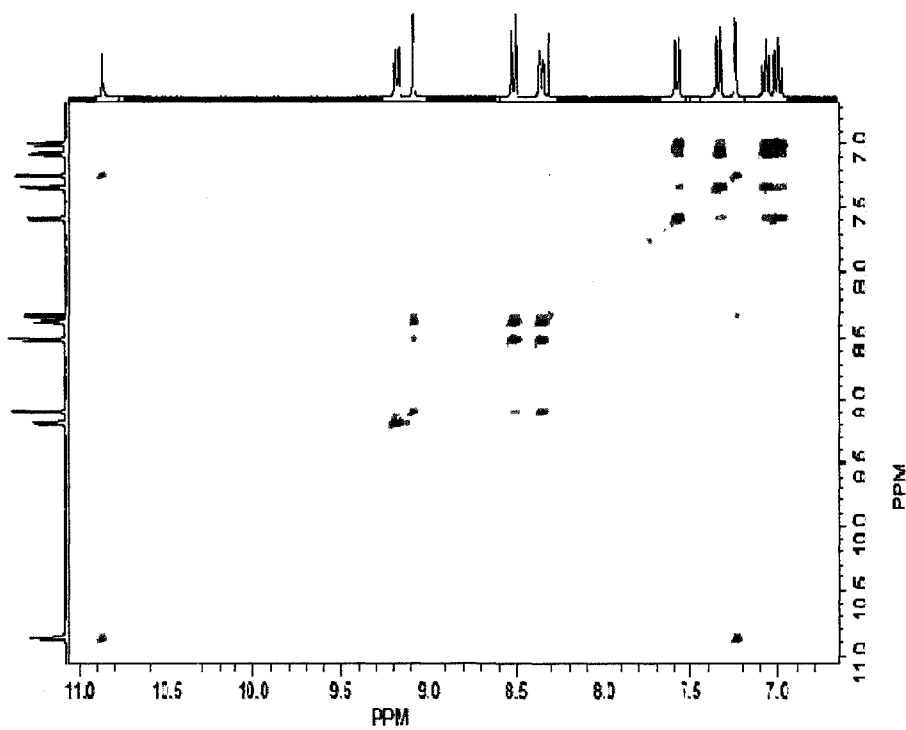


Figure 4.3 ^1H - ^1H COSY NMR of 5,5'-Bipyridine Tryptophan Ligand

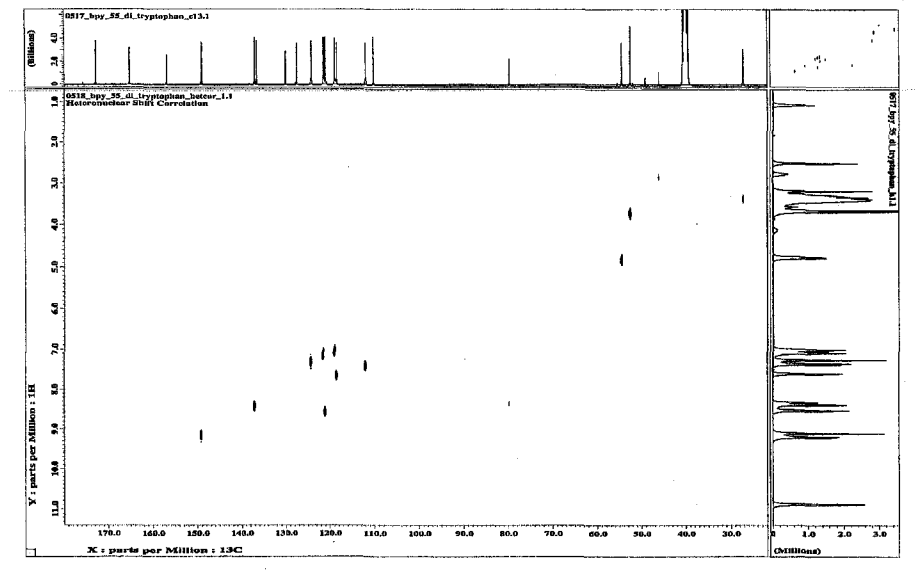


Figure 4.4 ^1H - ^{13}C HETCOR NMR of 5,5'-Bipyridine Tryptophan Ligand

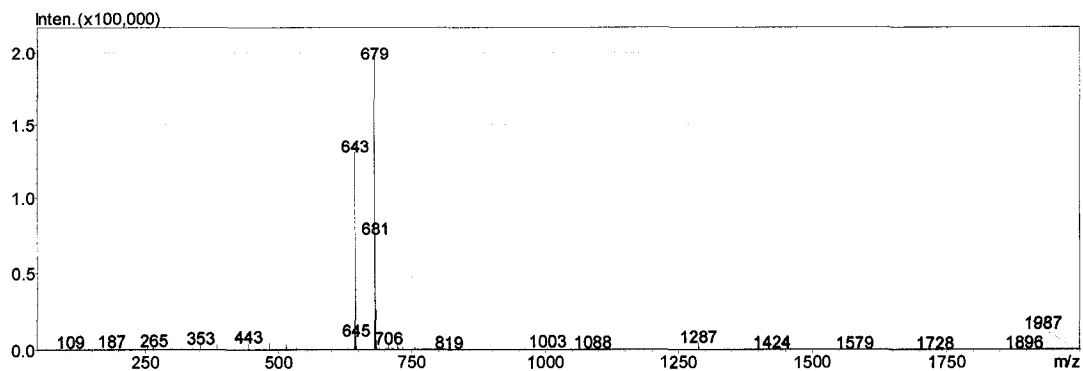


Figure 4.5 LC-MS ESI (-Ve) of 5,5'-Bipyridine Tryptophan Ligand

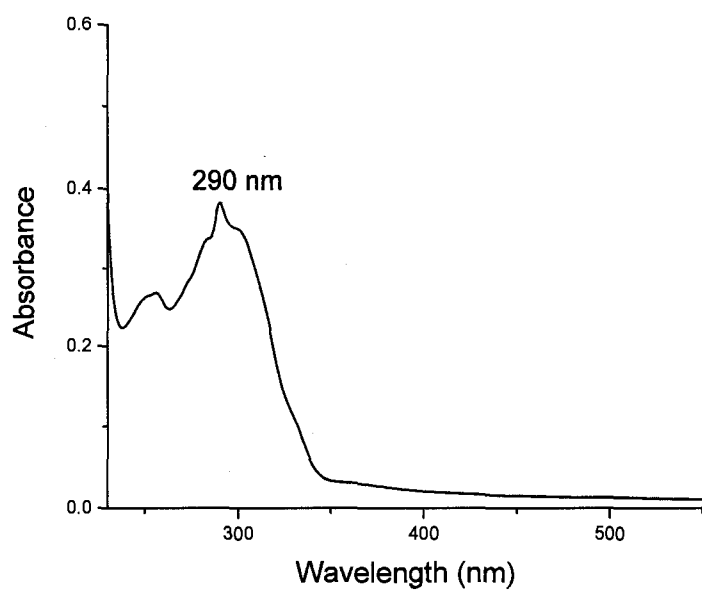


Figure 4.6 UV-Vis Spectrum of 5,5'-Bipyridine Tryptophan Ligand

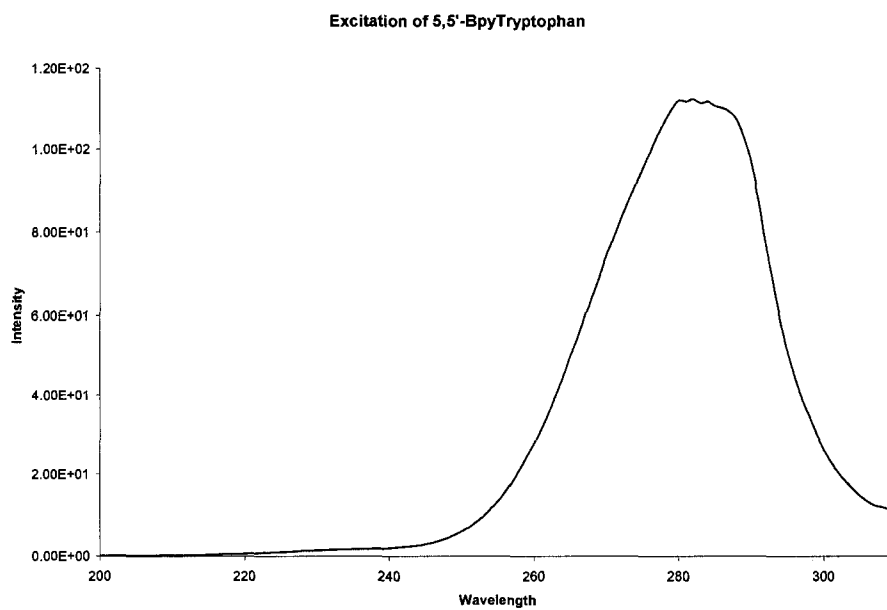


Figure 4.7 Excitation Spectrum of 5,5'-Bipyridine Tryptophan Ligand

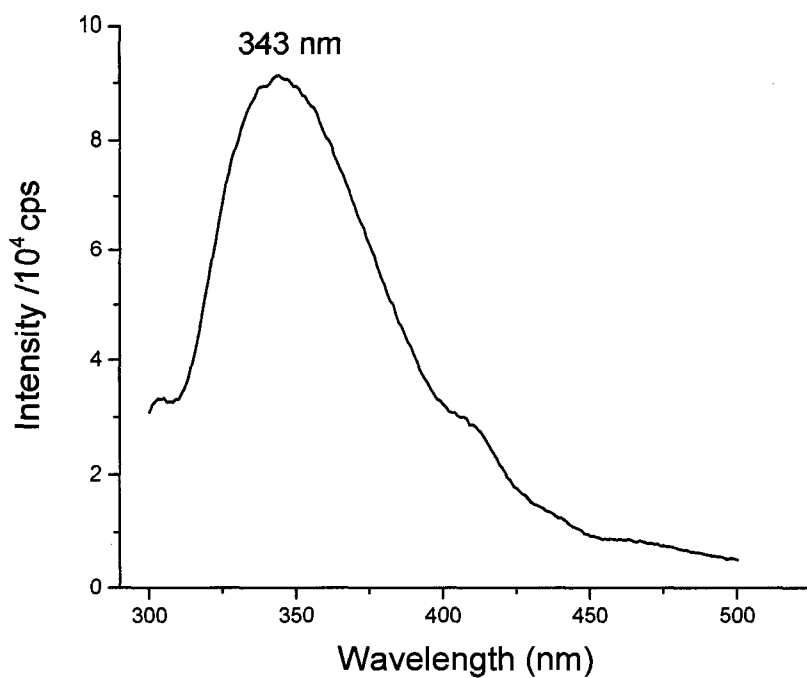


Figure 4.8 Emission Spectrum of 5,5'-Bipyridine Tryptophan Ligand

4.1.2 Emission of 5,5'-Bpy Tryptophan [12.5×10^{-6} M] Vs Variable DCP [50 μ M to 5 mM] [(at Exci 290 nm) (sol. Acetonitrile)]

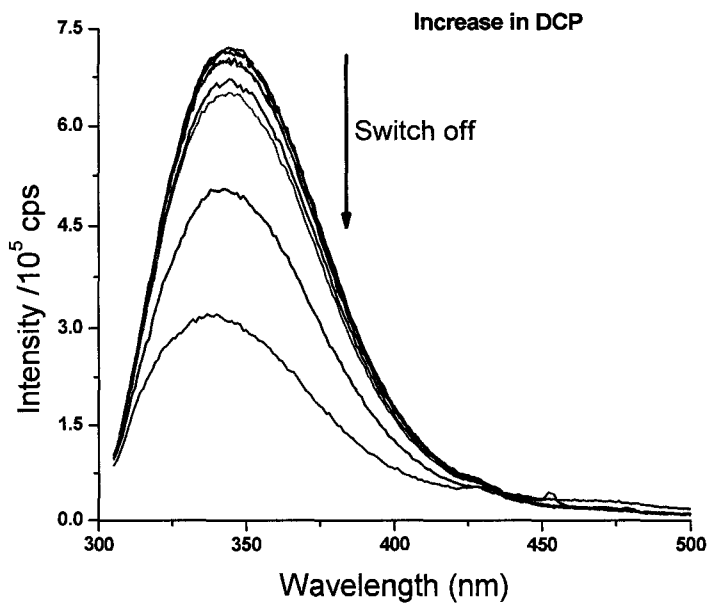


Figure 4.9 Emission Spectrum of 5,5'-Bpy Tryptophan with DCP

Association Constant: $K = 353 \pm 45 \text{ M}^{-1}$

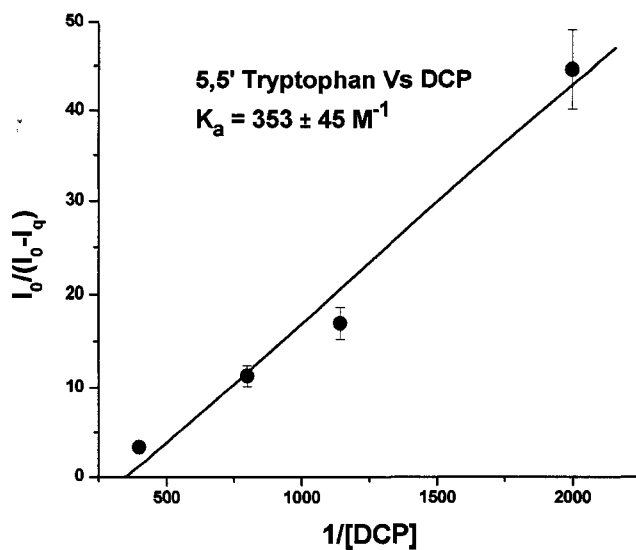


Figure 4.10 Association Constant of 5,5'-Bpy Tryptophan with DCP

Figure 4.9 shows the emission of 12.5 μM 5,5'-Bpy Tryptophan with various DCP (50 μM to 5 mM) concentrations excited at 290 nm. This ligand shows similar behavior (switch off) as 4,4'-Bipyridine tryptophan and with higher association constant. The emission quenches and shows hypsochromic shift as the concentration of DCP increases. At the initial concentrations, emission quenches slowly and after that emission it quenches rapidly.

4.1.3 Emission of 5,5'-Bpy Tryptophan [15×10^{-6} M] Vs Variable HCl [0 μ M to 54 μ M] [(at Exci 290 nm) (sol. Acetonitrile)]

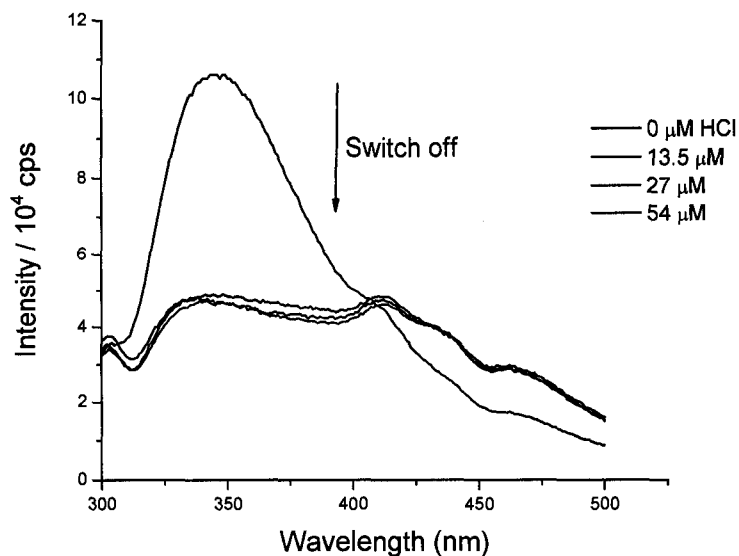


Figure 4.11 Emission Spectrum of 5,5'-Bpy Tryptophan with HCl

4.1.4 Emission of 5,5'-Bpy Tryptophan [7×10^{-6} M] Vs Variable DMMP [0 μ M to 345 μ M] [(at Exci 290 nm) (sol. Acetonitrile)]

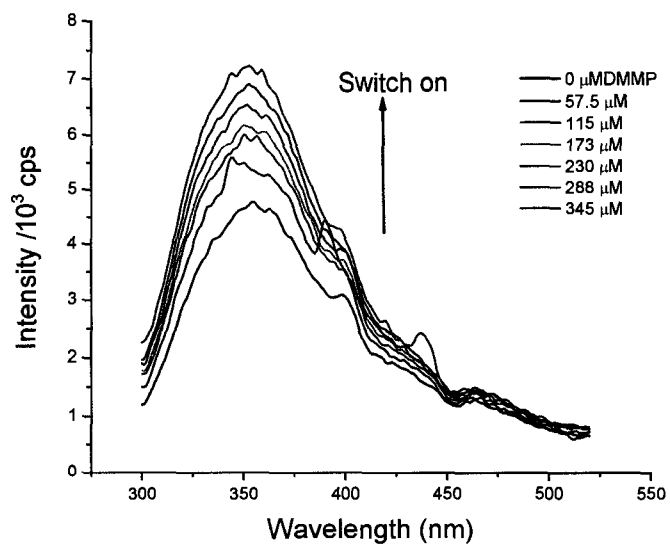


Figure 4.12 Emission Spectrum of 5,5'-Bpy Tryptophan with DMMP

Association Constant: $K = (2.6 \pm 0.9) \times 10^3 \text{ M}^{-1}$

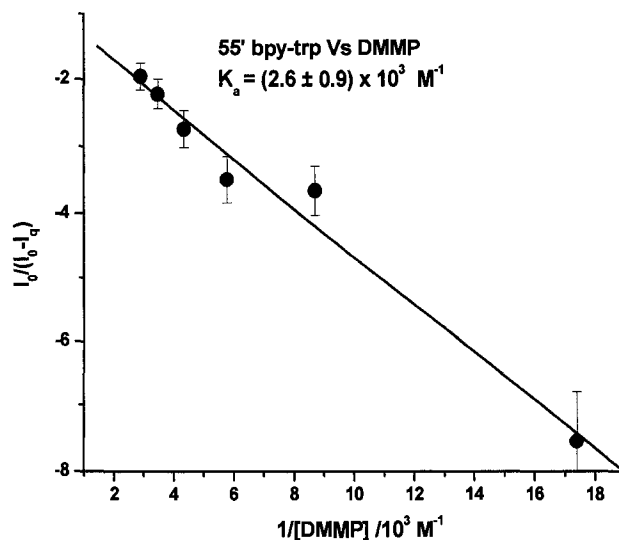
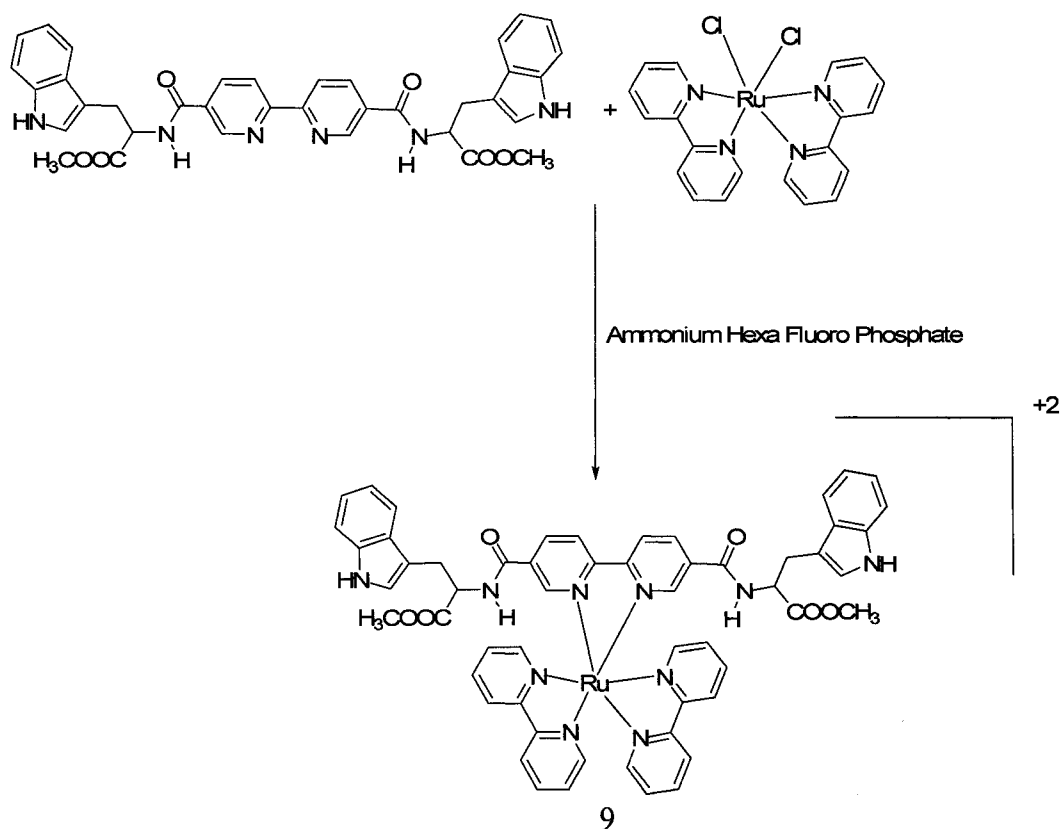


Figure 4.13 Association Constant of 5,5'-Bpy Tryptophan with DCP

Figure 4.11 shows the emission spectrum of 5,5'-Bpy Tryptophan with HCl. The emission was quenched drastically on the first addition of HCl, and then remained constant. Figure 4.12 shows the emission of 5,5'-ligand with DMMP. Here it differs from the 4,4'-ligand, and has a very high association constant (Figure 4.13). This could be attributed to the change in the position of bipyridyl ring.

4.1.5 Preparation of Ru(bpy)₂(5,5'-Bpy Tryptophan) Complex



Scheme 4.2 Synthetic Scheme of Preparation of Ru(bpy)₂(5,5'-Bpy Tryptophan) Complex

387mg of 4,4'-Bipyridine Tryptophan ligand(7) and 243mg of cis-(bpy)₂ RuCl₂·2H₂O (4) were taken in a sealed tube and heated at 110° C overnight, after cooling to room temperature any unreacted compound was filtered off and to the solution 200mg of ammonium hexafluorophosphate was added , this precipitate was filtered off and washed with cold water and cold ethanol to give Ru(bpy)₂(5,5'-Bpy Tryptophan) compound (9). Figure 4.14.shows the ¹H NMR, Figure 4.15.shows the LCMS spectrum, Figure 4.16 shows the UV-Vis spectrum which has two absorbance values, one at 440nm

is due to the ruthenium metal center and the other at 290 nm is due to the tryptophan.

Figure 4.17 shows the emission spectrum of Ru(bpy)₂(5,5'-Bpy Tryptophan) Complex.

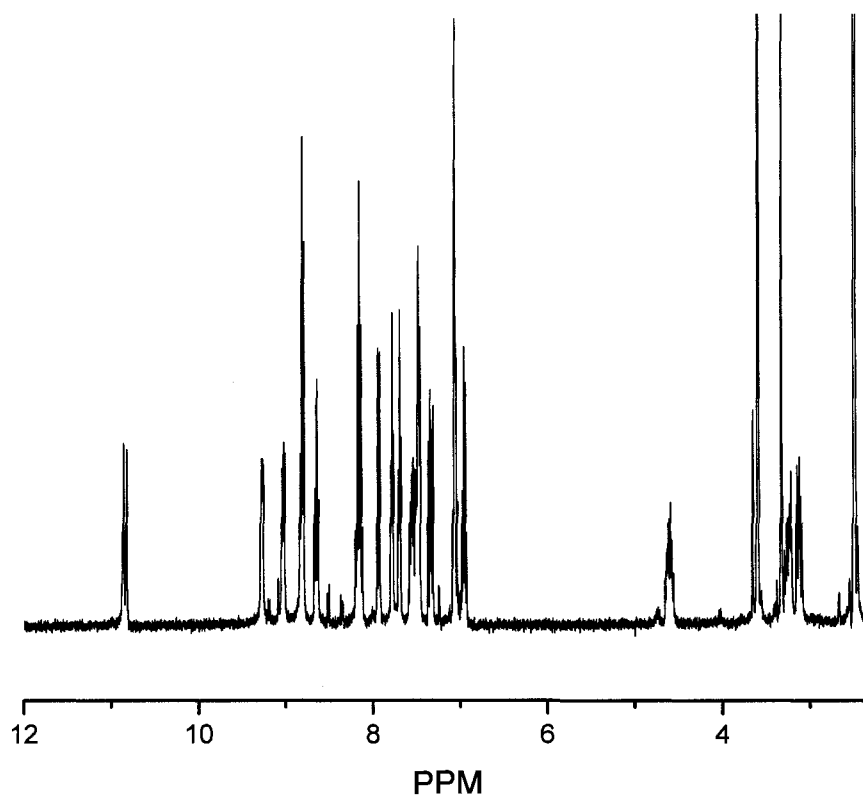


Figure 4.14 ¹H NMR of Ru(bpy)₂(5,5'-Bpy Tryptophan) Complex

¹H NMR (400 MHz, DMSO-d₆): δ 3.10-3.30 (4H, m), 3.60 (6H, d, *J* = 3.6Hz), 4.59 (2H, m), 6.92-7.09 (6H, m), 7.31-7.37 (2H, m), 7.46-7.58 (6H, m), 7.69 (2H, t, *J* = 5.1Hz), 7.79 (2H, t, *J* = 5.4Hz), 7.93 (2H, d, *J* = 9.1Hz), 8.11-8.20 (4H, m), 8.64 (2H, m), 8.79-8.83 (4H, m), 9.01-9.04 (2H, m), 9.27 (2H, dd, *J* = 7.3, 3.3Hz).

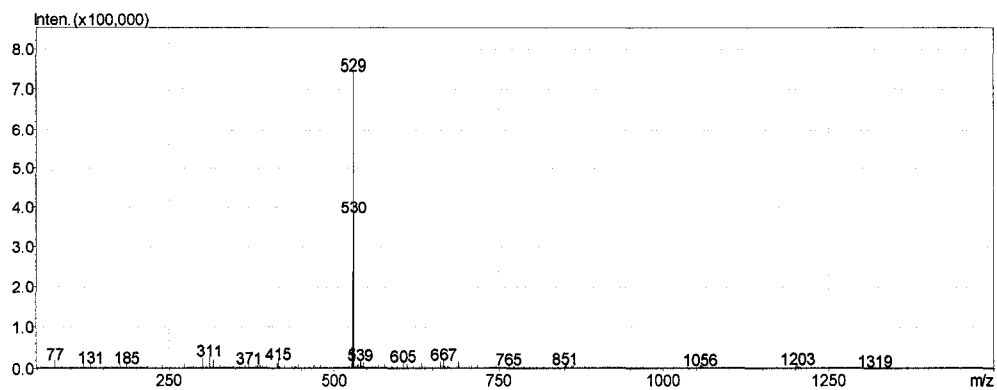


Figure 4.15 LC-MS ESI (+Ve) mode of Ru(bpy)₂(5,5'-Bpy Tryptophan) Complex

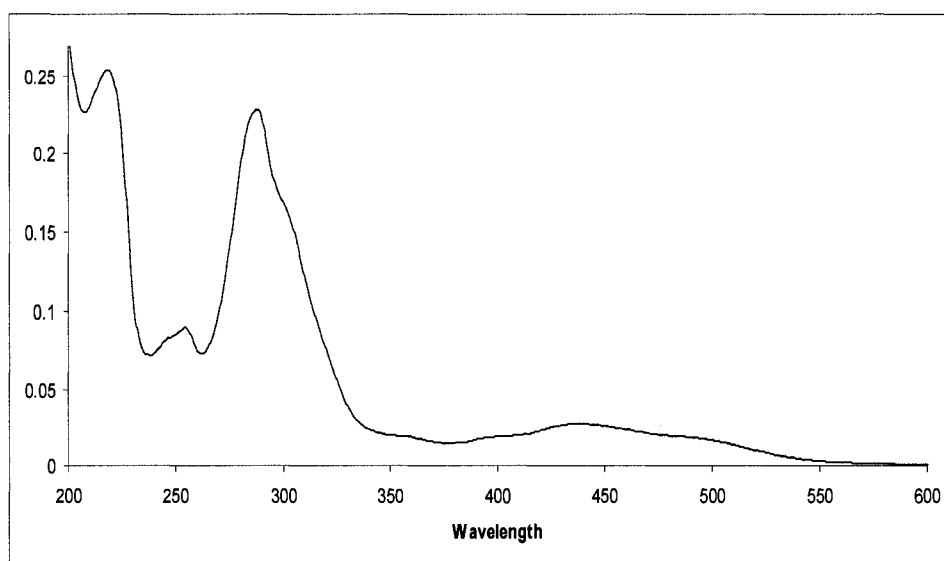


Figure 4.16 UV-Vis Spectrum of Ru(bpy)₂(5,5'-Bpy Tryptophan) Complex

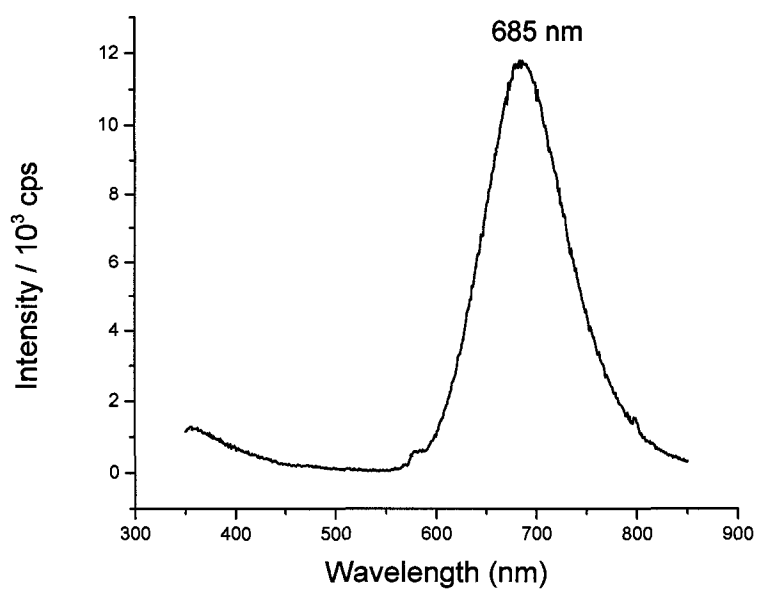


Figure 4.17 Emission Spectrum of Ru(bpy)₂(5,5'-Bpy Tryptophan) Complex

4.1.6 Emission of Ru(bpy)₂(5,5'-Bpy Tryptophan) Complex [5x10⁻⁶M] Vs Variable DCP [50 μM to 875 μM] (at Exci 290 nm)

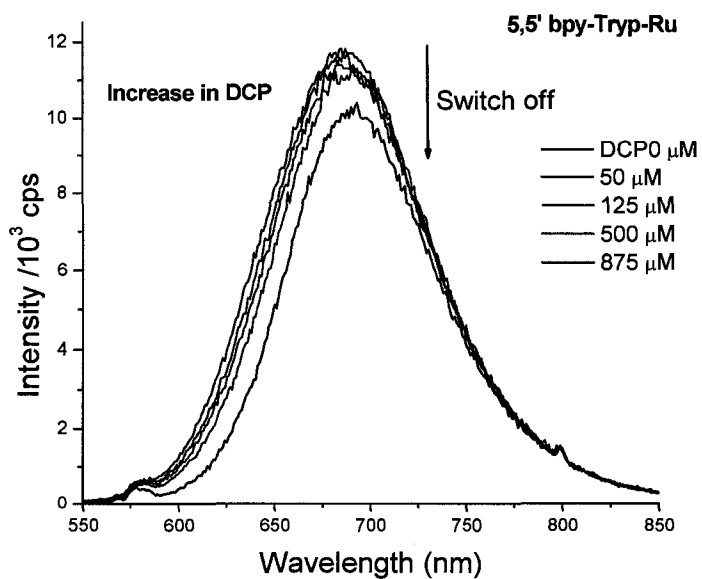


Figure 4.18 Emission Spectrum of Ru(bpy)₂(5,5'-Bpy Tryptophan) Complex with DCP

Association Constant : $K = (2.6 \pm 0.9) \times 10^3 \text{ M}^{-1}$

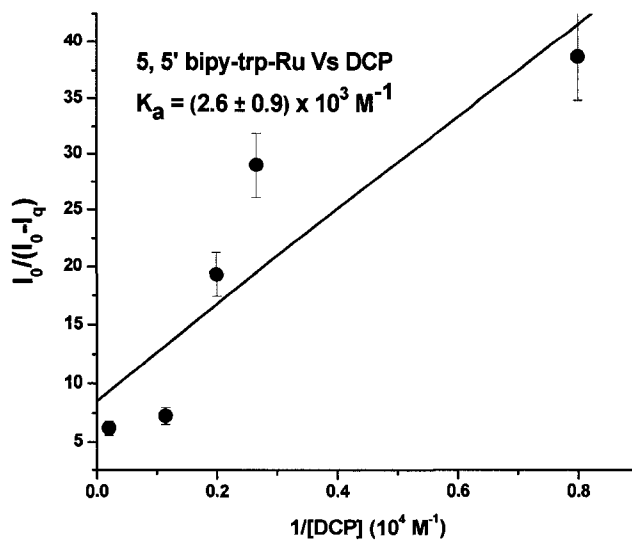


Figure 4.19 Association Constant of $\text{Ru}(\text{bpy})_2(5,5'\text{-Bpy Tryptophan})$ Complex with DCP

Figure 4.18 shows the emission of $5\mu\text{M}$ $\text{Ru}(\text{bpy})_2(5,5'\text{-Bpy Tryptophan})$ Complex with various DCP ($50\mu\text{M}$ to $875\mu\text{M}$) concentrations. This complex acts as a switch off sensor, as the DCP concentration increases emission of the complex decreases and shows a 7 nm bathochromic shift. Association constant (Figure 4.19) for this complex was $(2.6 \pm 0.9) \times 10^3 \text{ M}^{-1}$.

4.1.7 Emission of Ru(bpy)₂(5,5'-Bpy Tryptophan) Complex [10x10⁻⁶M] Vs Variable HCl [0 μM to 450 μM] (at Exci 290 nm)

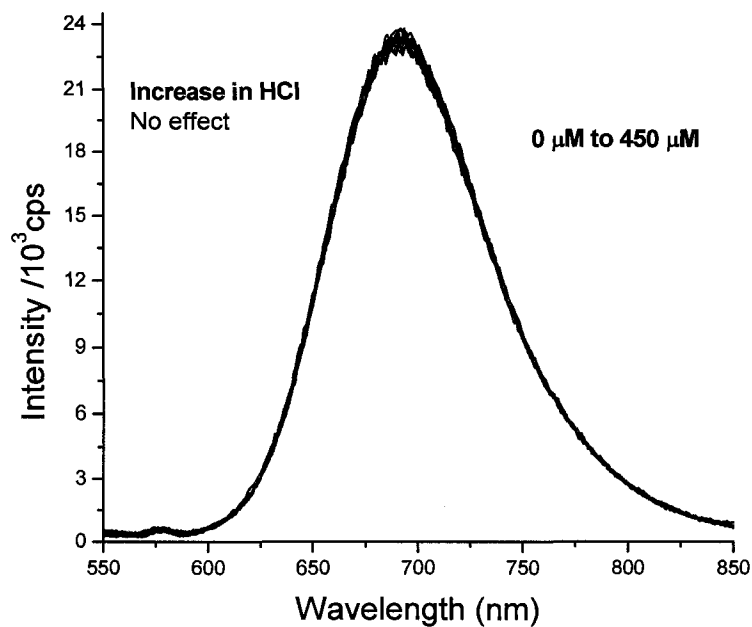


Figure 4.20 Emission Spectrum of Ru(bpy)₂(5,5'-Bpy Tryptophan) Complex with HCl

4.1.8 Emission of Ru(bpy)₂(5,5'-Bpy Tryptophan) Complex [7.5x10⁻⁶M] Vs Variable DMMP [0 μM to 450 μM] (at Exci 290 nm)

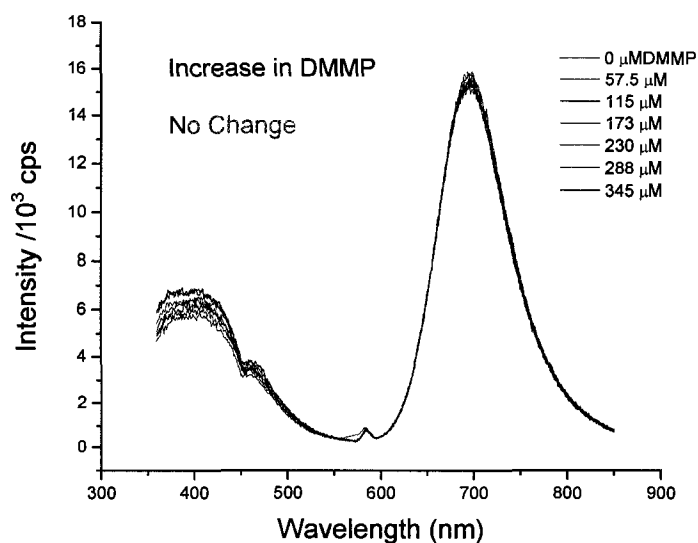
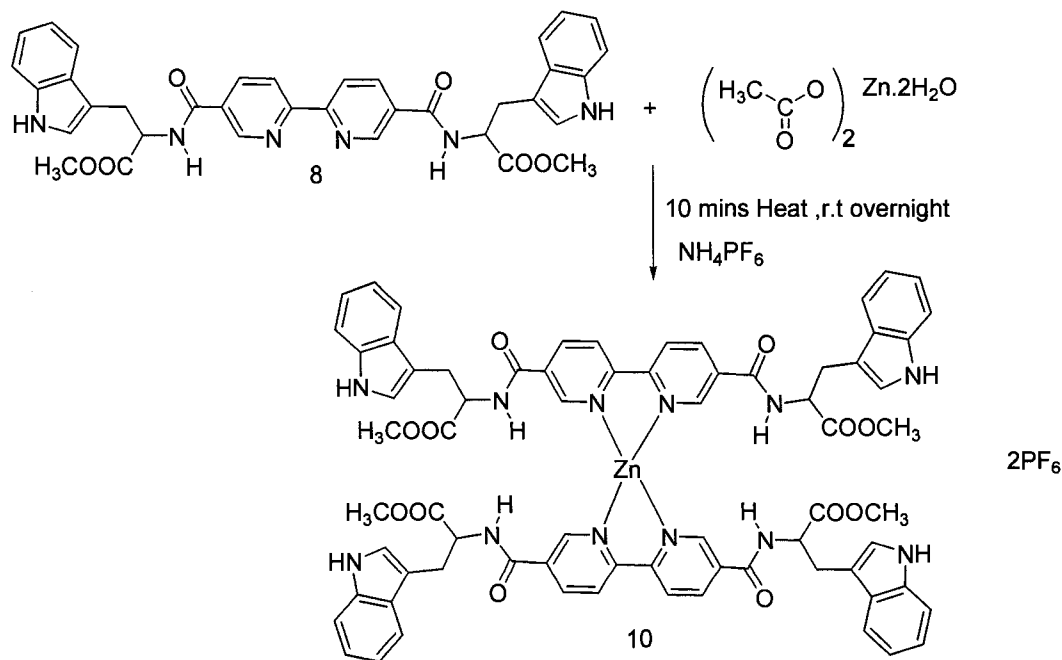


Figure 4.21 Emission Spectrum of Ru(bpy)₂(5,5'-Bpy Tryptophan) Complex with DMMP

Figures 4.20 and 4.21 show the emission of Ru(bpy)₂(5,5'-Bpy Tryptophan) complex with HCl and DMMP respectively. Increasing concentrations of HCl or DMMP will not change the intensity of the complex. This is ascribed to steric factors.

4.1.9 Preparation of Zinc (5,5'-Bpy Tryptophan)₂ Complex

.110 g (0.5 mmol) of zinc acetate dihydrate and 0.690 g (1mmol) of 5,5'-Bpy Tryptophan were dissolved in acetonitrile by warming for 10 mins, then stirring was continued over night at room temperature. To this 0.5 g of ammonium hexa fluorophosphate was added to get the required complex. A light yellow color precipitate (10) was formed when ammonium hexa fluorophosphate was added; this precipitate was filtered off and washed with cold ether to remove any impurities.



Scheme 4.3 Synthetic Scheme of Preparation of 5,5'-Bipyridine Tryptophan Zinc Complex

4.2.0 Emission of 11.75 μM $\text{Zn}(5,5'\text{BpyTrp})_2$ Complex Vs DCP [0 μM to 282.5 μM] (at Exci 290 nm)

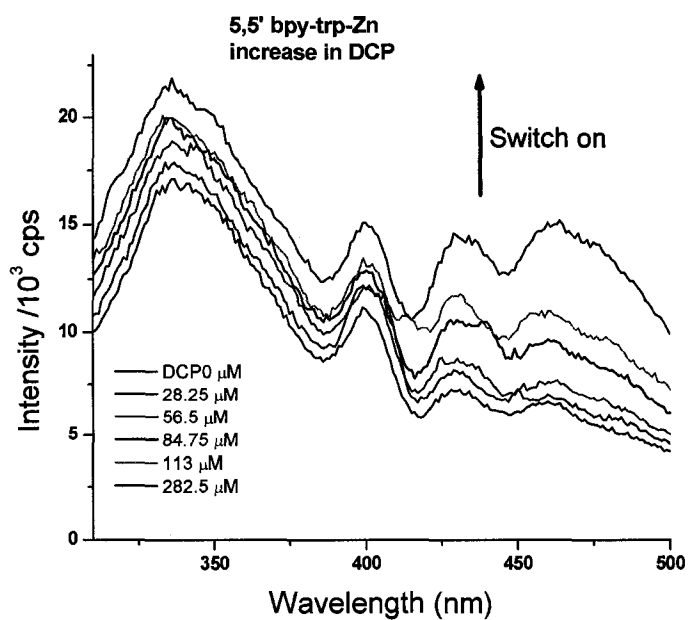


Figure 4.22 Emission Spectrum of $\text{Zn}(5,5'\text{BpyTrp})_2$ Complex with DCP

Association Constant: $K = (7.4 \pm 0.9) \times 10^3 \text{ M}^{-1}$

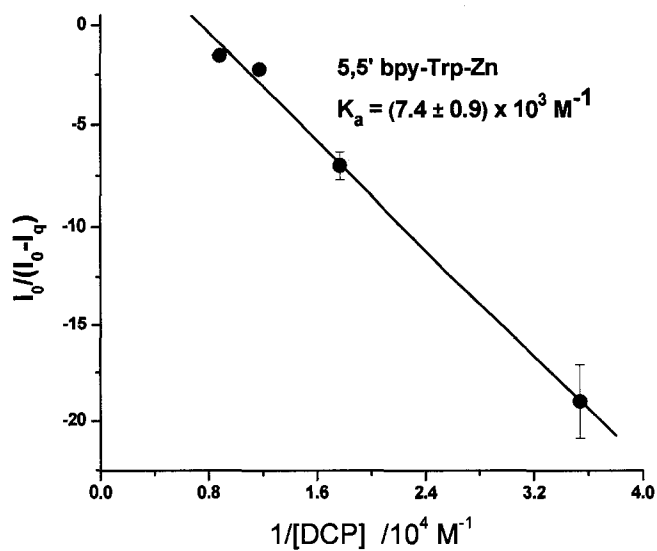


Figure 4.23 Association Constant of $\text{Zn}(5,5'\text{BpyTrp})_2$ Complex with DCP

Figure 4.22 shows the emission of 11.75 μM $\text{Zn}(5,5'\text{-Bpytryp})_2$ Complex Vs various DCP (0 μM to 282.5 μM) concentrations. Like 4,4' zinc complex(Figure 3.25), this zinc complex has two emissions, the emission at 340 nm is the tryptophan emission and the emissions at 440 and 460 nm are the zinc emissions. Increasing DCP concentration increases the emission intensity at both the tryptophan and the zinc regions. The association constant for this complex is $(7.4 \pm 0.9) \times 10^3 \text{ M}^{-1}$. When compared to the ruthenium complex, the association constant of the zinc complex is weak. This complex shows switch on behavior and has a 4 nm bathochromic shift.

4.2.1 Emission of 11.75 μM $\text{Zn}(5,5'\text{BpyTryp})_2$ Complex Vs Variable HCl [0 μM to 508 μM] (at Exci 290 nm)

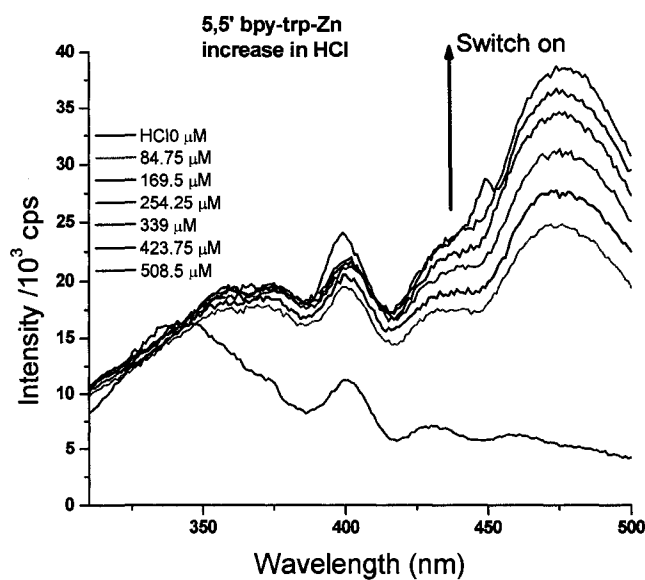


Figure 4.24 Emission Spectrum of $\text{Zn}(5,5'\text{BpyTryp})_2$ Complex with HCl

Association Constant: $K = (6.0 \pm 0.5) \times 10^3 \text{ M}^{-1}$

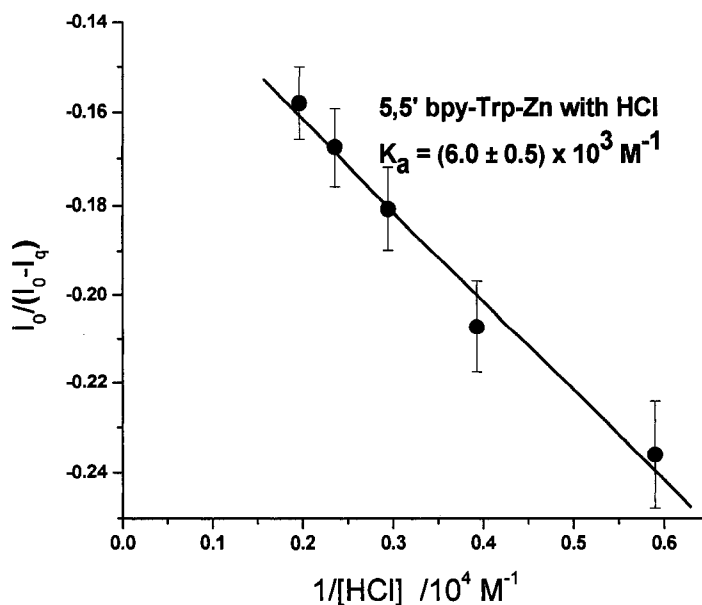


Figure 4.25 Association Constant of $\text{Zn}(5,5'\text{BpyTrp})_2$ Complex with HCl

Figure 4.24 shows the Emission of $11.75 \mu\text{M}$ $\text{Zn}(5,5'\text{BpyTrp})_2$ Complex with various HCl ($0 \mu\text{M}$ to $508 \mu\text{M}$) concentrations. Figure 4.25 shows the association constant of $\text{Zn}(5,5'\text{BpyTrp})_2$ Complex with HCl. This complex demonstrated very good sensitivity with switch on behavior corresponding to a 16 nm bathochromic shift with increasing concentrations.

4.2.2 Emission of 11.75 μM Zn(5,5'BpyTrp)₂ Complex Vs Variable DMMP
[0 μM to 280 μM] (at Exci 290 nm)

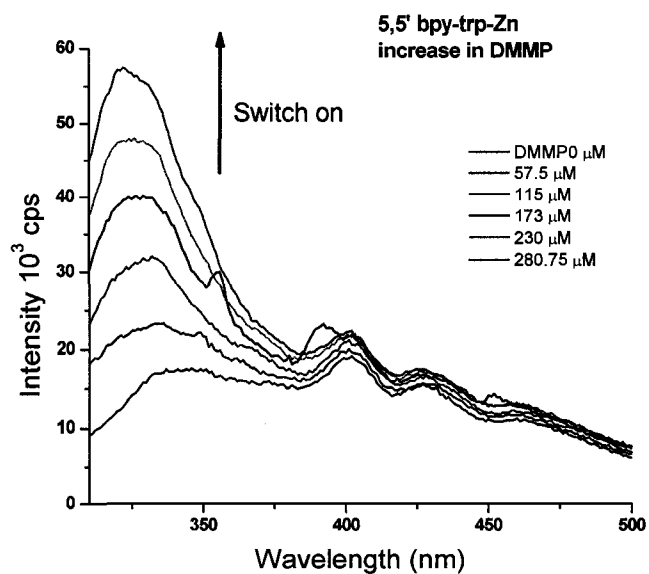


Figure 4.26 Emission Spectrum of Zn(5,5'BpyTrp)₂ Complex with DMMP

Association Constant: $K = 14 \pm 7 \text{ M}^{-1}$

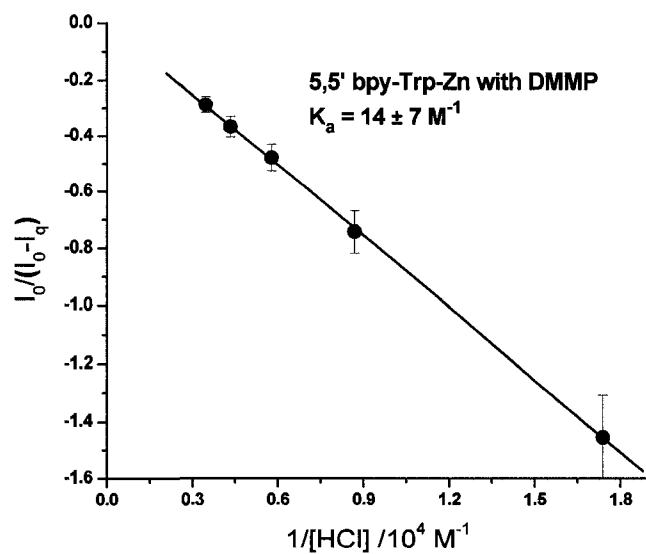


Figure 4.27 Association Constant of Zn(5,5'BpyTrp)₂ Complex with DMMP

Figure 4.26 shows the emission of 11.75 μM $\text{Zn}(5,5'\text{BpyTrp})_2$ complex with various DMMP (0 μM to 280 μM) concentrations. Here it shows switch on behavior with a 21 nm hypsochromic shift at the tryptophan region and as expected it gives a very weak association constant value of (14 ± 7) .

Table 4.1 Association Constants of 5,5'-Bpy Tryptophan and its Complexes

	$K_{\text{DCP}} \text{ M}^{-1}$	$K_{\text{HCl}} \text{ M}^{-1}$	$K_{\text{DMMP}} \text{ M}^{-1}$
5,5'-Bipyridine tryptophan	353 ± 45		$(2.6 \pm 0.9) \times 10^3$
$\text{Ru}(\text{bpy})_2(5,5'\text{'-Bpy Tryptophan})$	$(2.6 \pm 0.9) \times 10^3$	No change	No change
Zinc (5,5'-Bpy tryp) ₂	$(7.4 \pm 0.9) \times 10^3$	$(6.0 \pm 0.5) \times 10^3$	14 ± 7

Table 4.1 shows the association constants of 5,5'-Bipyridine tryptophan receptor and its ruthenium and zinc complexes with nerve gas analogs DCP, DMMP and hydrolyzed product HCl. 5,5' zinc complex shows better sensitivity towards DCP when compare to the 5,5' ruthenium complex.

CHAPTER V

SYNTHESIS AND SPECTRAL STUDIES OF FULL SENSOR SYSTEM

5.1 Introduction

The field of optical chemical sensors has been a growing research area over the last thirty years. The Cambridge definition is an appropriate definition for a chemical sensor, which indicates “chemical sensors are miniaturized devices that can deliver real-time and on-line information in the presence of specific compounds or ions in even complex samples”.⁷³

The bottom up approach was used to build up nanosensors for nerve gas agents (Figure 1.13). Silica nanoparticles and quantum dots are used as a solid base for the nanosensors. Silica NPs made are monodispersed and are small sized (40 nm), these small silica NPs can produce uniform monolayers which can be used on glass slides or on any chip. Quantum dots can also be used in sensors because, they have large range of wavelength and we can tune the properties based on the size of QDs.

Stilbene type monomer compounds are used in sensors, because they have excellent luminescent properties and can improve the signal intensity because of their inherent high conjugation.

Ruthenium, zinc and europium metals were used to synthesize complexes. These highly conjugated metal complexes can shift the signal into the visible region and we can easily observe the signal.

4,4'-Bipyridine tryptophan and 5,5'-Bipyridine tryptophan were used as the receptors, these receptors can form adducts with the nerve gas analogs such as DCP and gives the signal. The assembling of the constituents (nanoparticles, monomer, complex and receptor) through a bottom up approach will enhance selectivity and sensitivity to the nanosensors.

In this chapter individual components will be discussed, firstly the discussion is based on emission properties with only the stilbene monomer, secondly, I will discuss the combination of silica NPs or QDs with the monomer and their properties with nerve gas analogs, and then the complete sensor synthesis and its spectral properties with DCP, DMMP and HCl will be discussed in the ensuing pages.

5.2 Spectral Properties of Stilbene Monomer

5.2.1 Emission of Stilbene Monomer with DCP (excitation 290 nm)

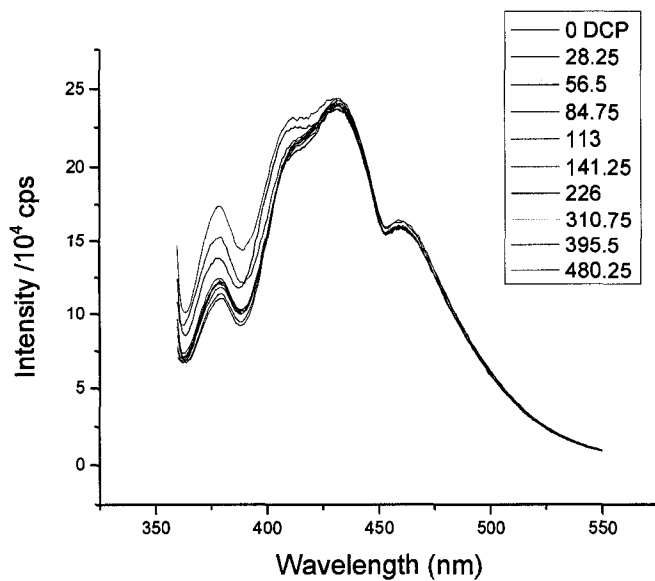


Figure 5.1 Emission Spectrum of Stilbene Monomer with DCP

5.2.2 Emission of Stilbene Monomer with HCl

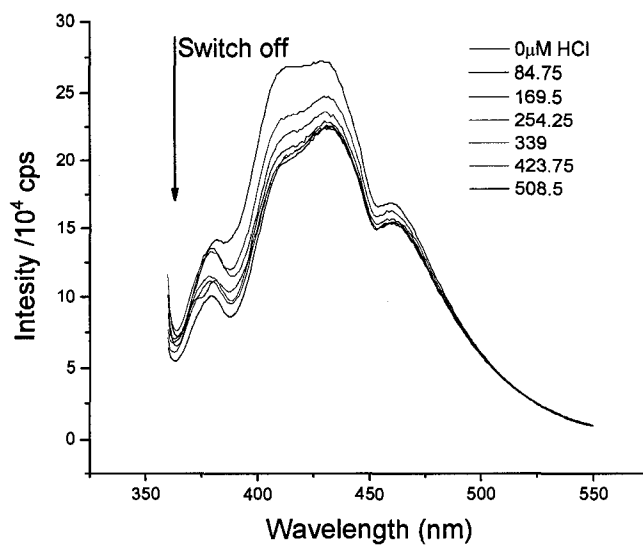


Figure 5.2 Emission Spectrum of Stilbene Monomer with HCl

Association Constant: $K = (6.4 \pm 0.4) \times 10^3 \text{ M}^{-1}$

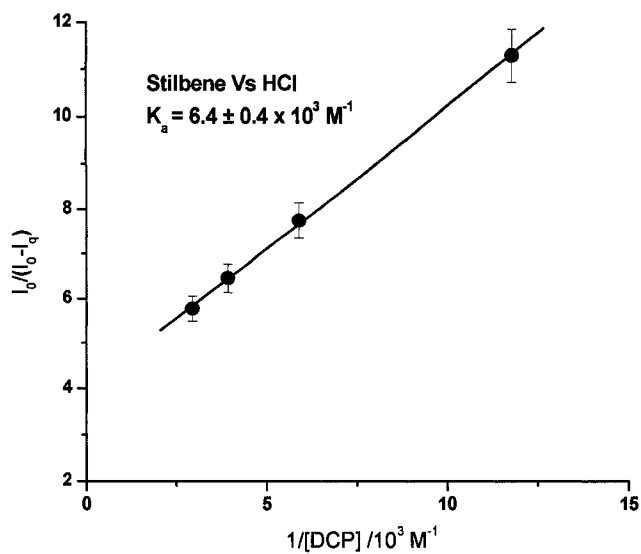


Figure 5.3 Association Constant of Stilbene Monomer with HCl

5.2.3 Emission of Stilbene Monomer with DMMP

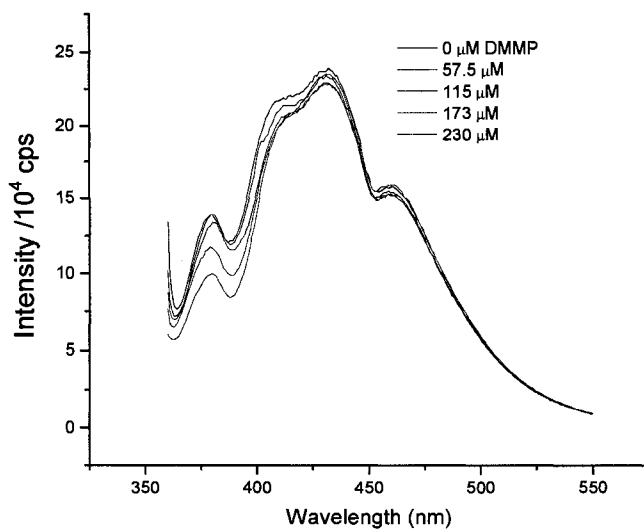


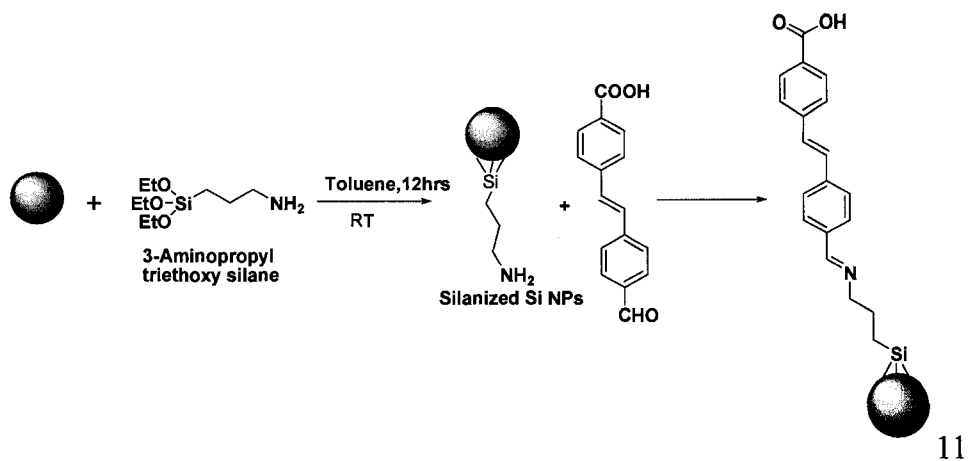
Figure 5.4 Emission Spectrum of Stilbene Monomer with DMMP

Figures 5.1, 5.2 and 5.4 show the emission of stilbene monomer with increasing concentrations of DCP, HCl and DMMP. All these emission spectrums were obtained by exciting the system at 290 nm and the emission maxima was observed at 430 nm. The emission maxima of the stilbene monomer does not show any change on addition of DCP or DMMP as it does not carry a receptor which will attach to the target analyte. Stilbene shows a faint interaction (switch off behavior) with HCl and the association constant was found to be $(6.4 \pm 0.4) \times 10^3 \text{ M}^{-1}$ (Figure 5.3).

5.3 Synthesis and Spectral Studies of Silica Nanoparticles with Stilbene Monomer

5.3.1 Synthesis of Silica NPs with Stilbene Monomer

First silica NPs were silanized with APTS according to procedure 2.4. Then 100 mg of these silanized silica NPs were reacted with 100 mg of stilbene monomer in toluene at room temperature for 12 hours. Then it was filtered and washed with hot ethanol to remove any excess stilbene monomer. The aldehyde group of the monomer is more reactive and reacts with the amine group of silanized silica NPs and forms enamine bond. This compound was characterized by the emission, absorption and IR spectrometry.



Scheme 5.1 Synthesis of Silica NPs with Stilbene Monomer

5.3.2 IR Spectra of Silica NPs with Stilbene Monomer

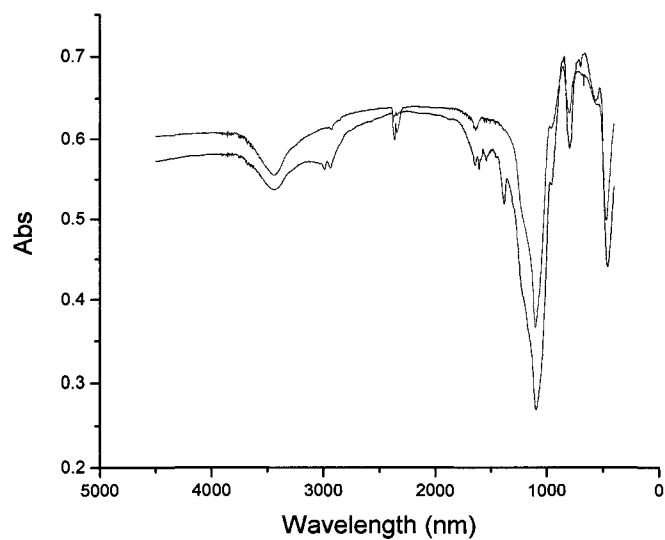


Figure 5.5 IR Spectra of Silica NPs with Stilbene Monomer

The peak (two spikes) around 3000 cm^{-1} in the silanized silica NPs disappears on binding to the stilbene monomer, this indicates the bond formation.

5.3.3 Emission of Silica NPs with Stilbene Monomer

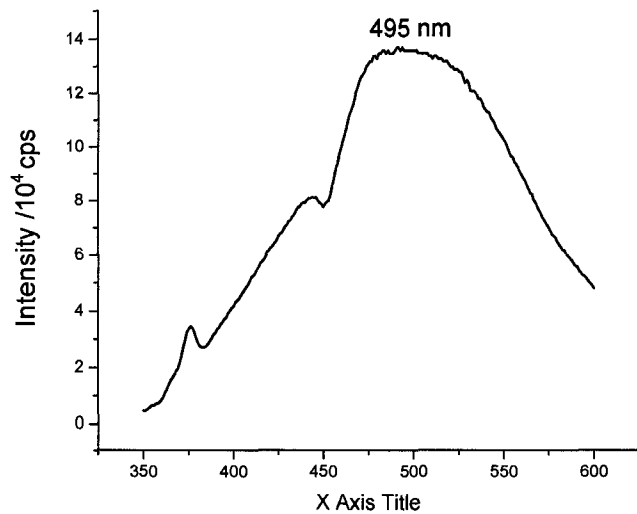


Figure 5.6 Emission Spectrum of Silica NPs with Stilbene Monomer

5.3.4 Emission of Silica NPs with Stilbene Monomer Vs Various DCP

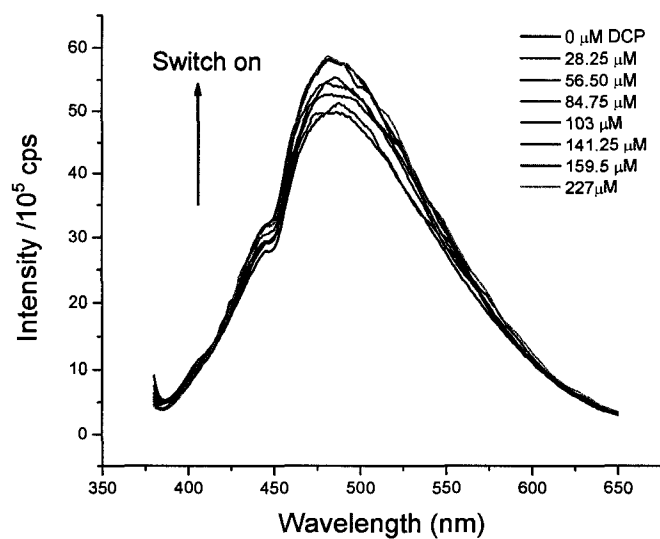


Figure 5.7 Emission Spectrum of Silica NPs with Stilbene Monomer with Various DCP

Association Constant: $(952 \pm 90) \text{ M}^{-1}$

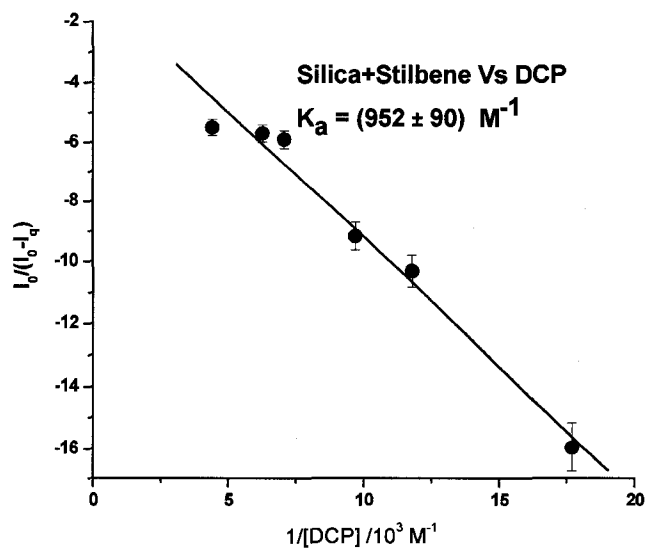


Figure 5.8 Association Constant of Silica NPs with Stilbene Monomer with Various DCP

5.3.5 Emission of Silica NPs with Stilbene Monomer Vs Various HCl

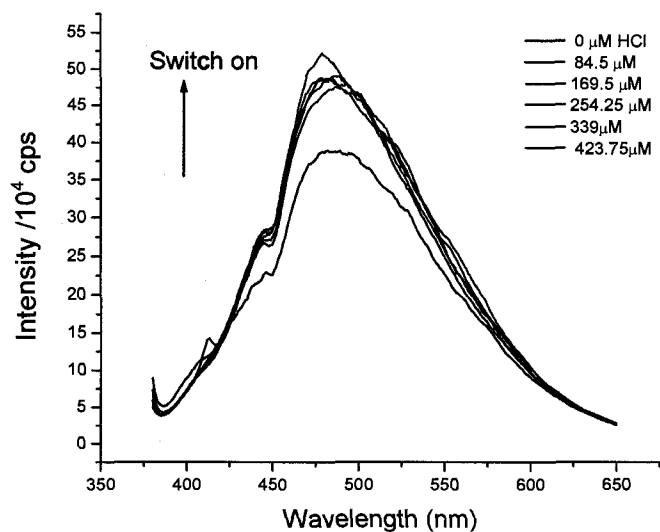


Figure 5.9 Emission Spectrum of Silica NPs with Stilbene Monomer Vs Various HCl

Association Constant: $(8 \pm 5) \times 10^3 \text{ M}^{-1}$

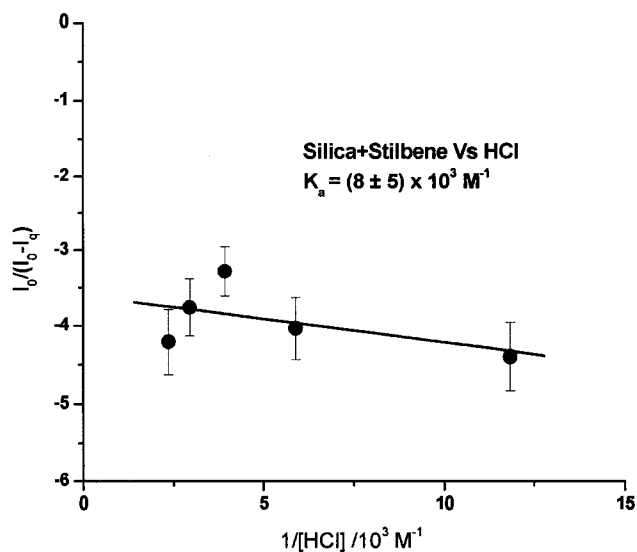


Figure 5.10 Association Constant of Silica NPs with Stilbene Monomer Vs Various HCl

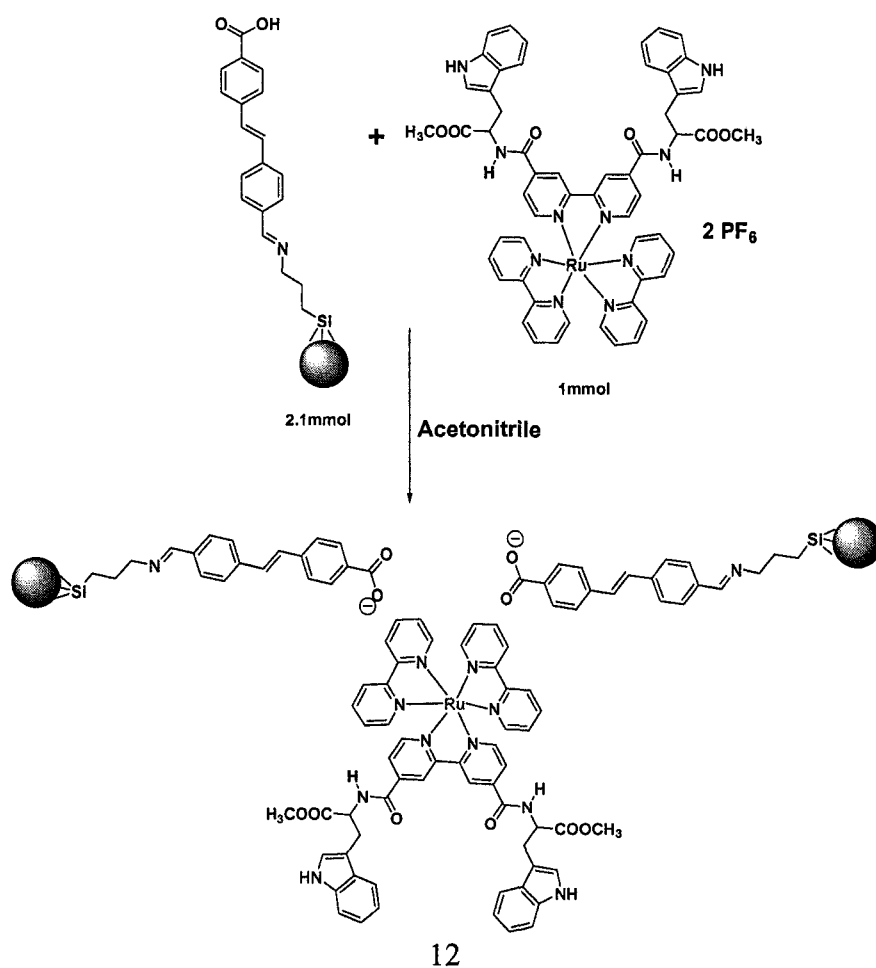
The emission spectrum of the stilbene monomer (Figure 5.6) after reacting with the silica NPs, shows the emission maxima at 495nm. This emission spectrum is different from the original stilbene monomer (Figure 2.16) which has an emission maxima at 445 nm. Figure 5.7 shows the Emission spectrum of silica NPs with stilbene monomer with various DCP concentrations. Emission of this compound increases with the increasing DCP concentrations (switch on) and shows 4 nm hypsochromic shift. Association constant of this compound is very weak (Figure 5.8) because there is no active receptor in this compound to react with the nerve gas analog.

Figure 5.9 shows the Emission spectrum of silica NPs with stilbene monomer with various concentrations of HCl. Emission increases with increasing

concentrations and shows a 7 nm hypsochromic shift. Figure 5.10 shows the Association constant of silica NPs with stilbene monomer with variable HCl concentrations.

5.4 Synthesis of Silica NPs + Stilbene Monomer + 4,4'-Bpy Tryp ruthenium Complex (Sensor I) and its Spectral Characterization

5.4.1 Synthetic Scheme of Sensor I



Scheme 5.2 Synthesis of Sensor I

1 mmol $\text{Ru}(\text{bpy})_2(4,4'\text{-Bpy Tryptophan})$ complex (compound 6) and 2.1 mmol silanized silica nanoparticles (compound 11) were dissolved in acetonitrile and

stirred overnight to form an ion pair between compound 6 and 11 (compound 12). Compound 12 was characterized with emission spectroscopy.

5.4.2 Emission of Silica NP + Stilbene Monomer (9.45 μM) + Ru(bpy)₂(4,4'-Bpy Tryptophan) (4.7 μM) (Sensor I) Vs Various DCP

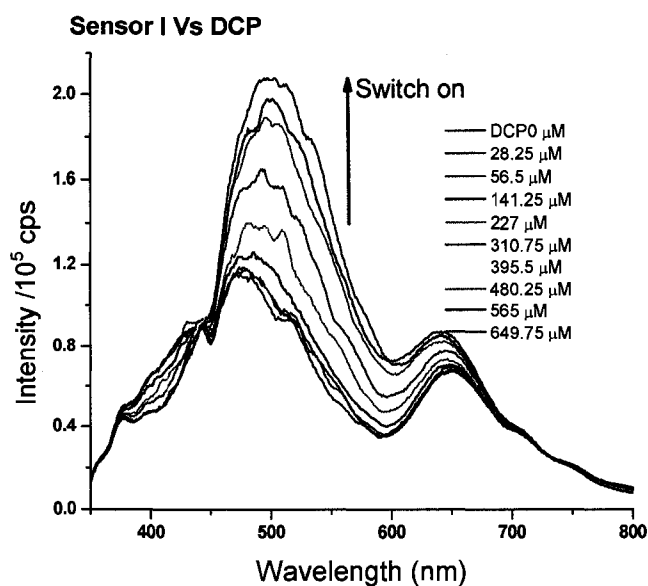


Figure 5.11 Emission Spectrum of Sensor I with Various DCP Concentrations

Association Constant: $K = 620 \pm 140 \text{ M}^{-1}$

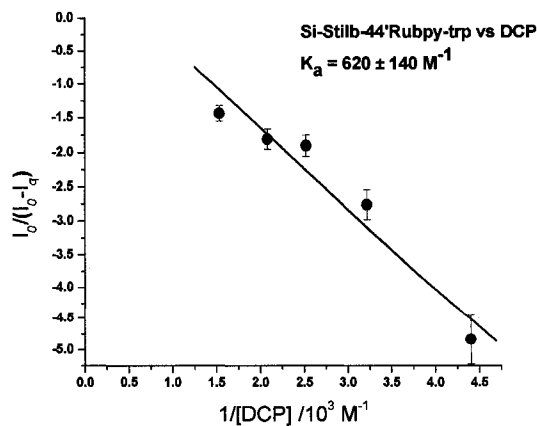


Figure 5.12 Association Constant of Sensor I with DCP

5.4.3 Emission of Silica NP + Stilbene Monomer (9.45 μM) + Ru(bpy)₂(4,4'-Bpy Tryptophan) (4.7 μM) (sensor I) Vs Various HCl

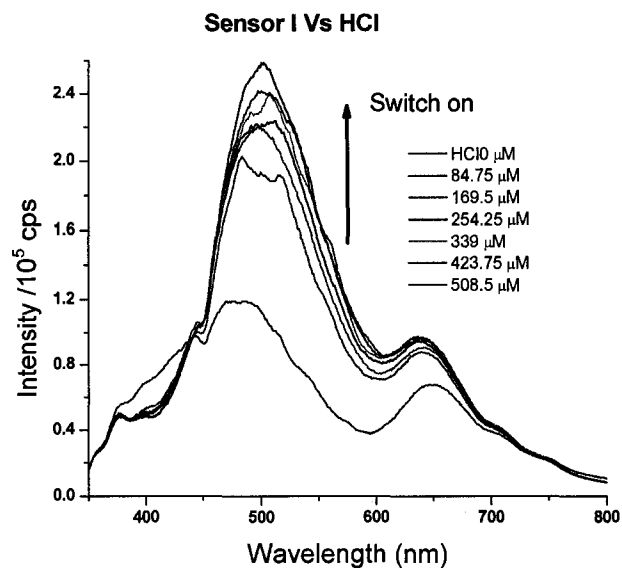


Figure 5.13 Emission Spectrum of Sensor I with HCl

Association Constant: $K = (1.2 \pm 0.5) \times 10^4 \text{ M}^{-1}$

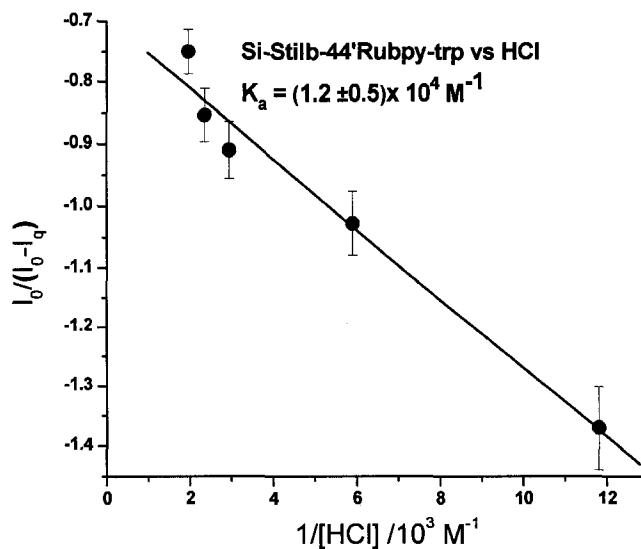


Figure 5.14 Association Constant of Sensor I with HCl

5.4.4 Emission of Silica NP + Stilbene Monomer (9.45 μM) + Ru(bpy)₂(4,4'-Bpy Tryptophan) (4.7 μM) (sensor I) Vs Various DMMP

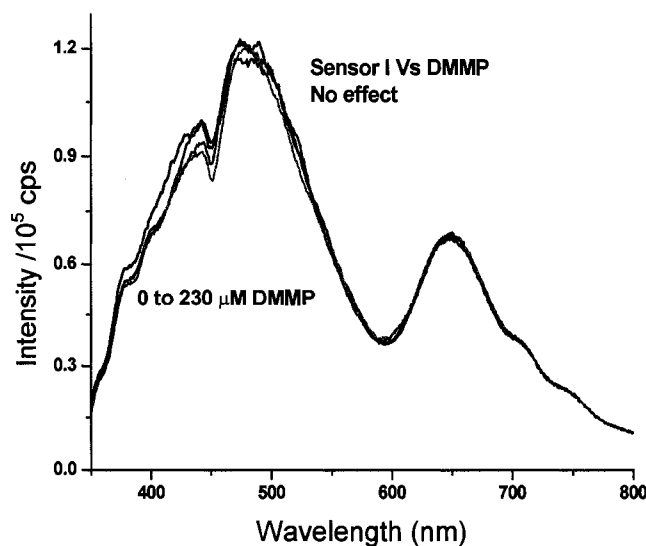


Figure 5.15 Emission Spectrum of Sensor I with DMMP

Figures 5.11, 5.13 and 5.15 show the emission spectra of sensor I. Sensor I has two emission maxima, one at 477 nm due to the stilbene monomer and the other at 650 nm due to the ruthenium complex. The emission spectrum (Figure 5.11) demonstrated switch on behavior with increasing concentrations of DCP. The emission due to the stilbene moiety increases with the increasing concentrations of DCP and displayed a 23 nm bathochromic shift. The ruthenium emission also increases with the increasing concentrations of DCP and here it shows a 11 nm hypsochromic shift. The association constant (Figure 5.12) was very weak and the value was found to be $(620 \pm 140) \text{ M}^{-1}$. This association constant value is very weak when compared to the bare 4,4'-Bpy ruthenium complex (Figure 3.21). This might be due to the interaction between free carboxylate ions and the free nitrogen on the receptor. Thereby the lone pair electrons are not freely available for binding with the target analyte.

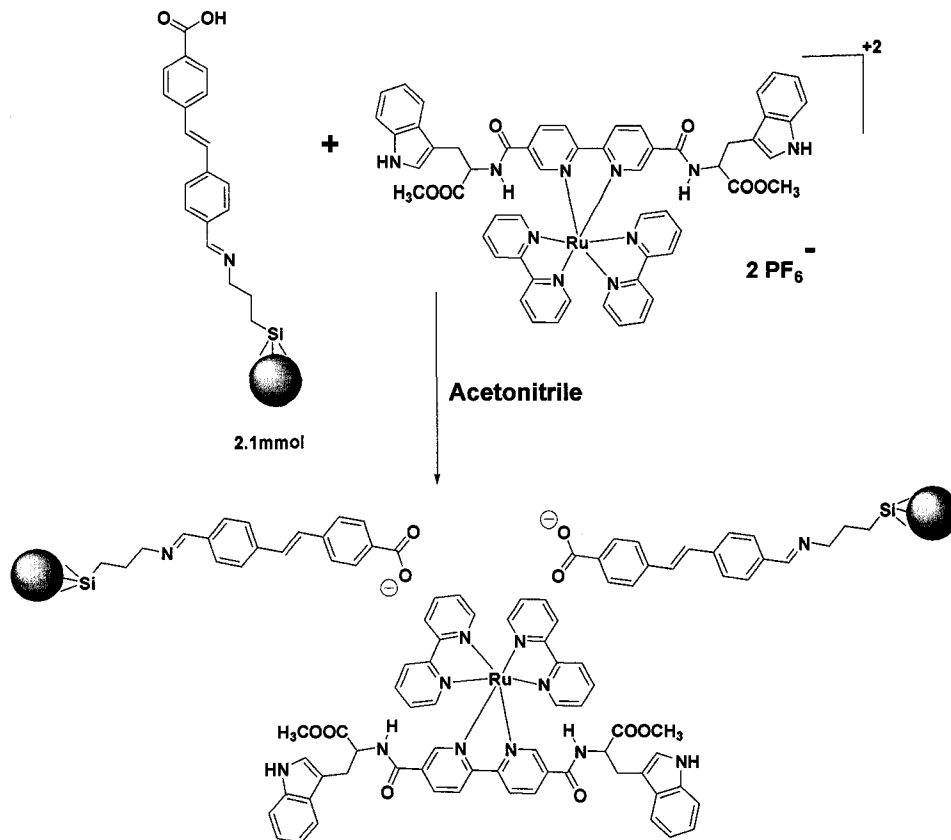
Figure 5.13 shows the emission of sensor I with increasing concentrations of HCl. After the first addition (87.75 μM) of HCl, the emission increases rapidly and then it increases slowly and shows some irregular behavior on increasing the concentrations of HCl. The association constant for this compound (Figure 5.14) is very high and the value is $(1.2 \pm 0.5) \times 10^4 \text{ M}^{-1}$. This association constant is almost same as the association constant of the free complex (Figure 3.23).

Figure 5.15 shows the emission of sensor I with DMMP and it does not show any change. It might be due to the chemical nature of DMMP, it does not have a good leaving group to attach with the receptor.

5.5 Synthesis of Silica NPs + Stilbene Monomer + 5,5'-Bpy Trypruthenium Complex (Sensor II) and its Spectral Characterization

The synthetic procedure for the sensor II is same as that of sensor I. An ion pair was formed by mixing 1 mmol $\text{Ru}(\text{bpy})_2(5,5'\text{-Bpy Tryptophan})$ complex (compound 9) and 2.1 mmol silanized silica nanoparticles (compound 11) in acetonitrile. The resultant mixture was stirred overnight to obtain compound 13.

5.5.1 Synthetic Procedure of Sensor II



13

Scheme 5.3 Synthesis of Sensor II

5.5.2 Emission of Silica NP + Stilbene Monomer (9.45 μM) + Ru(bpy)₂(5,5'-Bpy Tryptophan) (4.7 μM) (sensor II) Vs Various DCP

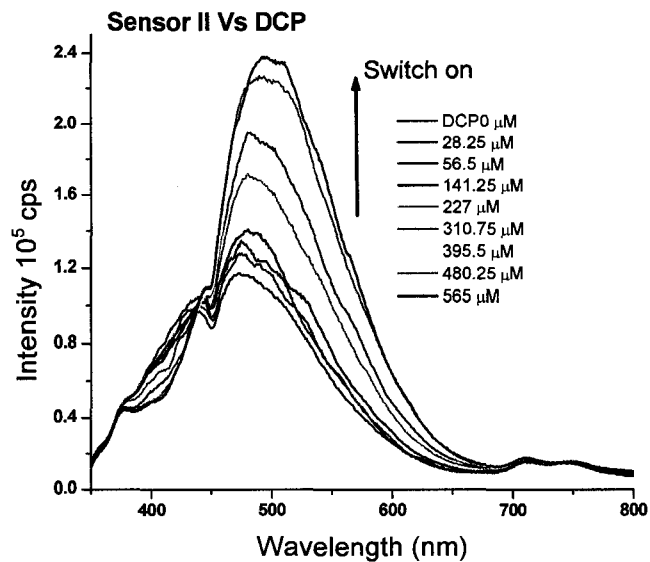


Figure 5.16 Emission Spectrum of Sensor II with DCP

Association Constant: $(813 \pm 60) \text{ M}^{-1}$

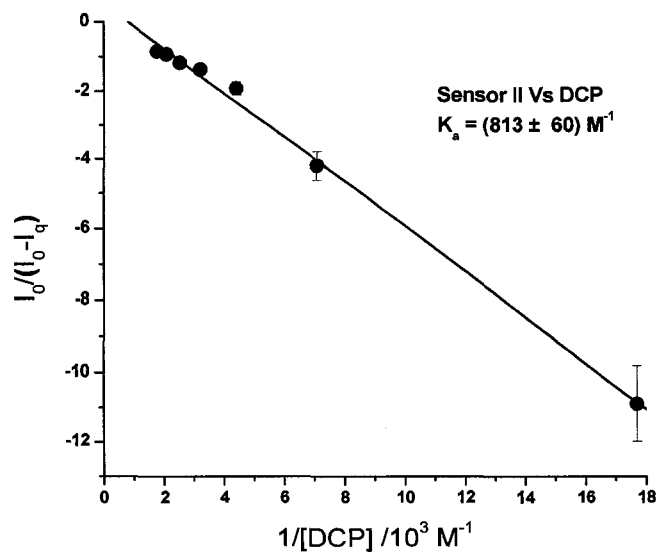


Figure 5.17 Association Constant of Sensor II with DCP

5.5.3 Emission of Silica NP + Stilbene Monomer (9.45 μM) + Ru(bpy)₂(5,5'-Bpy Tryptophan) (4.7 μM) (Sensor II) Vs Various HCl

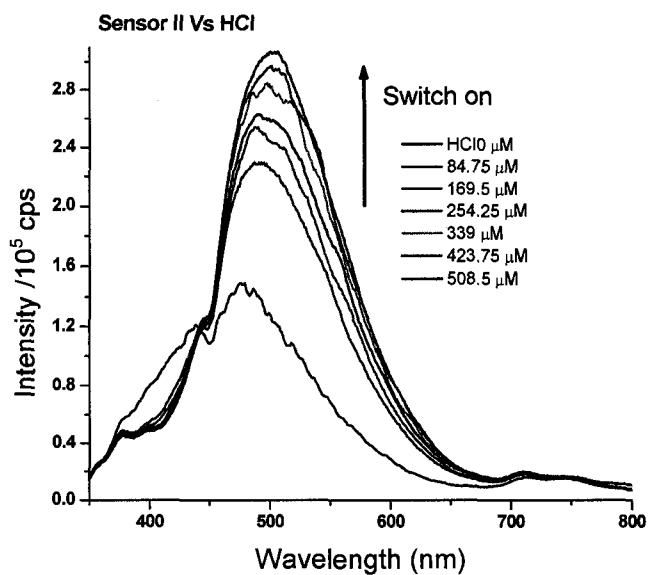


Figure 5.18 Emission Spectrum of Sensor II with HCl

Association Constant: $K = (5.7 \pm 0.8) \times 10^3 \text{ M}^{-1}$

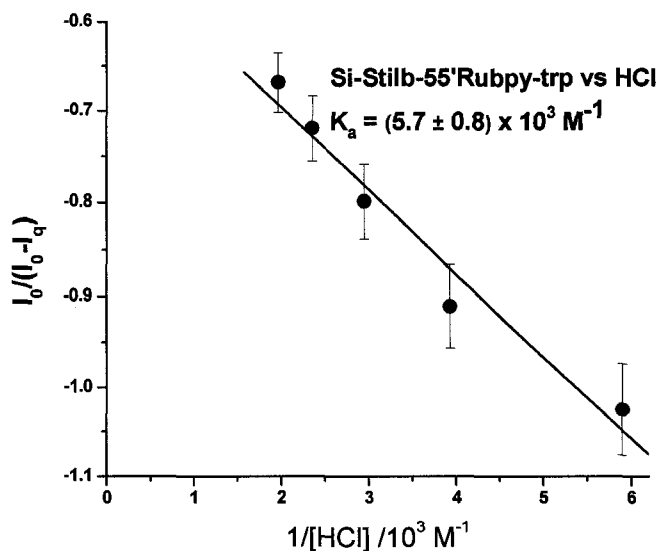


Figure 5.19 Association Constant of Sensor II with HCl

5.5.4 Emission of Silica NP + Stilbene Monomer (9.45 μM) + Ru(bpy)₂(5,5'-Bpy Tryptophan) (4.7 μM) (Sensor II) Vs Various DMMP

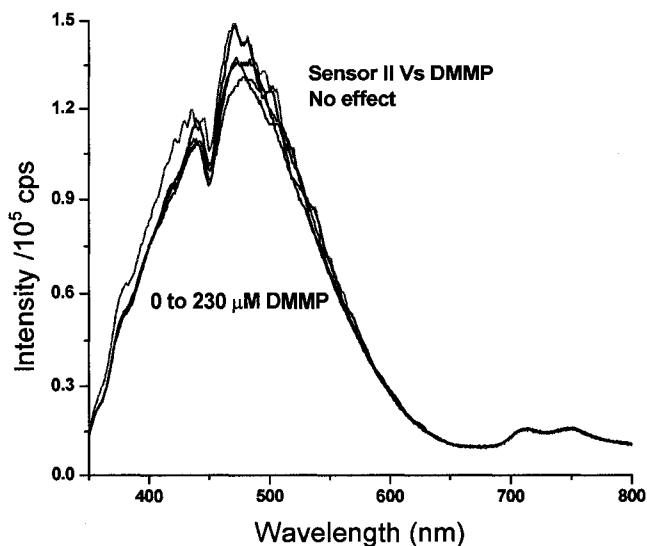


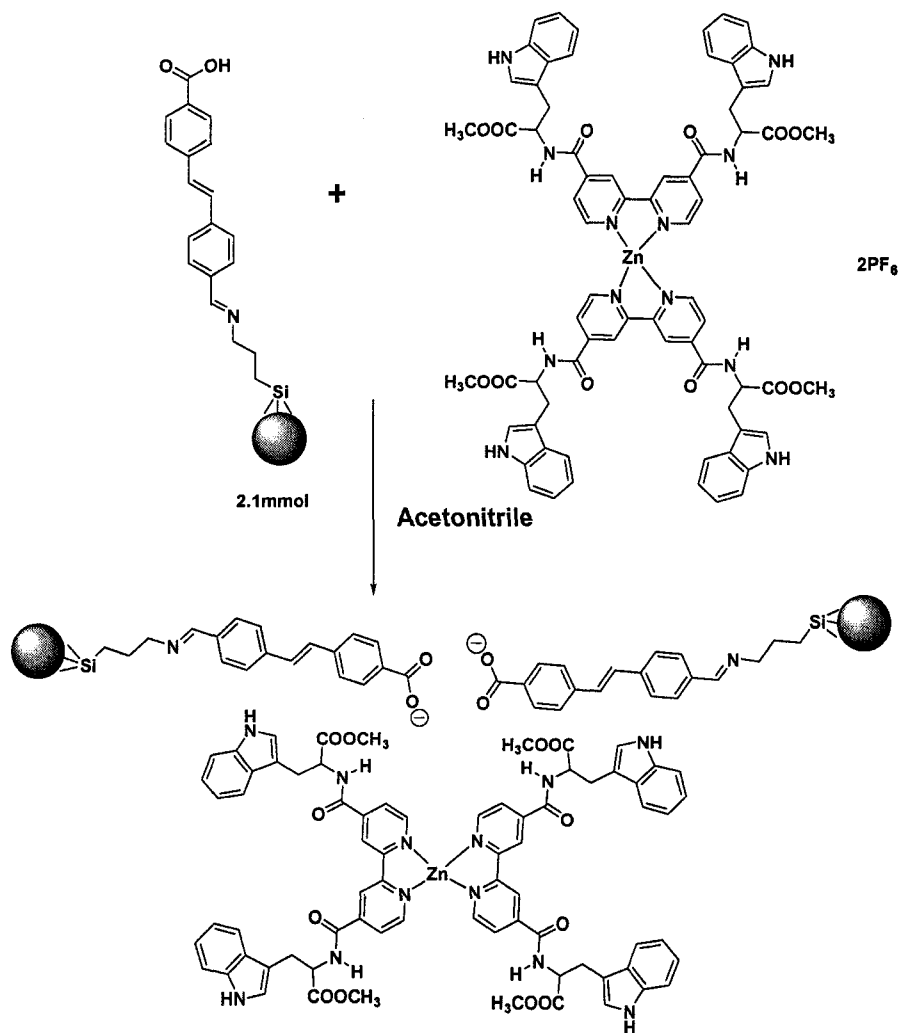
Figure 5.20 Emission Spectrum of Sensor II with DMMP

Figures 5.16, 5.18 and 5.20 show the emission of sensor II with DCP, HCl and DMMP. Sensor II shows switch on behavior with increasing concentration of DCP and has an association constant of $(813 \pm 60) \text{ M}^{-1}$ (Figure 5.17). This association constant is very weak when compared to the Ru(bpy)₂(5,5'-Bpy Tryptophan) complex (Figure 4.19) association constant. Sensor II shows the switch on behavior with increasing concentrations of HCl. Here the association constant is very high $(5.7 \pm 0.8) \times 10^3 \text{ M}^{-1}$ (Figure 5.19) when compared to the Ru(bpy)₂(5,5'-Bpy Tryptophan) complex (Figure 4.20) which does not have any change with increasing concentrations of HCl.

Figure 5.20 shows the emission spectrum of sensor II with increasing concentrations of DMMP, which shows no change in the emission maxima.

5.6 Synthesis of Silica NPs + Stilbene Monomer + 4,4'-Bpy tryp Zinc Complex (Sensor III) and its Spectral Characterization

5.6.1 Synthetic Scheme of Sensor III



Scheme 5.4 Synthesis of Sensor III

2.1 mmol silanized silica and 1mmol of 4,4'-Bpy Tryp zinc complex were dissolved in 4mL acetonitrile and stirred overnight at room temperature to get the desired sensor III.

5.6.2 Emission of Sensor III with DCP

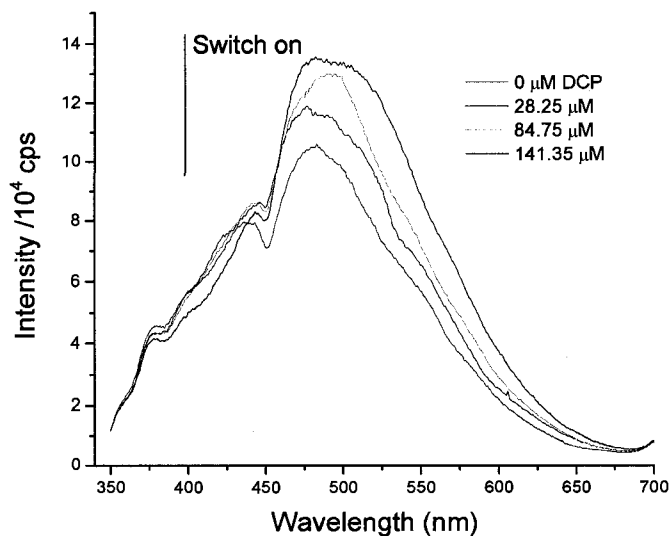


Figure 5.21 Emission Spectrum of Sensor III with DCP

Association Constant: $K = (1.3 \pm 0.3) \times 10^4 \text{ M}^{-1}$

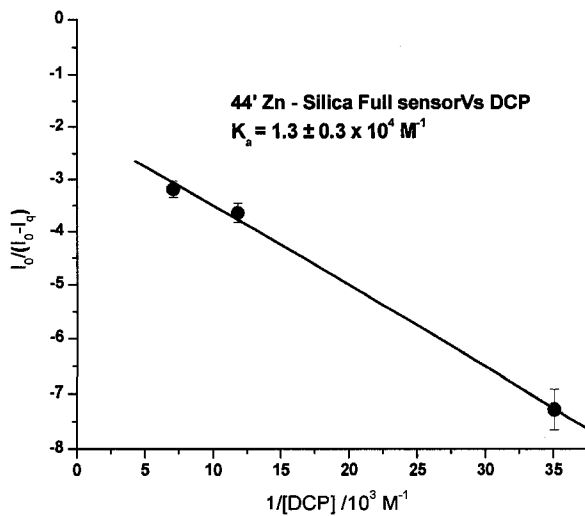


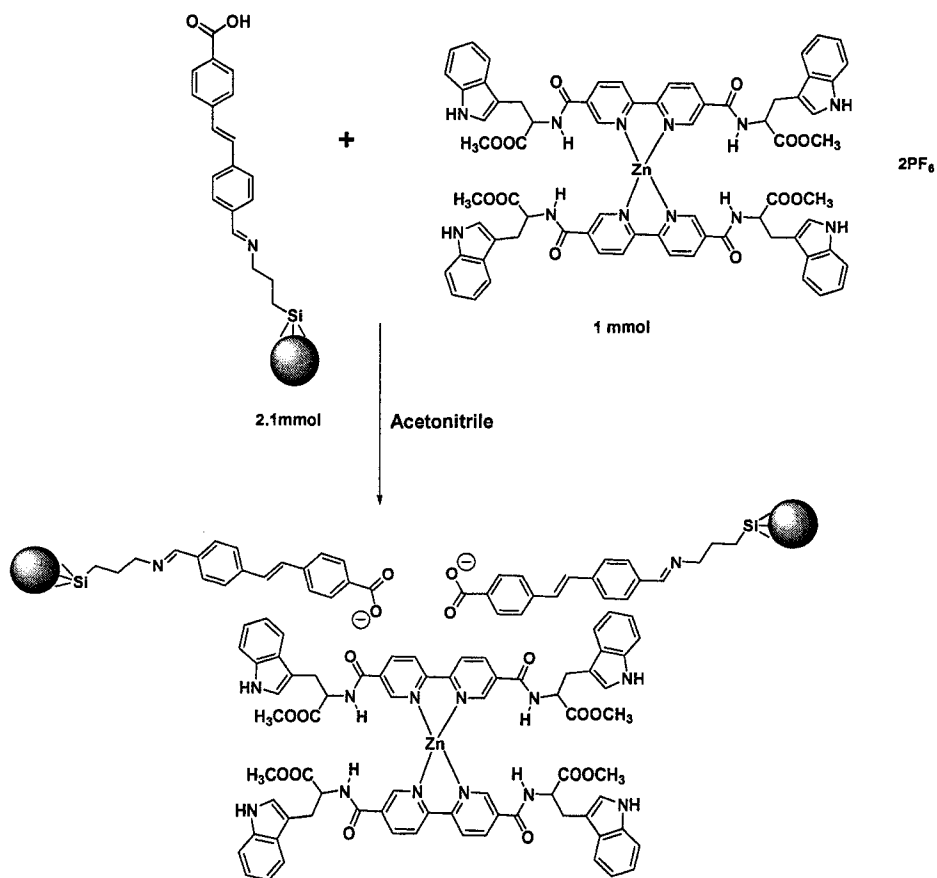
Figure 5.22 Association Constant of Sensor III with DCP

Figure 5.21 shows the emission spectrum of sensor III with increasing concentrations of DCP, and has a high association constant $(1.3 \pm 0.3) \times 10^4 \text{ M}^{-1}$ (Figure

5.22). This association constant is very high when compared to the association constant of $\text{Zn}(4,4'\text{-Bpy tryp})_2$ with DCP (Figure 3.26).

5.7 Synthesis of Silica NPs + Stilbene Monomer + 5,5'-Bpy Tryp Zinc Complex (Sensor IV) and its Spectral Characterization

5.7.1 Synthetic Scheme of Sensor IV



15

Scheme 5.5 Synthesis of Sensor IV

5.7.2 Emission of Sensor IV with DCP

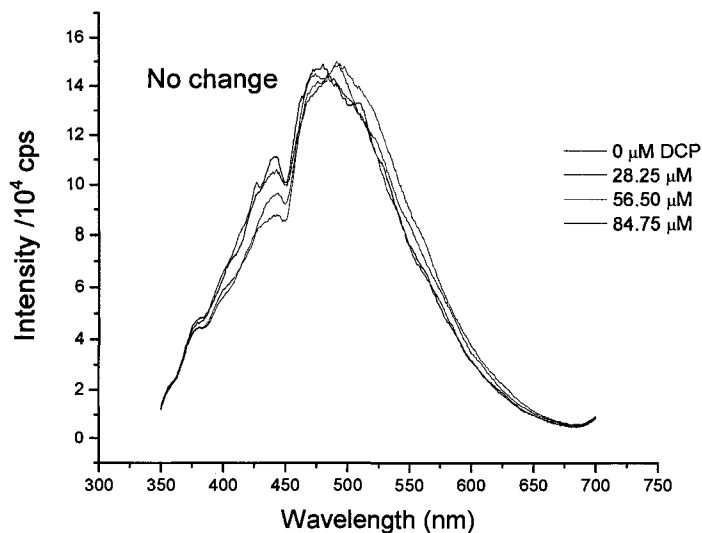


Figure 5.23 Emission Spectrum of Sensor IV with DCP

Figure 5.23 shows the emission spectrum of sensor IV with increasing concentrations of DCP. It does not exhibit any effect on increasing concentrations of DCP, because in sensor IV, the attached tryptophans at 5,5' position render very high steric hindrance. This may be due to the unavailability of nitrogen groups on the receptor for binding with the target analyte.

5.8 Synthesis of ZnS: Mn/ZnS QDs + Stilbene Monomer + 4,4'-Bpy Tryp Ruthenium Complex (Sensor V) and its Spectral Characterization

5.8.1 Synthetic Procedure for Sensor V

Sensor V was constructed based on conjugating ZnS: Mn/ZnS (1/16th) QDs to the Ru(bpy)₂(4,4'-Bpy Tryptophan) complex (compound 6). Ion pairing of QDs with the ruthenium complex was achieved by the mixing of the two compounds in acetonitrile by titration method. Firstly the ruthenium complex was dissolved in 4 mL of acetonitrile and to this solution QD solution was added drop wise till the QD emission and Ruthenium complex emission are equal. The QD solution was sonicated before the addition to avoid aggregation.

5.8.2 Emission of Sensor V Vs DCP

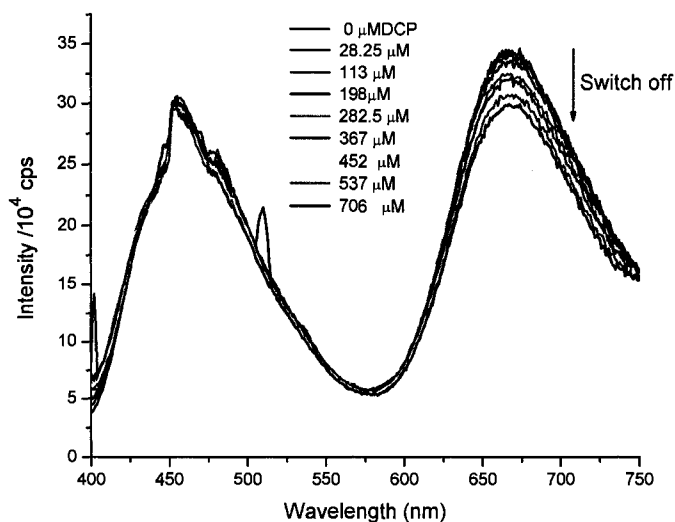


Figure 5.24 Emission Spectrum of Sensor V with DCP

Association Constant: $K = (425 \pm 50) \text{ M}^{-1}$

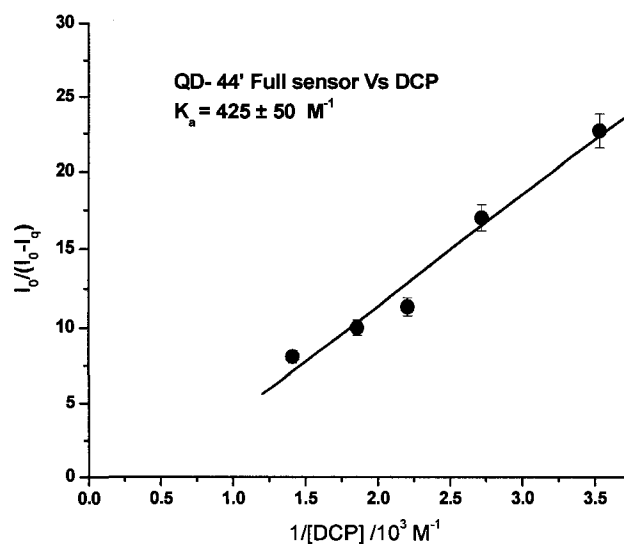


Figure 5.25 Association Constant of Sensor V with DCP

Figure 5.24 shows the emission spectrum of sensor V with increasing concentrations of DCP. The sensor V shows two emission maxima at 452nm and 670 which correspond to the QD and ruthenium metal centered emission respectively. The emission band at 670nm showed quenching with the increasing concentration of DCP while the other emission band at 452nm remained constant. Sensor V has very weak association constant $(425 \pm 50) \text{ M}^{-1}$ (Figure 5.25) with DCP.

5.8.3 Emission of Sensor V Vs HCl

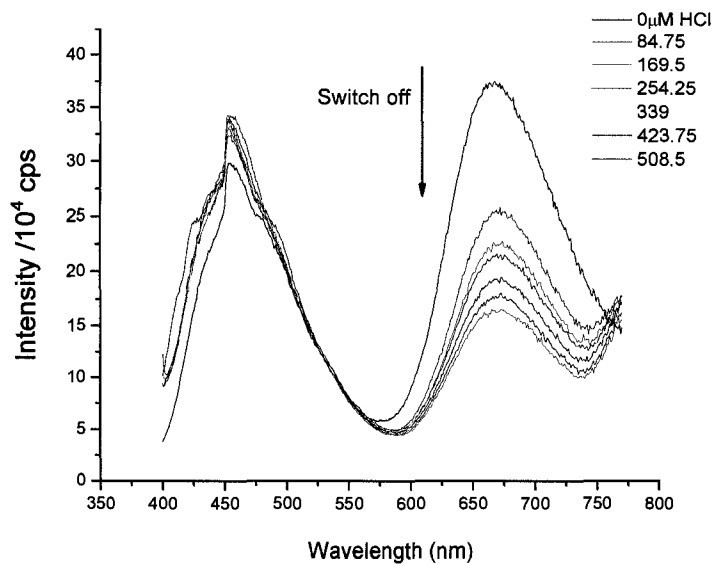


Figure 5.26 Emission Spectrum of Sensor V with HCl

Association Constant: $K = (1.6 \pm 0.3) \times 10^4 \text{ M}^{-1}$

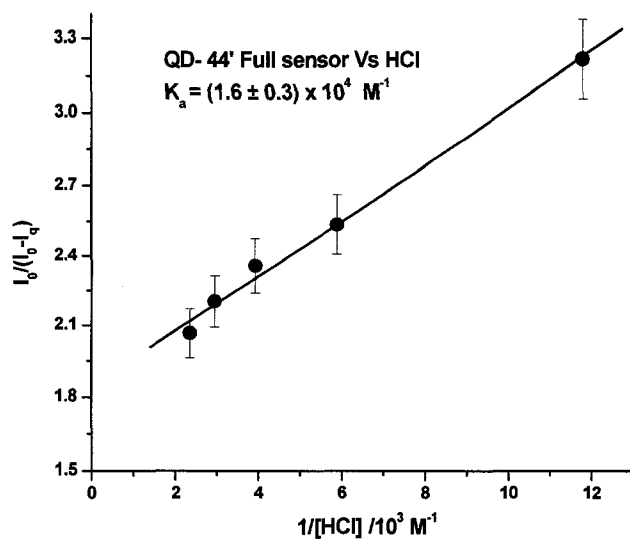


Figure 5.27 Association Constant of Sensor V with HCl

Figure 5.26 shows the emission spectrum of sensor V with increasing concentrations of HCl. The emission maxima corresponding to the ruthenium metal center quenches with increasing concentrations of HCl and shows very high association constant $(1.6 \pm 0.3) \times 10^4 \text{ M}^{-1}$.

5.8.4 Emission of Sensor V Vs DMMP

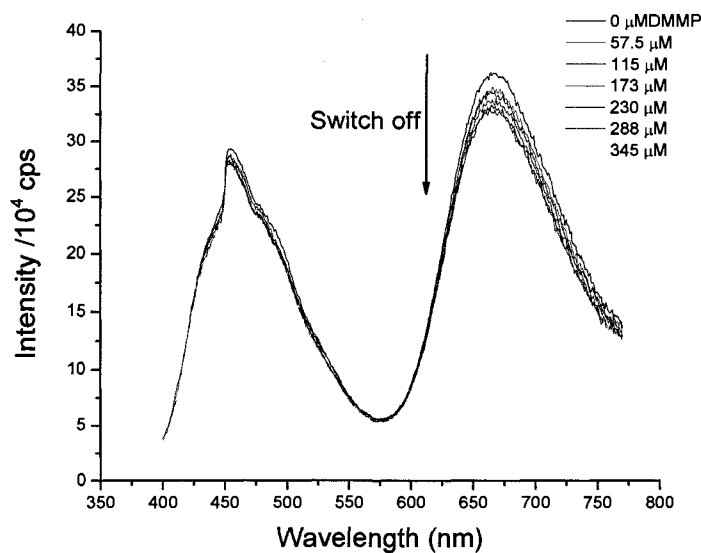


Figure 5.28 Emission Spectrum of Sensor V with DMMP

Association Constant: $K = (1.5 \pm 0.4) \times 10^3 \text{ M}^{-1}$

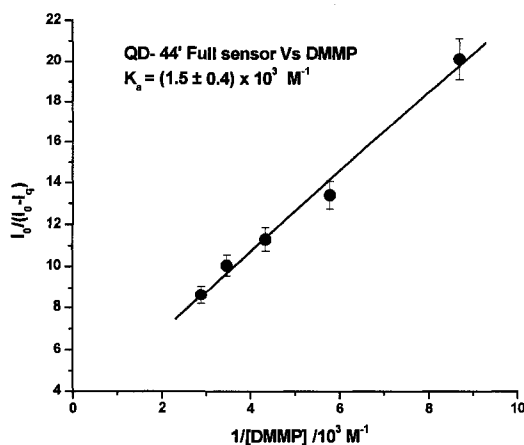


Figure 5.29 Association Constant of Sensor V with DMMP

Figure 5.28 shows the emission spectrum of sensor V with the increasing concentrations of HCl. Sensor V emission was quenched at the ruthenium center with increasing concentrations of HCl. The association constant is very high $(1.5 \pm 0.4) \times 10^3 \text{ M}^{-1}$ (Figure 5.29) when compared to the $\text{Ru}(\text{bpy})_2(4,4'\text{-Bpy Tryptophan})$ complex.

Table 5.1 Association Constants of Sensor Systems

	$K_{\text{DCP}} \text{ M}^{-1}$	$K_{\text{HCl}} \text{ M}^{-1}$	$K_{\text{DMMP}} \text{ M}^{-1}$
Sensor I	620 ± 140	$(1.2 \pm 0.5) \times 10^4$	No change
Sensor II	813 ± 60	$(5.7 \pm 0.8) \times 10^3$	No change
Sensor III	$(1.3 \pm 0.3) \times 10^4$		
Sensor IV	No change		
Sensor V	425 ± 50	$(1.6 \pm 0.3) \times 10^4$	$(1.5 \pm 0.4) \times 10^3$

Table 5.1 shows the association constants of the sensor systems developed. Sensor III with Zinc metal as complex, 4,4'-Bpy Tryptophan as receptor, Silica NPs and Stilbene monomer shows high sensitivity with DCP.

CHAPTER VI

CONCLUSION

6.1 Conclusion

This research was focused on building Nanoparticles-Monomer-Complex-Receptor (NMCR) nanosensors for the detection of nerve gas agents with a bottom up approach. Nerve gas analogs such as DCP and DMMP are used as target analytes.

Tryptophan has been used as the receptor for all five sensors. Ruthenium and zinc bipyridyl systems are used as complexes. Ruthenium bipyridyl systems show better results when compared to zinc bipyridyl systems. Ruthenium metal has advantages because of its metal to ligand charge transfer and we can tune ruthenium metal emission based on the ligand attached to it.

Silica nanoparticles and ZnS: Mn/ZnS (1/16th) core/ shell Quantum dots are used as building blocks of sensors. Highly conjugated stilbene type compounds are used as monomers.

Five types of nanosensors have been developed with different constituents based on the fundamental building blocks of the sensors which are outlined below. Table 6.1 shows the association constants and behavior of all sensors with DCP, DMMP and HCl.

Table 6.1 Association Constants and Behavior of Sensors Developed

	$K_{\text{DCP}} (\text{M}^{-1})$	$K_{\text{HCl}} (\text{M}^{-1})$	$K_{\text{DMMP}} (\text{M}^{-1})$
4,4'-Bpy Tryp	146 ± 60 Switch off	Switch off	Switch on
5,5'-Bpy Tryp	353 ± 45 Switch off	Switch off	(2.6 ± 0.9) x 10 ³ Switch on
Ru(bpy) ₂ (4,4'-Bpy Tryptophan)	(5.8 ± 0.6) x 10 ⁴ Switch on	(1.0 ± 0.4) x 10 ⁴ Switch off	No change
Ru(bpy) ₂ (5,5'-Bpy Tryptophan)	(2.6±0.9) x 10 ³ Switch off	No change	No change
Zinc (4,4'-Bpy Tryp) ₂	(5.4 ± 0.6) x 10 ³ Switch on	Switch on	Switch on
Zinc (5,5'-Bpy Tryp) ₂	(7.4±0.9) x 10 ³ Switch on	(6.0±0.5) x 10 ³ Switch on	14 ± 7 Switch on
Sensor I (4,4'Rubpy+Stilbene+Silica NP)	620 ± 140 Switch on	(1.2 ± 0.5) x 10 ⁴ Switch on	No change
Sensor II (5,5'Rubpy+Stilbene+Silica NP)	813 ± 60 Switch on	(5.7 ± 0.8) x 10 ³ Switch on	No change
Sensor III (4,4'Znbpy+Stilbene+Silica NP)	(1.3 ± 0.3) x 10 ⁴ Switch on	No data	No data
Sensor IV (5,5'Znbpy+Stilbene+Silica NP)	No change	No data	No data
Sensor V (4,4'Rubpy+Stilbene+QDs)	425 ± 50 Switch off	(1.6 ± 0.3) x 10 ⁴ Switch off	(1.5 ± 0.4) x 10 ³ Switch off

6.1.1 Sensor I

Sensor I was constructed with Silica NPs, Stilbene analog, Ruthenium-4,4'-Bpy Tryptophan as receptor. The interaction of this sensor with DCP, DMMP and HCl was determined by using emission studies. Sensor I showed a better interaction with HCl compared to DCP. Sensor I demonstrated no interaction with DMMP as it does not have a good leaving group.

6.1.2 Sensor II

Sensor II was synthesized by using Silica NPs, Stilbene analog, Ruthenium and 5,5'-Bpy Tryptophan as receptor. Sensor II shows similar behavior as sensor I, sensor II displayed "Switch on" behavior with DCP, DMMP and has no effect on DMMP. Sensor II shows better efficiency with DCP when compared to HCl.

6.1.3 Sensor III

Sensor III was developed by using Silica NPs, Stilbene analog, Zinc and 4,4'-Bpy Tryptophan as receptor. Sensor III confirmed "Switch on" behavior with increasing DCP concentrations and better sensitivity when compared to sensor I and II. This behavior is due to the two ligands attached to the zinc metal center and hence augments the number of binding sites for the interaction of target analytes.

6.1.4 Sensor IV

Sensor IV was constructed by Silica NPs, Stilbene analog, Ruthenium and 5,5'-Bpy Tryptophan as receptor. Sensor V confirmed no response towards DCP.

6.1.5 Sensor V

Sensor V was synthesized by using ZnS: Mn/ZnS (1/16th) QDs, Stilbene analog, Ruthenium and 4,4'-Bpy Tryptophan as receptor. Sensor V displayed “switch off” behavior with DCP, DMMP and HCl. The sensitivity of Sensor V for DCP was weak when compared to DMMP and HCl.

We were able to show a design strategy for making flexible and sensors that are processable in the solid state for nerve agents through the bottom up construction. This bottom up assembling of a sensor concept is flexible and can be altered based on the type of target that we need to sense.

From the above discussion it is conclusive that Sensor III demonstrated the maximum sensitivity and maximum selectivity towards DCP when compared to other sensor systems used in this study. We can improve the sensitivity and selectivity of this sensor system by varying the receptor moiety which would have a greater affinity towards the nerve gas analogs.

REFERENCES

1. Jortani, S.A.; Snyder, J.W and Valdes, R. "The role of the clinical laboratory in managing chemical or biological terrorism". *Clinical Chemistry*, **2000**, 46(12), 1883-1893.
2. Cannard, K "The acute treatment of nerve agent exposure", *Journal of Neurological Sciences*, **2006**, 249, 86-94.
3. Seto, Y.K.M.; Tsuge, K.; Ohsawa, I.; Matsushita, K.; Sekiguchi, H.; itoi,T.; Iura, K.; Sano, Y.; Yamashiro, S. "Sensing technology for chemical-warfare agents and its evaluation usng authentic agents". *Sensors and Actuators B*, **2005**, 108,193-197.
4. Royo, S.M.R.; Sancenon, F.; Costero, A.; Margarita, P.; Gil, S. "Chromogenic and fluorogenic reagents for chemical warfare nerve gas agents detection". *Chemical communications*, **2007**, 4839-4847.
5. Tsuge, K.; Seto, Y. "Detection of human butyrylcholinesterase-nerve gas adduct by liquid chromatography-mass spectrometric analysis after in gel chymotryptic digestion". *Journal of Chromatograpy B*, **2006**, 838, 21-30.
6. Rudolph H. de Jong. "Nerve gas terrorism: A grim challenge to Anesthesiologists". *Anesth. Analog.* **2003**, 96, 819-825.
7. Wiener, S.W.; Hoffman, R.S. "Nerve agents: A comprehensice review". *Journal of Intensive Care Medicine.* **2004**, 19, 22-37.

8. Paukku, Y.; Michalkova, A.; Muzumdar, D.; Leszczynski, J. "Investigation on the low energy conformational surface of tabun to probe the role of its different conformers on biological activity". *Chemical physics letters*, **2006**, 422, 317-322.
9. Kuca, K.; Bielavsky, J.; Cabal, J and Kassa, J. "Synthesis of a new reactivator of Tabun-inhibited acetylcholinesterase". *Bioinorganic and medicinal chemistry letters*. **2003**, 13, 3545-3547.
10. Pavlov, V.; Xiao, Y and Willner, I. " Inhibition of the Acetylcholine esterase-stimulated growth of Au nanoparticles: Nanotechnology-based sensing of Nerve Gases". *Nano letters*. **2005**, 5, 649-653.
11. Simpson, B. "Sarin Nerve Gas- Or how I learned to stop worrying and love pon-1". *Bio Teach Journal*, **2004**, 2, 100-105.
12. Lee, E.C. "Clinical manifestations of sarin nerve gas exposure". *The Journal of the American Medical Association*. **2003**.290(5), 659-662.
13. Thompson, C.H.; Hu, J.; Kaganove, S.N.; Keinath, S.E.; Keeley, D.L and Dvornic, P.R. "Hydrogen-bond acidic hyperbrached polymers for surface acoustic wave (SAW) sensors". *Chemistry of material*. **2004**, 16, 5357-5364.
14. Nieuwenhuizen, M.S and Harteveld, J.L.N. "Studies on a surface acoustic wave (SAW) dosimeter sensor for organophosphorous nerve agents". *Sensors and actuators B*. **1997**, 40, 167-173.
15. Williams, D and Pappas, G. "Rapid identification of nerve agents Sarin (GB) and soman (GD) with the use of a field-portable GC/SAW vapor detector and liquid deoction front-end device". *Field analytica chemistry and technology*. **1999**, 3, 45.

16. Russel, R.J and Pishko, M.V. "Poly(ethylene glycol) hydrogel-encapsulated fluorophore-enzyme conjugates for direct detection of organophosphorous neurotoxins". *Analytical Chemistry*, **1999**, 71, 4909-4912.
17. Lejuene, K.E.; Wild, J.R and Russel, A.J. "Nerve agents degraded by enzymatic foams". *Nature*, **1998**, 395, 27-28.
18. La Rosa, C.; Pariente, F.; Hernandez, L and Lorenzo, E. "Amperometric flow-through biosensor for the determination of pesticides". *Analytical Chimica Acta*, **1995**, 308, 129-136.
19. Kumaran, S and Morta, M. "Application of a cholinesterase biosensor to screen for organophosphorus pesticides extracted from soil". *Talanta*, **1995**, 42(4), 649-655.
20. Sohn, H.; Letant, S.; Sailor, M.J and Trogler, W.C. "Detection of fluorophosphate chemical warfare agents by catalytic hydrolysis with a porous silicon interferometer". *Journal of American Chemical Society*, **2000**, 122, 5399-5400.
21. Gamson, R.M.; Robinson, D.W and Goodman, A. "Test for anticholinesterase materials in water". *Environmental Science and Technology*, **1973**, 7(13), 1137-1140.
22. Novak, T.J.; Daasch, L.W and Epstein, J. "Decomposition at 90° C of the cholinesterase substrate indoxyl acetate impregnated on paper supports". *Analytical Chemistry*, **1979**, 51(8), 1271-1275.
23. Yang, Y.; Feng, H and Thunda, T. "Nerve agents detection using a Cu²⁺/L-Cysteine bilayer-coated microcantilever". *Journal of American Chemical Society*, **2003**, 125(5), 1124-1125.
24. Van Houten, K.A.; Heath, D.C and Pilato, R.S. "Rapid luminescent detection of phosphate esters in solution and the gas phase using (dppe)Pt{S₂C₂(2-

- pyridyl)(CH₂CH₂OH)}”. *Journal of American Chemical Society*, **1998**, 120, 12359-12360.
25. Levitsky, I and Krivoslykov, S.G. “Rational design of a Nile red/polymer composite film for fluorescence sensing of organophosphonate vapors using hydrogen bond acidic polymers”. *Analytical Chemistry*, **2001**, 73, 3441-3448.
26. Gehauf, B.; Epstein, J.; Wison, GB.; Witten, B.; Sass, S.; Bauer, V.E and Rueggeberg, W.H.C. “Reaction for colorimetric estimation of some phosphorus compounds”. *Analytical Chemistry*, **1957**, 29, 278-281.
27. Zhang, W and Swager, T.M. “Fluorescent detection of chemical warfare agents: functional group specific ratiometric chemosensors”. *Journal of American Chemical Society*, **2003**, 125, 3420-3421.
28. Dale, T.J and Rebek Jr, J. “Fluorescent sensors for organophosphorus nerve agent mimics”. *Journal of American Chemical Society*, **2006**, 128, 4500-4501.
29. Nagale, S.; Stemfeld, T and Walt, D.R. “Microbead chemical switches: an approach to detection of reactive organophosphate chemical warfare agent vapors”. *Journal of American Chemical Society*, **2006**, 128, 5041-5048.
30. Swapna, K.; “Nitrogen heterocyclic compounds as receptors in nanosensors for nerve gas agent analogs”. A thesis submitted to the Western Michigan University graduate college. August 2007.
31. Blatt, E.; Chatelier, R.C and Sawyer, W.H. “Effects of quenching mechanism and type of quencher association on Stern-Volmer plots in compartmentalized systems”. *Biophysical Journal*. **1986**, 50, 349-356.

32. Chow, C.; Lam, M.H.W and Wong, W.Y. "A heterobimetallic ruthenium (II)-copper(II) donor-acceptor complex as a chemodosimetric ensemble for selective cyanide detection". *Inorganic Chemistry*, **2004**, 43, 8387-8393.
33. Chang, S.Y.; Liu, L and Asher, S.A. "Creation of templated complexed topological morphologies in colloidal silica". *Journal of American Chemical Society*, **1994**, 116, 6745-6747.
34. Santra, S.; Tapeç, R.; Theodoropoulou, N.; Dobson, J.; Hebard, A and Tan, W. "Synthesis and characterization of silica-coated iron oxide nanoparticles in microemulsion: The effect of nonionic surfactants". *Langmuir*, **2001**, 17, 2900-2906.
35. Rao, K.S.; El-Hami, K.; Kodaki, T.; Matsushige, K and Makino, K. "A novel method for synthesis of silica nanoparticles". *Journal of colloidal and interface science*, **2005**, 289, 125-131.
36. Matsoukas, T and Gulari, E. "Dynamics of growth of silica particles from ammonia-catalyzed hydrolysis of tetra ethyl orthosilicate". *Journal of colloidal and interface science*, **1988**, 124, 252-261.
37. Lindberg, R.; Sundholm, G.; Pettersen, B.; Sjoblom, J and Friberg, S.E. "Multivariate analysis of the size dependence of monodisperse silica particles prepared according to the sol-gel technique". *Colloids and surfaces A*, **1997**, 123, 549-560.
38. Tolnai, G.; Csempesz, F.; Faix, M.K.; Kalman, E.; Desesztes, Z.; Kovacs, A.L.; Ramsden, J.J.; and Horvolgy, Z. "Preparation and characterization of surface-modified silica nanoparticles". *Langmuir*, **2001**, 17, 2683-2687.
39. Bagwe, R.P.; Hilliard, L.R and Tan, W. "Surface modification of silica nanoparticles to reduce aggregation and nonspecific binding". *Langmuir*, **2006**, 22, 4357-4362.

40. Asare, K.O and Arriagada, F.J. "preparation of SiO₂ nanoparticle in a non-ionic reverse micellar system". *Journal of colloids and surfaces*, **1990**, 50, 321-339.
41. Stober, W.; Fink, A and Bohn Ernst. "Controlled growth of monodisperse silica spheres in the micron size range". *Journal of colloid and interface science*, **1968**, 26, 62-69.
42. Liu, S.; Zhang, H.; Lie, T.; Lie, B.; Cao, Y.; Huang, Z.; Zhao, Y and Luo, Q. "Optimization of the methods for introduction of amine groups onto the silica nanoparticle surface". *Journal of Biomedical Materials Research Part A*, **2006**, 752-758.
43. Bruce, I.J and Sen, T. "Surface modification of magnetic nanoparticles with alkoxy silanes and their application in magnetic bioseparations". *Langmuir*, **2005**, 21, 7029-7035.
44. Murphy, C.J.; "Optical sensing with quantum dots". *Analytical Chemistry*, **2002**, 74(19), 520A-526A.
45. Wang, X.; Ruedas Rama, M.J and Hall, E.A.H. "The emerging use of quantum dots in analysis". *Analytical letters*, **2007**, 40, 1497-1520.
46. Gomez, D.E.; Califano, M and Mulvaney, P. "Optical properties of single semiconductor nanocrystals". *Physical chemistry chemical physics*, **2006**, 8, 4989-5011.
47. Fernandez, J.M.C.; Pereiro, R.; Medel, A.S. "The use of luminescent quantum dots for optical sensing". *Trends in analytical chemistry*, **2006**, 25 (3), 207-218.
48. Costa Fernandez, J.M. "Optical sensors based on luminescent quantum dots". *Analytical and Bioanalytical Chemistry*, **2006**, 384, 37-40.

49. Raymo, F.M and Yildiz, I. "Luminescent chemosensors based on semiconductor quantum dots". *Physical chemistry chemical physics*, **2007**, 9, 2036-2043.
50. Jorge, p.; Martins, M.A.; Trindade, T.; Santos, J.L and Farahi, F. "Optical fiber sensing using quantum dots". *Sensors*, **2007**, 7, 3489-3543.
51. Jin, W.J.; Costa Fernandez, J.M.; Pereiro, R and Sanz-Medel, A. "Surface-modified CdSe quantum dots as luminescent probes for cyanide determination". *Analytica Chimica Acta*, **2004**, 522, 1-8.
52. Shi, G.H.; Shang, Z.B.; Wang, Y.; Jin, W.J and Zhang, T.C. "Fluorescence quenching of CdSe quantum dots by nitroaromatic explosives and their relative compounds". *Spectrochimica Acta Part A*, **2008**, 70, 247-252.
53. Riegler, J and Nann, T. "Applications of luminescent nanocrystals as labels for biological molecules". *Analytical and Bioanalytical Chemistry*, **2004**, 379, 913-919.
54. Alivisatos, P. "The use of nanocrystals in biological detection". *Nature biotechnology*, **2004**, 22(1), 47-52.
55. Somers, R.C.; Bawendi, M.G and Nocera, D.G. "CdSe nanocrystals based chem -/bio-sensors". *Chemical Society Reviews*, **2007**, 36, 579-591.
56. Cordes, D.B.; Gamsey, S and Singaram, B. "Fluorescent quantum dots with boronic acid substituted viologens to sense glucose in aqueous solution". *Angewandte Chemie International Edition*. **2006**, 45, 3829-3832.
57. Mattoussi, H et al. "Self-assembly of CdSe-ZnS quantum dot bioconjugates using an engineered recombinant protein". *Journal of American Chemical Society*, **2000**, 122, 12142-12150.

58. Beermann, P.A.G.; McGarvey, B.R.; Muralidharan, S and Sung, R.C.W. "EPR spectra of Mn²⁺ doped ZnS quantum dots". *Chemistry of Materials*, **2004**, 16, 915-918.
59. Tao, Y.; Donat-Bouillud, A.; Iorio, M.D.; Lam, J.; Gorjanc, T.C.; Py, C.; Wong, M.S.; Li, Z.H. "Organic light emitting diodes based on end-substituted oligo(phenylenevinylene)s". *Thin solid films*, **2000**, 363, 298-301.
60. Neuteboom, E.E et al. "Altering oligo(p-phenylene vinylene)-perylene bisimide copolymers: synthesis, photophysics, and photovoltaic properties of a new class of donor-acceptor materials". *Journal of American Chemical Society*, **2003**, 125, 8625-8638.
61. Hulvat, J.F.; Sofos, M.; Tajima, K and Stupp, S.I. "Self-assembly and luminescence of oligo(p-phenylenevinylene) amphiphiles". *Journal of American Chemical Society*, **2005**, 127, 366-372.
62. Surin, M et al. "Solid state assemblies and optical properties of conjugated oligomers combining fluorine and thiophene units". *Journal of material chemistry*, **2007**, 17, 728-735.
63. Kraft, A.; Grimsdale, A.C and Holmes, B. "Electroluminescent conjugated polymers-seeing polymers in a new light". *Angewandte Chemie International Edition*, **1998**, 37, 402-428.
64. Dimitrakopoulos, C.D and Malenfant, P.R. "Organic thin film transistors for large area electronics". *Advanced materials*, **2002**, 14(2), 99-117.
65. Halls, J.J.M et al. "Efficient photodiodes from interpenetrating polymer networks". *Nature*, **1995**, 376, 498-500.

66. McQuabe, D.T.; Pullen, A.E and Swager, T.M. "Conjugated polymer based chemical sensors". *Chemical Reviews*, **2000**, 100, 2537-2574.
67. Aggarwal, V.K.; Fulton, J.R.; Sheldon, C.G and Vicente, J. "Generation of phosphoranes derived from phosphites. A new class of phosphorus ylides leading to high E selectivity with semi-stabilizing groups in witting olefinations". *Journal of American Chemical Society*, **2003**, 125, 6034-6035.
68. Chun Wang.; "Synthesis and characterization of stilbenoids and their aza-analogs as photoluminescent materials for the detection of nerve agent mimics". Dissertation submitted to the Western Michigan University graduate college. December 2007.
69. Sprintschnik, G.; Sprintschnik, H.W.; Kirsch, P.P and Whitten, D.G. "Preparation and photochemical reactivity of surfactant ruthenium (II) complexes in monolayer assemblies and at water-solid interfaces. *Journal of American Chemical Society*, **1997**, 99(15), 4947-4954.
70. Garelli, N and Vierling, P. "Synthesis of new amphiphilic perfluoroalkylated bipyridines". *Journal of Organic Chemistry*, **1992**, 57, 3046-3051.
71. Sullivan, B.P.; Salmon, D.J and Meyer, T.J. "Mixed phosphine 2,2'-Bipyridine complexes of ruthenium". *Inorganic chemistry*, **1978**, 17(12), 3334-3341.
72. <http://dwb.unl.edu/Teacher/NSF/C08/C08Links/pps99.cryst.bbk.ac.uk/projects/gmocz/fluor.htm>
73. Wolfbeis, O.S. "fiber optic chemical and biosensors". *Analytical Chemistry*, **2006**, 78, 3859-3874.

NEW YEAR, NEW CONNECTIONS!

Join us for a special evening of networking and celebration.

Event details and ticket information available at www.cosozo.com.

For more information, please contact us at (517) 974-2915.

We look forward to seeing you at the event!

2009

(517) 974-2915

www.CosoZo.com